Molecular Beam Epitaxy of Tailored (In,Ga)As/GaAs Quantum Dot Heterostructures

A thesis submitted to

Dept. of Physics, University of Paderborn

for the degree of

Doctoral of Philosophy

by

Nand Lal Sharma

(India)

Paderborn, Sept. 2017

1. Gutachter: Prof. Dr. Dirk Reuter

2. Gutachter: Prof. Dr. Artur Zrenner

Parts of this work have already been published in journals, conference proceedings. The publications are listed on page 128.

This page has been intentionally left blank.

Abstract

This work is focused on the growth of self-assembled (In,Ga)As/GaAs quantum dots (QDs) by the molecular beam epitaxy on the GaAs(100) substrate. The InAs/GaAs is a mature material system which allows precise fabrication of the complex heterostructures of a high quality. The InAs QDs are promising semiconductor quantum emitters and it is also possible to grow them in a spatially controlled manner which allows novel device fabrications. All this together makes InAs/GaAs a very attractive material system for the applications in the field of quantum communication.

In the first part of the thesis, the growth of low density (In,Ga)As QDs for single dot spectroscopy is realized by an In-gradient approach. In this approach, the substrate rotation is paused during InAs deposition, which results in a density gradient on the substrate surface. The emission wavelength of the QDs should be around 900-1000 nm so that the efficient Si-detection technology can be used. In this thesis the emission energy tuning of QDs is done by the In-flush technique or by growing $In_xGa_{1-x}As$ QDs.

In the second part of the thesis, we demonstrate a simplified gradient method to grow low density quantum dot molecules, utilizing the In-gradient approach and strain induced nucleation. The influence of the bottom QD layer on the growth of the top QD layer is studied by varying InAs amount for the top layer growth while keeping the interdot barrier thickness constant.

In the last part of the thesis, the patterning and regrowth technology for the site-controlled QDs fabrication is discussed. In the process, the nanohole arrays are patterned on the substrate for preferential nucleation of QDs during the regrowth process. The nanohole patterning and the QD growth process is optimized for single QD per hole occupancy.

Abstrakt

Diese Arbeit behandelt das Wachstum von selbstorganisierten (In,Ga)As/GaAs Quantenpunkten (QDs) mittels Molekularstrahlepitaxie auf GaAs(100)-Substraten. Das InAs/GaAs-Materialsystem ist ausgereift, was die Herstellung von komplexen Heterostrukturen mit hoher Qualität ermöglicht. (In,Ga)As-QDs sind mögliche Halbleiterquantenemitter, welche auch räumlich positioniert gewachsen werden können. Das macht InAs/GaAs zu einem attraktiven Materialsystem für Anwendungen in der Quantenkommunikation.

Zunächst wird das Wachstum von (In,Ga)AsAs QDs mit niedriger Dichte für Einzelpunktspektroskopie durch einen Indiumgradienten-Ansatz diskutiert. Dazu wird die Substratrotation während der InAs-Deposition gestoppt, wodurch ein In-Gradient auf der Oberfläche entsteht. Die Emissionswellenlängen der QDs sollen bei 900-1000 nm liegen damit Siliziumdetektoren genutzt werden können. Um die Emissionsenergie der QDs zu kontrollieren wird die Indiumflush-Technik angewandt oder $In_xGa_{1-x}As$ QDs hergestellt.

Anschließend wird eine vereinfachte Gradientenmethode zum Wachstum von QD-Molekülen mit niedrigen Dichten verwendet, wobei der Indiumgradienten-Ansatz mit verspannungsinduzierter Nukleation kombiniert wird. Dabei wird auch der Einfluss der unteren Quantenpunktschicht auf die obere Quantenpunktschicht untersucht, indem die abgeschiedene InAs-Menge bei konstanter Barrierendicke verändert wird.

Im letzten Teil wird eine Technologie behandelt, bei der positionierte QDs auf strukturierten Substraten gewachsen werden. Dazu werden Löcher mit einer Größe von wenigen Nanometern in das Substrat geätzt um als Nukleationsorte für QDs während des Überwachsens zu fungieren. Der Prozess wurde so optimiert, dass sich in jedem Loch ein einzelner QD bildet.

Acknowledgements

This thesis work is the result of research carried out in the Optoelectronic Materials and Devices (OMD) group at the University of Paderborn between October 2013 to 2017. I am grateful to the OMD group for providing excellent research facilities and to the staff who make it a social place to work.

Special thanks go to

- Prof. Dr. Dirk Reuter for supervising and giving me the opportunity to realize this fascinating work. His great expertise, encouragement and guidance helped me on the way to this thesis.
- Prof. Dr. Artur Zrenner for his work as second assessor and many helpful discussions. His valuable time, guidance and inputs enabled this project.
- apl. Prof. Dr. Donat. J. As is acknowledged for a lot of scientific discussions, support and useful advices.
- Prof. Dr. Cedrik Meier for access to the electron beam lithography system and the photoluminescence spectroscopy setup.
- Dr. Thomas Riedl for the TEM investigations and helpful discussions.
- my office mate Dr. Stepan Shvarkov for pleasant working atmosphere and teamwork. For his guidance and many helpful discussions during thesis writing. Furthermore, my other colleagues Victoryia Zolatanosha, Tobias Wecker, Alexander Karlisch, Sarah Blumenthal, Michael Deppe, Timo Langer and Tobias Henksmeier for their teamwork and help.
- former group members Prof. Dr. Alexander Pawlis, Dr. Ricarda Kemper and Dr. Matthias Bürger for their guidance during the beginning of my work.
- Dr. Amlan Mukherjee, Alex Widhalm and Nils Weber for their support and helpful discussions.
- Bastian Aisenbrey for the technical support during MBE growth and patterning.
- Anja Blank and Siegfried Igges for the administrative and technical support.

Furthermore, I thank the SFB TRR 142 for the funding of this project and the other members of the SFB TRR.

I would like to thank all coworkers of my collaboration partner at the University of Bochum, Bochum

- Dr. Arne Ludwig, Sascha R. Valentin, Julian Ritzmann, Rüdiger Schott and Prof. Dr. Andreas D. Wieck

At finally, I would like to express my gratitude to my family for their love and encouragement and for making everything possible.

This page has been intentionally left blank.

Table of Contents

Abstract v

Acknowledgement vii

List of Figures xi

List of Tables xviii

List of Abbreviations xix

1 Introduction 1

1.1 Motivation 1

1.2 Thesis outline 3

2 Fundamentals 5

2.1 Group III-arsenides 5

2.2 Semiconductor Nanostructures 8

2.3 Quantum Dots (QDs) 9

2.4 Self-Assembled Quantum Dots (SAQDs) 10

3 Experimental Techniques 13

3.1 Molecular Beam Epitaxy 13

3.1.1 Molecular Beam Epitaxy System 15

3.2 Reflection High Energy Electron Diffraction 19

3.2.1 Surface Morphology and Reconstruction 19

3.2.2 RHEED Oscillations 21

3.3 Atomic Force Microscopy 23

3.4 Photoluminescence Spectroscopy 25

3.5 Electron Beam lithography 28

4 Sample Preparation and Patterning Process 29

4.1 Sample preparation 29

4.2 Substrate Patterning 37

4.2.1 Optical Lithography 37

4.2.2 Electron-Beam Lithography 40

4.3 Chemical Cleaning 42

4.4 Atomic Hydrogen Cleaning 44

5 Growth of Self-Assembled (In,Ga)As QDs on GaAs(100) 51
5.1 Introduction 51
5.2 Quantum Dots Growth 53
5.3 Quantum Dots Characterization 57
5.3.1 Morphological Characterization 57
5.3.2 Optical Characterization 61
5.4 Growth of Low Density QDs 65
5.4.1 In-gradient Approach: Growth 65
5.4.2 In-gradient Approach: Characterization 67
5.5 Emission Energy Tunning 71
5.5.1 In-flush Technique 71
5.5.2 Growth of InGaAs QDs 76
5.5.3 InGaAs QDs: Growth Procedure 76
5.5.4 InGaAs QDs: Characterization 78
6 Quantum Dot Molecules 81
6.1 Introduction 81
6.2 QDMs: Growth Process 83
6.3 QDMs: Characterization 85
6.3.1 QDMs: Effect of In Amount for Top QD Layer 88
6.3.2 QDMs: Effect of Interdot Barrier Thickness 91
6.4 QDMs: Optical Properties 92
7 Site-Controlled Quantum Dots 97
7.1 Introduction 97
7.2 Growth of InAs QDs on Patterned Substrate 99
7.3 SCQDs: Morphological Characterization 101
7.4 SCQDs: Optical Characterization 108
7.5 Summary 109
8 Conclusions 111
Appendix 113
Bibliography 117
Curriculmn Viate 127
Publications 128

List of Figures

2.1 Bandgap energy and lattice constant of various III-V semiconductors at room temperature (after Tien 1988)……………………………………………………………………………6

2.2 Band alignment for different type of heterostructures: E_g is the bandgap of the semiconductor, E_c and E_v are conduction and valance band edge, respectively. (a) represents type-I heterostructure where both types of carriers are confined in the spatial region, (b) represents type-II (staggered), where one type of carriers are confined and (c) represents type-III heterostructures (broken gap), no overlap of the bandgaps…………………………………7

2.3 Top: Schematic diagram of three, two, one and zero-dimensional heterostructures. Bottom: corresponding electronic density of states [8]……………………………………………………8

2.4 Schematic diagram of formation of InAs quantum dot on GaAs ……..…...……………..10

2.5 Atomic force microscopy image ($2 \times 2\ \mu m^2$) of InAs quantum dots showing their random spatial distribution. The average height and base diameter of QDs is 6.6 nm and 35 nm, respectively…………………………………...…………………………………………11

2.6 (top) Schematic representation of the band edge diagram of the InAs/GaAs quantum dot system, (bottom) shows schematic sketch of InAs QD embedded in GaAs matrix…………...12

3.1 Schematic illustration of surface processes occurring during film growth by MBE: (a) surface diffusion, (b) lattice incorporation, (c) desorption, (d) surface aggregation, and (e) interdiffusion, after [23]...14

3.2 Schematic of the III/V molecular beam epitaxy system (MBE Komponenten)……………………15

3.3 Schematic sketch of the MBE growth chamber (MBE Komponenten)……………………………16

3.4 Schematic diagram of RHEED arrangement………….…………………………………19

3.5 Schematic representation of RHEED pattern: (a) from rough surface and (b). from atomically smooth surface. The intersection of Ewald sphere and reciprocal lattice defines the diffracted streaks and spots on RHEED screen ………………………………………………20

3.6 RHEED patterns observed along the (011) (a) and $(01\bar{1})$ (b) azimuths during the molecular beam epitaxy (MBE) growth of an epitaxial GaAs layer deposited on a GaAs(100) substrate; the surface reconstruction is the As-stabilized (2×4) one……………………………………21

3.7 RHEED intensity oscillations during growth of GaAs on GaAs (100) substrate. The growth rate of GaAs is 0.7ML/sec…………………………………………………………………22

3.8 (a) Schematic sketch of an AFM setup [30], (b) AFM image of single InAs quantum dots on GaAs(100) at low density area. The surface is atomically smooth and rms value of the roughness is 0.42 nm……………………………………………………………………….24

3.9 Illustration of photoluminescence process (a) a photon excites an electron-hole pair in the material (b) the carriers thermalization and diffuse (c) a photon is emitted from recombination of electron-hole pair……………………………………..……………………………25

3.10 (a) Schematic representation of PL process in InAs QD: (1) creation of electron-hole pairs in bulk GaAs by laser excitation; (2) capture in QD by phonon emission; (3) recombination and emission of photons from different states. (b) shows a room temperature PL spectrum of QD ensemble………………………………………………………………………………26

3.11 Schematic sketch of the photoluminescence setup………………………………………27

4.1 AFM image of GaAs(100) wafer (a) before and (b) after thermal removal of the surface oxide. The pit density is around $10^9/\text{cm}^2$. The height scale for (a) is 3 nm and for (b) is 6 nm……………………………………………………………………………………….31

4.2 AFM images and corresponding RHEED pattern of different types of GaAs surface. (a) shows an AFM image of epi-ready GaAs substrate after thermal degassing at 200°C in UHV and corresponding RHEED pattern, (b) shows an AFM image of GaAs surface after thermal removal of the surface oxide and corresponding RHEED pattern and (c) shows an AFM image of epitaxial grown smooth GaAs and corresponding RHEED pattern………………………...32

4.3 Different types of oval defects on MBE grown GaAs Surface. (a) These type of oval defects are due to Ga spitting on surface , (b) oval defect with notch in the centre, these are defects are related to chamber impurities and (c) & (d) these oval defects are related to the arsenic flux in the chamber [44-48]. In optimized growth temperature and As flux conditions, the defect density can be reduced to 20-30 defects/cm^2.................... 33

4.4 (a) Surface phase diagram for the epitaxial growth of GaAs from Ga and As_4 beams on GaAs (100) substrate [49], (b) AFM image of epitaxial grown GaAs surface and (c) line scan along the dotted line in (b)…………………………………………………………………34

4.5 GaAs surface at low As pressure ($P_{As_4} = 1.5 \times 10^{-5}$ mbar) An AFM image of GaAs surface with surface defects. The vertical scale of AFM image is 7 nm………………………36

4.6 GaAs surface at high As pressure ($P_{As_4} = 3.5 \times 10^{-5}$ mbar) (a) Laser microscopy image of GaAs surface with mound growth. (b) AFM shows mound traces with size of 1 µm to 2 µm. The vertical scale for AFM is 8 nm…………………………………………………………….36

4.7 Schematic of the optical lithography process……………………………………………..38

4.8 (a) Schematic of a ¼ 3" GaAs (100) wafer with optical lithography mask and (b) Laser microscope image of patterned mesa. The mesa size is 300 × 300 μm^2 and 400 nm deep etched……………………………………………………………………………………...39

4.9 Overview of the mask design, (a) Schematic of patterned mesa via optical lithography, (b) schematic of pattern mask for EBL, here different colours correspond to different layers for patterning nanoholes and (c) shows array of holes with alignment marks in the centre of the mesa………………………………………………………………………...………...40

4.10 AFM images of patterned nanoholes on GaAs (100), (a) after removing resist with acetone and IPA, (b) after chemical cleaning…………………………………………………………42

4.11 Nanopatterned holes with different spacing. (a), (b), (c) and (d) shows AFM images at different mesa structures with patterned nanoholes. (e) and (f) shows SEM images of such nanoholes……………………………………………………………………………………43

4.12 Photograph of the hydrogen atom beam source (HABS) unit (MBE Komponenten)…..45

4.13 Schematic sketch of the atomic hydrogen cleaning unit…………………………………46

4.14 (a) shows the diffusive spotty pattern on RHEED screen before AH cleaning and, (b) after removal of oxide shows sharp pattern on the RHEED screen…………………………………47

4.15 AH cleaning: (a) AFM image of thermally cleaned GaAs surface, and (b) shows AFM image of GaAs surface after AH cleaning……………………………………………………47

4.16 AFM image of InAs QDs (a) on as grown GaAs surface and (b) on atomic hydrogen cleaned surface on GaAs (100) substrate……………………………………………………….. 48

4.17 PL spectra of InAs QDs at different surfaces where (a) belongs to the reference sample, (b) atomic hydrogen cleaned sample and (c) chemical cleaning + atomic hydrogen cleaned and 15 nm GaAs buffer layer. In all cases QDs are optically active. The FWHM for the ground state also shown for each sample……………………………………...…………………49

5.1 (left) shows AFM images of 1.6ML of InAs grown on GaAs (100) at 510°C substrate temperature where atomic steps are visible and (right) shows AFM images of 4ML of $In_{0.5}Ga_{0.5}As$ grown on GaAs (100) at 510°C substrate temperature. The colour scale for AFM images is 4 nm. ……………………………………………………………………………….54

5.2 RHEED patterns at different stage of the growth process: (a) after growth of a GaAs buffer layer at 600°C substrate - a (2×4) reconstructed surface, (b) after cooling down the substrate to 510°C – a c(4×4) reconstructed surface, (c) after deposition of 5 cycles of InAs (0.6 ML), and (d) after deposition of 16 cycles of InAs (1.73ML) – a spotty pattern due to 2D-3D growth transition. ………………………………………………………………………………….55

5.3 Schematic process of InAs QDs growth on GaAs (100) substrate. …………….……….56

5.4 (a) shows a 2D AFM view of surface QDs, the density of QDs is 4.0×10^9QDs/cm^2, (b) shows a 3D AFM view of the dots, and (c) TEM image of a single InAs QD and (d) shows the height distribution of these QDs, the average height of the dots is 6.1 nm. …………………57

5.5 Growth of InAs QDs on a GaAs(100) surface (left) Shows an AFM image of 9.8×9.8 µm^2 area with InAs QDs, QD clusters are present around the oval defects. (right) shows an AFM image of 2×2 µm^2 area of the same image. Due to high surface energy at the oval defects, QD cluster around them. ……………………………………………………………………….58

5.6 (a-e) AFM images (1×1 µm^2) of InAs QDs grown on GaAs(100) substrate with different In amount, (a) grown with 4 ML; QDs coalesced and large island forms, (b) grown with 1.84 ML(17 cycles); QD density is 4.2×10^{10}, (c) grown with 1.73 ML (16 cycles); QD density is 6.8×10^9, and (d) grown with 1.62 ML; QD density is 1.0×10^9, and (e) grown with 1.30 ML (12 cycles); no QDs growth, and (f) shows density of QDs as a function of InAs amount deposited……………………………………………………...………………………59

5.7 PL spectra of an InAs QD ensemble embedded in a GaAs matrix at 0.045mW laser power. The QDs show ground state emission at 1284.65 nm (0.965 eV) with FWHM of 31.7 meV at RT. At 8K, the ground state emission is at 1178.88 nm (1.053 eV) with FWHM of 30.3 meV..59

5.8 Photoluminescence spectra of a self-assembled InAs QD ensemble at room temperature for different excitation powers. High laser excitation power stimulates emission of the higher order confined states……………………………………………………………………..………62

5.9 Room temperature PL spectra of QD ensemble of two different samples grown at different As(Arsenic) to In (Indium) flux ratio…………………………………………..………….63

5.10 (left) A normalized room temperature PL spectra of InAs QD ensemble at different excitation power, (right) AFM image of surface QDs. The scanned area is 1×1 µm^2. The average height of such QDs is 5.5±.5 nm and diameter is 35±2 nm. The triangular shape of the dots is due to tip art effects……………………………………………………………64

5.11 (a) Monte Carlo simulations of the flux distribution on a stationary substrate from the In-cell. Each black circle indicates 10% change in the flux and the red circle in the centre shows the position of the substrate. (b) shows the flux distribution over the substrate. A schematic of ¼ 3” substrate is shown in the centre of the image……………………………………………66

5.12 (a) Schematic sketch of MBE growth chamber with In cell geometry for In-gradient approach to grow low density QDs, (b) schematic of InAs thickness profile with substrate rotation and without substrate rotation deposition……………………………………………67

5.13 (i) Schematic of a sample structure for low density approach and (ii) ¼ 3” wafer sketch with marked positions where AFM measurements are performed, (a) & (b) shows the AFM image of surface QDs at high density site ($6\text{-}4 \times 10^9$/cm^2), (c) shows AFM image at transition region where density is 5.5×10^8/cm^2, and (d) shows AFM image at low density region (2.5×10^7/cm^2)……………………………………………………………………………68

5.14 PL spectra of InAs QD ensemble embedded in a GaAs matrix on GaAs (100) substrate at room temperature. QDs are grown with gradient (rotation of substrate paused). Positions a, b, c, and d corresponds to Figure 5.13ii……………………………………………………….69

5.15 PL spectra of InAs QDs at room temperature grown with gradient approach. The PL spectra shows redshift along the gradient direction due to the presence of slightly high arsenic pressure. The inset shows a sketch of ¼ 3" wafer with marked positions where PL spectra are recorded...70

5.16 Schematic of In-flush technique (a) a self-assembled InAs QD, (b) partially capping of the QD by defined GaAs thickness, (c) reevaporation of uncapped part of QDs by heating the substrate to 600°C and (d) overgrowth after flushing………………………………..…………………………………72

5.17 Change in QD confinement potential induced by In-flush technique. Lateral and in-growth direction are depicted after [93]……………………………………………………………72

5.18 (left) An AFM image (2 × 2 μm^2) of 2.3 nm flushed QDs capped with 4 nm GaAs. Underneath the GaAs, flushed QDs are disk shaped with average diameter of 40 nm.(right) HRTEM images of as grown QD and 5 nm flushed QD………………………………………73

5.19 PL spectra of InAs QD ensemble grown with different capping layer thickness (d_{QD}) at room temperature. For each sample, the spectra is normalised for ground state emission. Spectra shows blue shift with decreasing d_{QD}……………………………………………...74

5.20 PL spectra of 2.5 nm flushed InAs QDs at room temperature grown with In-gradient approach. Inset show schematic of ¼ 3" wafer with marked positions along the gradient axis where PL measurement are performed……………………………………………………75

5.21 (a) Schematic sketch of MBE growth chamber with In cell and Ga cluster cell geometry for low density InGaAs QDs growth, (b) schematic of InGaAs thickness profile with substrate rotation and without substrate rotation deposition……………………………………………77

5.22 (a-c) AFM images of $In_xGa_{1-x}As$ QDs grown with gradient approach. (a) shows QDs at high density area, (b) shows QDs at low density area, (c) shows only WL at no QDs area, and (d) shows the height histogram of InGaAs QDs at high density region……………………...78

5.23 Room temperature PL spectra of InGaAs QDs along the In-gradient axis. The inset shows wafer sketch with positions marked along the In-gradient axis. The inset (top left) shows the wafer sketch with mark positions along the gradient direction where PL measurement is performed……………………………………………………………………………..……..79

6.1 Schematic of QDMs growth process (a) growth of bottom QD layer at 510°C with the In-gradient approach. In this step substrate rotation is paused and InAs QDs are grown with a density gradient along [011] direction, (b) In-flush process to define the height of QDs to tune emission energy, (c) interdot barrier growth at 610°C, and (d) top QD layer growth with homogeneous InAs deposition……………………………………………………………..83

6.2 Schematic of the sample structure of quantum dot molecules for optical investigations….84

6.3 Schematic of the sample structure, (ii) Sketch of ¼ 3" wafer with marked positions where AFM measurements have been performed, and (a-d) AFM images at various positions along the gradient axis. Images (a) and (b) represents the high density region, (c) is from the transition region and (d) represents the low density region…………………………………………...85

6.4 (i) QDMs sample structure and (ii) ¼ 3" wafer sketch. The Bottom QDs are 2.2 nm flushed and grown with gradient approach. The top QDs are grown with homogeneous InAs deposition. In wafer sketch, rectangular squares show the positions where AFM is performed…………..86

6.5 AFM images (a-f) along the In-gradient axis for top layer quantum dots grown with 15 cycles with substrate rotation. The positions of the recorded images are indicated in Fig. 6.4(ii)……………………………………………………………………………………87

6.6 AFM images of top QDs with different In amount. The images are taken from high density region in bottom QD layer………………………………………………………………89

6.7 Density and height of top QDs as a function of growth cycles at high density region. The density stays almost constant for 17 to 14 cycles. The height decreases with decreasing cycles……………………………………………………………………………………89

6.8 AFM images of top QDs with for different In amount. The images are taken from the low density region in bottom QD layer…………………………………………………………90

6.9 AFM images from the high density region along the In-gradient for the top QD layer for different interdot barrier thickness d_B. The interdot barrier d_B is (a) 6 nm (b) 12 nm (c) 18 nm. For 6 nm the arrows in Figure (b) indicate humps on the surface due to bottom QDs. The arrows in Fig. (c) shows 2d islands (~ 3 Å) which are a consequence of the strained growth…………91

6.10 Room temperature PL spectra of QDMs at various positions along the gradient. (main graph) The inset (top left) shows the wafer sketch with marked positions where PL measurement are performed and the inset (top right) shows the PL spectra at position (c) and (d)with higher resolution……………………………………………………………………..92

6.11 PL spectra of 2.2 nm flushed QDs and QDMs (B-QDs_2.2 nm / T-QDs 1.8 nm) for high density region at 77K. For both spectra the same excitation and detection parameters have been used (0.045mW power and 1 sec integration time). The intensity of QDMs is comparable to the QDs. The slight change in the intensity is probably due to the density variations between the samples…………………………………………………………………………………...93

6.12 Power dependent PL spectra of QDMs at high density region at 77K. The spectra is vertically displaced for clarity. Inset shows the band structure of a QDM along the growth direction (neglecting the band tilting due to built-in field). At low powers emission from bottom QDs is observed. As power increased emission form top QDs, wetting layers and from GaAs

is observed. Two peaks at WL position also indicate the presence of two WLs with different thickness…………………………………………………………………………………...94

7.1 Schematic diagram of the mechanism of site-controlled InAs QD formation on GaAs(100) substrate after [117]………………………………………………………………………..98

7.2 Schematic of the fabrication process for site-controlled InAs quantum dots on GaAs(100) substrate………………………………………………………………………………..100

7.3 AFM images (8.8×8.8 μm^2) of patterned nanoholes on GaAs (a) after chemical cleaning and (b) after growth of 25 nm GaAs buffer layer. Inset AFM images (500×500 nm^2) shows the shape evolution of the nanoholes after buffer layer growth, in more detail………………101

7.4 AFM images (5×5 μm^2) of positioned InAs QDs on GaAs (a) at 1.73 ML of InAs and (b) at 1.57 ML of InAs deposited at 510°C. In the inset of both images (500×500 nm^2) shows QDs in single nanohole……………………………………………………………...102

7.5 SEM image of site-controlled InAs/GaAs QDs on patterned nanoholes. Appropriate position control is achieved with 1.46 ML InAs deposition. The inset shows a histogram of dot occupancy per hole…………………………………………………………………103

7.6 AFM images of positioned InAs QDs grown on GaAs(100). The deposited InAs amount is 1.46 ML. (a) shows 500 nm pitch, (b) shows 1 μm pitch and (c) shows 2 μm pitch. Almost each of holes contain 2 QDs. The height of QDs is in the range of 3-4 nm and diameter is in the range of 25-30 nm. The dotted circle in (a) indicates the presence of defect during regrowth process...104

7.7 (a) An AFM images of 50 nm diameter nanohole arrays on PMMA defined by e-beam lithography technique. (b) Shows an AFM image of nanoholes after transferring the pattern by WCE process. Inset of the (b) shows the line scan over the nanohole………………………..105

7.8 AFM images of positioned InAs QDs with different pitch; (a) with 500 nm pitch, (b) with 1 μm pitch and (c) with 2 μm pitch. Most of the holes contain a single QD…………………105

7.9 SEM image of positioned InAs QDs grown at patterned nanoholes by MBE. The inset shows histogram of QDs occupancy per hole………………………………………………..106

7.10 PL spectra of positioned QDs with different pitch. For 1 μm pitch, around 10-15 QDs contributes to the emission…………………………………………………………...……108

7.11 Low temperature PL spectra of positioned InAs QDs. The higher arsenic pressure reduces the Ga-In intermixing and shifts the spectra to lower energy. Around 10-15 QDs contributes the PL emission……………………………………………………………………………...109

List of Tables

2.1 Lattice constants and band gap energies of GaAs, AlAs and InAs at room temperature [14]..................... 7

3.1 Different source cells with their description……………………………………………18

4.1 Temperature of group III cells and their fluxes..30

4.2 Process steps for nanohole patterning by electron beam lithography process……………..41

5.1 In flux and corresponding growth rate of InAs at different In cell temperatures. The growth rate of InAs is measured by RHEED oscillations while growing $In_xGa_{1-x}As$ layers at 510°C. Here T_B and T_P correspond to the temperature of the cell at the bottom and the top part of the cell………………………………………………………………………………………53

List of Abbreviations

Abbreviations	Expansions
AFM	Atomic Force Microscopy
AlAs	Aluminium Arsenide
AlGaAs	Aluminium Gallium Arsenide
EBL	Electron Beam Lithography
FWHM	Full-Width at the Half Maximum
HABS	Hydrogen Atom Beam Source
InAs	Indium Arsenide
InGaAs	Indium Gallium Arsenide
MBE	Molecular Beam Epitaxy
ML	Monolayer
NMP	n-methyl pyrrolidine
PBN	Pyrolytic Boron Nitride
PL	Photoluminescence
PMMA	Ploy Methyl Methacrylate
QD	Quantum Dot
QDM	Quantum Dot Molecule
RHEED	Reflection High Energy Electron Diffraction
RIE	Reactive Ion Etching
RTA	Rapid Thermal Annealing
SAQD	Self-Assembled Quantum Dot
SCQD	Site-Controlled Quantum Dot
SEM	Scanning Electron Microscopy
SK	Stranski-Krastanov
TCE	Trichloroethylene
TEM	Transmission Electron Microscopy
UHV	Ultra High Vacuum
WCE	Wet Chemical Etching
WL	Wetting Layer

This page has been intentionally left blank.

Chapter 1

Introduction

1.1 Motivation

The modern optoelectronic and electronic technology is based on semiconductor devices where the III-V semiconductors are playing key role like light-emitting diodes, lasers, transistors etc. There are different fabrication processes for them but molecular beam epitaxy (MBE) is one of the important one which provides precise control over composition and dimensionality with high purity possible. This process allows growth of abrupt semiconductor layers on each other with atomically sharp interfaces.

In this thesis we deal with semiconductor structures which provide confinement in all three dimensions and known as quantum dots (QDs). The self-assembly growth of QDs in a semiconductor system by epitaxial growth techniques provides excellent optical and electrical properties. The QDs formed in the region between semiconductor which provides higher potential energy than the QDs. This provides three-dimensional confinement for electrons and holes in the QD which results in the discrete energy levels similar to the atoms and therefore QDs are also known as "artificial atoms". Their optical and electrical properties can be manipulated during growth process for the desired applications. The QD ensemble can be used in the lasers as a broad-band gain medium with high output power and low threshold current [1]. In the photovoltaic, QDs are used to increase the efficiency of the photoconversion step [2]. The QDs also have great importance in the field of medical research as a source of drug carriers, monitoring, and localized treatments of specific disease sites. The cadmium and selenium based QDs are playing key role in the selective imagining of tumour cells [3, 4].

The strain induced fabrication of QDs has become a well-developed approach and widely used in III-V semiconductors and other material systems [5]. The self-assembled InAs QDs, which formed during epitaxial growth of InAs on GaAs. Due to the lattice mismatch between GaAs and InAs, after 1.7-2 ML deposition of InAs, the strain energy in the layer could not sustain and coherent 3D islands forms. These islands buried in GaAs are known as InAs QDs. The dimensions of the islands are in the order of the de Broglie wavelength (λ_B) and provide quantum confinement to the carriers. In the last years, the progress has been made to improve the size homogeneity, density control, emission energy control and spatial control of QDs for

application in the field of information technology. Modern research work focused on the single QD application in the field of quantum computing and single photon sources [6, 7]

Combining self-assembled growth with nanoengineering provides a variety of nanostructures as well as control over geometry and electronic spectrum [8]. An example is the growth of vertically stacked QDs separated by a thin interdot barrier. In vertical stacking, the QD of the top layer is located above the QD of the bottom layer forming a quantum dot molecule (QDM). The vertical alignment is induced by the strain from the buried QD layer [9, 10]. A thin interdot barrier provides the electronic coupling between the QDs and allows the engineering of the electronic states.

The aim of this thesis is fabrication of (In,Ga)As QDs on a newly installed MBE system for high optical and electrical quality. Initially, the growth of InAs, AlAs and GaAs layers on GaAs(100) substrate have been optimized for good optical and electrical quality of the heterostructures. To improve the quality of the growing surface, the effect of different substrate temperatures and III/V ratio are investigated.

The main work is dedicated to the fabrication of InAs/GaAs QDs on GaAs(100) substrate by Stranski-Krastonav growth mode. The fabrication of InAs/GaAs QDs is done by migration enhanced MBE where InAs deposition is done in cycled growth and with low growth rate (≈ 0.03ML/sec.). The effect of III/V flux ration, growth temperature and In-amount is studied by means of optical and structural characterization of QDs. The growth of low density InAs(InGaAs) QDs ($\approx 10^8/cm^2$) for single dot spectroscopy with the reproducible approach is realized by the In-gradient approach. The emission energy tuning of QDs has been done by an In-flushing approach where the height of QD is defined by the capping layer and by Ga-incorporation during InAs deposition.

The growth of self-assembled InAs QDs on patterned GaAs(100) substrate allows site-controlled growth otherwise on a planner GaAs surface it happens with random spatial distribution. The patterned surface enhances the migration of adatoms and provides a preferential nucleation site for InAs QD growth [11]. In this approach, the spatial control of self-assembled InAs QDs array growth is achieved by patterning and regrowth technology. The patterning of nanoholes is performed by electron beam lithography and wet chemical etching process. For successful regrowth process by MBE, intensive chemical cleaning and *in-situ* atomic hydrogen cleaning is carried out prior to the growth.

1.2 Thesis outline

This work concerns the growth, structural and optical characterization of InAs(InGaAs) QDs. The thesis is organised into the following structure:

- **Chapter 1** describes the status of the research work, challenges and the aim of the thesis work and thesis approach with complete overview.
- **Chapter 2**, the basic methods of QD fabrication are discussed. This thesis deals with SAQDs, which is described in detail in the next section.
- **Chapter 3** serve as an overview of the main growth and characterization techniques which are used during the thesis work.
- **Chapter 4** focus on substrate preparation which is essential for the epitaxial growth. Pre-patterning, chemical cleaning and atomic hydrogen cleaning for the patterned substrate is described in the last section of chapter 4.
- **Chapter 5** deals with the fabrication and characterization of InAs (InGaAs) QDs. The fabrication process of QDs is described in detail where different techniques are used to define the optical and structural properties.
- **Chapter 6**, a simplified gradient approach is demonstrated to grow low density quantum dot molecules (QDMs) which are vertically aligned and coupled.
- **Chapter 7** is dedicated to the regrowth technology by which site-controlled QDs are grown on the pre-patterned substrate.
- **Chapter 8** concludes the results of the present thesis work and gives an outlook for the future work.

This page has been intentionally left blank.

Chapter 2

2 Fundamentals

In this chapter, the fundamental properties of group III-arsenides are described briefly followed by an introduction to the low dimensional semiconductors. First, we describe different methods of quantum dot fabrication process and later we focus on self-assembled InAs quantum dots growth on GaAs(100) substrate. In the last section of the chapter, the growth and properties of self-assembled QDs are discussed.

2.1 Group III-arsenides

The III-V compound semiconductors are the most studied materials which are technologically important due to their band structure characteristic. They provide excellent optical and electrical properties and they allow tailoring possibility to their bandgap and lattice constant by changing their composition. The arsenide based III-V semiconductors generally have a zinc blende crystal structure and it may be viewed as consisting of two interpenetrating face-centre cubic (FCC) sub-lattices, each with lattice constant a. These sub-lattices are displaced from one another by (¼, ¼, ¼)a.

Figure 2.1 shows the bandgap energy versus lattice constant diagram for the most common III-V semiconductors (Tien 1988). The bandgap and lattice constants of the ternary compounds can be achieved by Vegard's law [12]. For $Al_xGa_{1-x}As$, the lattice constant can be expressed by

$$a^{AlGaAs}(x) = xa^{GaAs} + (1 - x)a^{AlAs}$$

where a^{GaAs} and a^{AlAs} are the lattice constants of GaAs and AlAs, respectively.

Also the bandgap of ternary compound semiconductor $Al_xGa_{1-x}As$ can be given by

$$E^{AlGaAs}(x) = xE^{GaAs} + (1 - x)E^{AlAs} - cx(1 - x)$$

where E^{GaAs} and E^{AlAs} are the bandgap of GaAs and AlAs respectively and c is the bowing parameter.

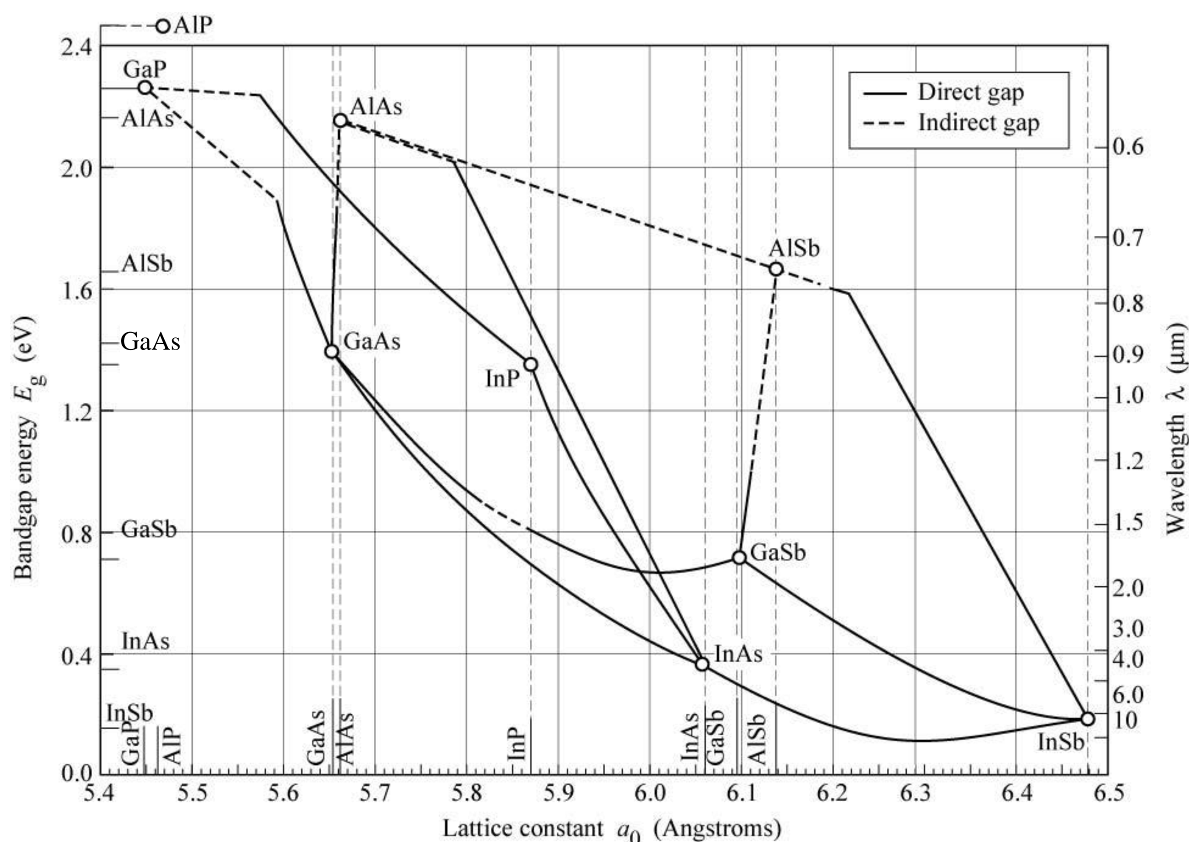

Figure 2.1: *Bandgap energy and lattice constant of various III-V semiconductors at room temperature (after Tien 1988).*

The band alignment at the interface of the two semiconductors in a heterostructure plays key role in the device fabrication. A proper band alignment can form a confinement potential which constrains the motion of charge carriers in the certain region. Figure 2.2 shows different type band alignment Three different alignments are possible [13] which are shown in Fig. 2.2:

- Type-I: The conduction band and the valence band of one semiconductor lie completely within the bandgap of the other semiconductor (Fig. 2.2a). In such band alignment, charge carriers can be spatially confined and restricted to move. Material systems of this kind are InAs/GaAs, GaAs/AlGaAs, which are grown during this thesis work.
- Type-II staggered: The bandgap of one semiconductor does not lie completely within the bandgap of the other semiconductor, but there is still some overlap (Fig. 2.2b). In such a heterostructure, charge carriers of one type can be confined, while the other type is not confined or even experiences a barrier. GaSb/GaAs is such material system.

- Type-II broken-gap: The conduction and the valence band of one semiconductor lie completely above or below the conduction and valence band of the other semiconductor (Fig. 2.2c), the bandgaps of the two semiconductors do not overlap. An example for type-III band alignment is the material combination InAs/GaSb.

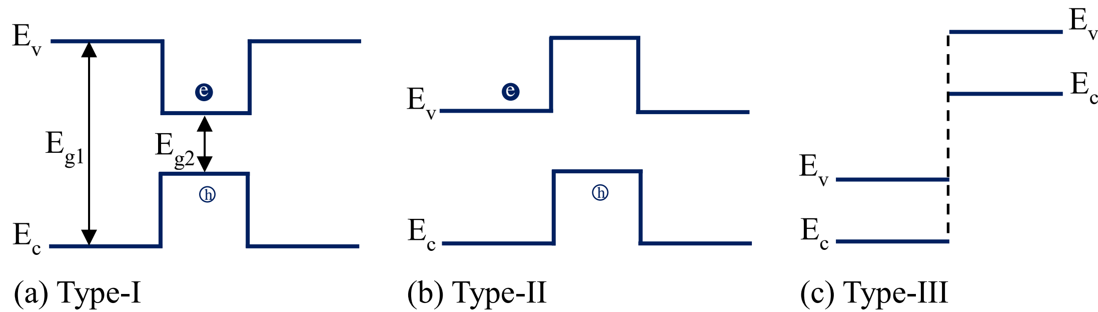

Figure 2.2: *Band alignment for various type of heterostructures: E_g is the bandgap of the semiconductor, E_c and E_v are conduction and valance band edge, respectively. (a) represents type-I heterostructure where both types of carriers are confined in the spatial region, (b) represents type-II (staggered), where one type of carriers are confined and (c) represents type-III heterostructures (broken gap), no overlap of the bandgaps.*

The samples in the thesis are made of alternating layers of GaAs, AlAs, AlGaAs and InAs grown by MBE. Important material parameters like lattice constants and bandgap energies of GaAs, AlAs and InAs is listed in Table 2.1.

Semiconductor	*Lattice constant*	*Bandgap energy*
GaAs	*5.65 Å*	*1.43 eV (direct)*
AlAs	*5.661 Å*	*2.35 eV (indirect)* *3.03 eV (direct)*
InAs	*6.058 Å*	*0.354 eV (direct)*

Table 2.1: *Lattice constants and band gap energies of GaAs, AlAs and InAs at room temperature* [14].

2.2 Semiconductor Nanostructures

In a bulk semiconductors material, the charge carriers behave like free carriers for all three directions because the three dimensions of the semiconductor is much larger that the wavelength of the charge carriers, i.e. de Broglie wavelengths. When the size of the semiconductor is reduced in one direction in the order of the de Broglie wavelength of the carriers, quantum confinement effects come into play [8]. Due to reduction in the size, the energy levels and density of states follow the quantum size effect and behave accordingly.

Here Figure 2.3 shows the change in the density of states for reducing the semiconductor dimensions. For a bulk semiconductor, the density of states D(E) for free electrons is proportional the square root of the energy $\sqrt{E}$ and for one dimension confinement (in quantum wells), the density of states is described by constant steps. The confinement of charge carriers in two dimensions (e.g. a quantum wire) results in a density of states proportional to $\left(\sqrt{E}\right)^{-1}$. A zero-dimensional system in which the carriers are confined in three dimensions is called QD and characterized by discrete delta peaks in the density of states. Due to their sharp density of states, QDs are also known as “artificial” atoms. The confinements of charge carriers is achieved by reducing the size

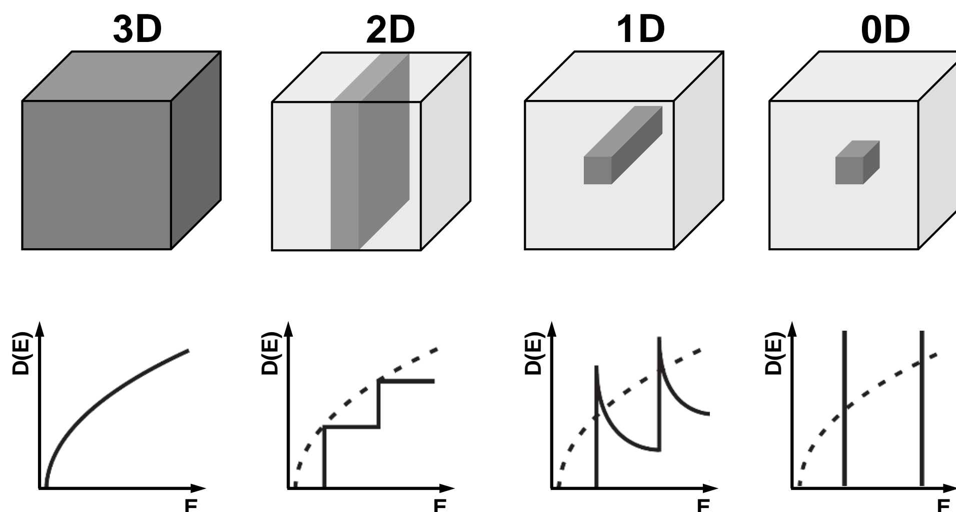

Figure 2.3: *Top: Schematic diagram of three, two, one and zero-dimensional heterostructures. Bottom: corresponding electronic density of states* [8].

2.3 Quantum Dots (QDs)

The term “quantum dot” (QD) is referred to a system which is crystalline and so small that the electronic energies resembles the atom like properties rather that the bulk crystal. The carrier confinement in the QDs is achieved by embedding them into higher bang gap materials. In this way the electronic and optical properties of QDs can be manipulated precisely for specific application, making them useful for different technologies. To fabricate such small nanostructures (1-100 nm), we need a great control over the technological point. Due to advanced fabrication techniques for materials, QDs are having a great interest in the research and industrial level for modern technology [15].

QDs made of semiconductor materials are attracting great attention towards the optoelectronic technologies. There are several methods to fabricate QDs. In the top-down approach, QDs are defined by patterning and etching process. The fabrication of QD by patterning of a quantum well structure has a great interest due to their combability with the large-scale integrated semiconductor technology. In this process the impurities and crystal defects incorporation increases during patterning and etching process, which may degrade the quality of the dots.

In second type approach, the QDs are formed by nanometer-scale semiconductor crystals capped with surfactant molecules and dispersed in the solution. They are known as colloidal QDs. These QDs have provided a powerful platform for the development of numerous classes of solution-processed optoelectronic devices over the past decade, including photovoltaic cells, photodetectors and light-emission devices [16]

The self-assembly growth of QDs by strained heteroepitaxy is currently the most widely used technique. Basically in this technique, the growth of 2-dimensional layers transforms to islands growth due to the strain accumulation in the layer which is known as Stranski-Krastanov growth mode. The size of QDs are in several nanometers in high and 30-45 nm in base diameter.

2.4 Self-Assembled Quantum Dots (SAQDs)

Self-assembling is a most promising approach for fabrication of QDs with good optical and electrical quality. In this process lattice-mismatched semiconductors are used to grow three dimensional islands. There are multiple examples of such system have been realized in the recent years such as InAs/GaAs, InAs/InP, InP/GaAs, Ge/Si, CdSe/ZnSe and GaN/AlGaN [8]. The epitaxial growth of InAs on a GaAs substrate is a most studied system, where the lattice mismatch between InAs and GaAs is about 7%.

In MBE growth process, initially InAs growth starts as layer by layer growth on GaAs. In the growing layer the strain is accumulating due to lattice mismatch. After a critical thickness, the InAs layer could not sustain the strain and 3-dimensional dislocation free coherent islands forms. Such growth process is known as Stranski-Krastanov (S-K) growth mode. These islands are known as self-assembled InAs quantum dots (SCQDs). The schematic diagram of the growth of SCQDs is shown in Figure 2.4. In this thesis, InAs and InGaAs QDs are grown by molecular beam epitaxy. During growth of InGaAs, the critical thickness of InGaAs layer is increased due to strain relaxation by Ga incorporation. At 50% Ga incorporation the critical thickness increased from 1.8 ML for pure InAs to 4.5 ML. The growth process in detail is discussed in Chapter 5.

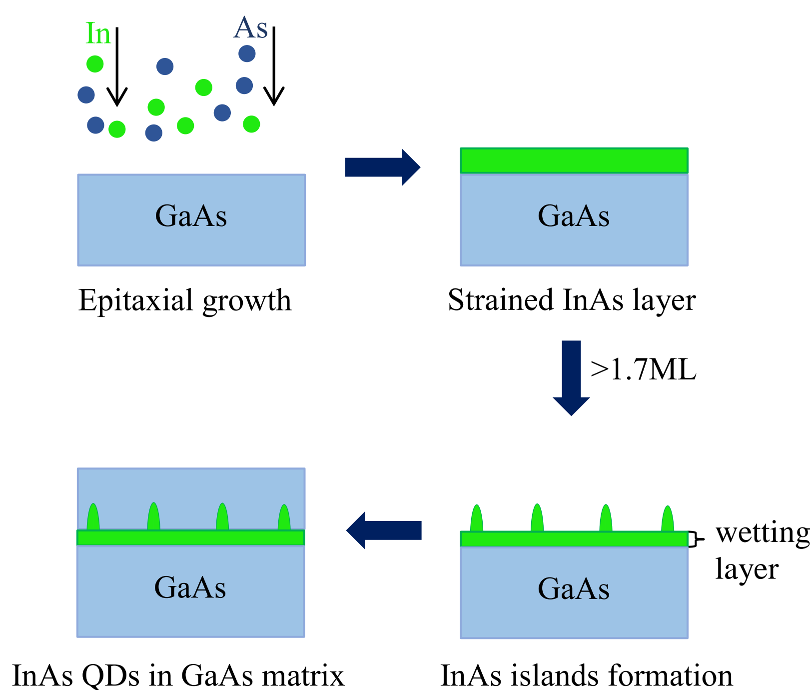

Figure 2.4: *Schematic diagram of formation of InAs quantum dot on GaAs*

After growth of the QDs, GaAs capping layer is grown to isolate them from surface states. The typical size of InAs/InGaAs islands are 20-30 nm in the lateral direction and 6-8 nm in the vertical direction. Since the typical exciton Bohr radius for InAs and GaAs system is in the range of 10-20 nm, the island size is small enough to exhibit the three-dimensional quantum confinement effects.

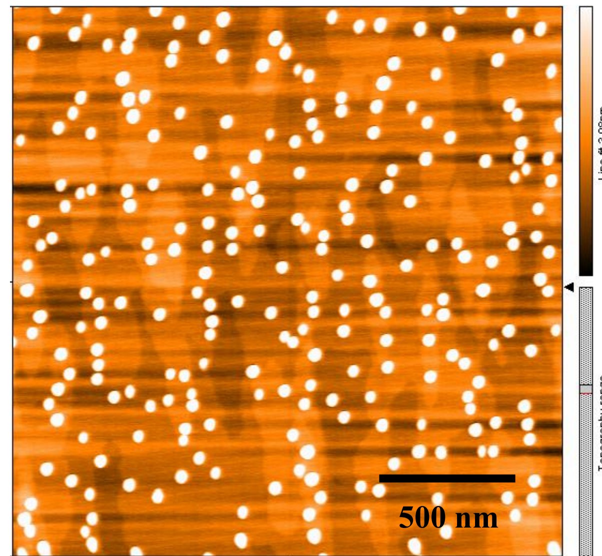

Figure 2.5: *Atomic force microscopy image (2 × 2 μm^2)of InAs quantum dots showing their random spatial distribution.The average height and base diameter of QDs is 6.1 nm and 35 nm, respectively.*

The InAs QDs shows random spatial distribution and additionally they also show randomness in shape and size. Figure 2.5 shows typical AFM image of InAs QDs grown by MBE self-assembly process, where the density of QDs is in the order of 10^{10} QDs/cm^2. Such high density QD samples are not suitable for single dot based experiments where the required density is around 10^8 QDs/cm^2 or below. The growth of low density QDs can be realized by In(Indium)-gradient approach [17, 18] or by annealing approach [19, 20, 21]. In this thesis work, In-gradient approach is utilized for the growth of low density QD, which is described in Chapter 5.

The GaAs has a bandgap of 1.43 eV and the InAs has 0.35 eV. Due to this band gap difference between GaAs and InAs, these QDs form a three-dimensional potential well, which confines the electrons and holes (type-I heterostructures). Such confinement causes the energy levels of QDs to be discrete. A schematic representation of the energy levels in the QD is

shown in Figure 2.6. The InAs QDs exhibit the emission in the entire near infrared spectrum. In the Quantum information technology, the desired emission wavelength QDs is around 1000 nm or below to use high performance of Si-based detection technology. The emission energy tuning of QDs can be done by various techniques such In-flush technique, Ga incorporation during InAs growth (or growth of $In_xGa_{1-x}As$ QDs) [22], and by ex-situ annealing technique. The In-flush technique and growth of QDs is described in Chapter 5.

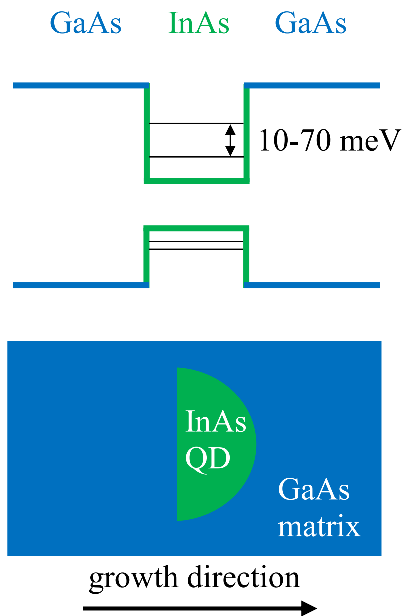

Figure 2.6: *(top) Schematic representation of the band edge diagram of the InAs/GaAs quantum dot system, (bottom) shows a schematic sketch of InAs QD embedded in GaAs matrix.*

Chapter 3

3 Experimental Techniques

This chapter is dedicated to a brief description of the growth and characterization techniques which are used during this work. First, concisely discuss the molecular beam epitaxy (MBE) system and the in-situ characterization method RHEED (reflection high energy electron diffraction). Later, ex-situ characterization techniques are discussed. For structural analysis of GaAs surface, quantum dots and patterned substrate, atomic force microscopy, and scanning electron microscopy are used. For optical characterization of the quantum dots, photoluminescence spectroscopy is used. In the last section, e-beam lithography system is briefly described, which is used for patterning of nanoholes on GaAs (100) substrates for positioning of quantum dots.

3.1 Molecular Beam Epitaxy

MBE is an advanced crystal growth technique, developed in the 1970s and has played a remarkable role in the research field of semiconductor devices [23, 24]. The key point of this technique is that all the growth process is done in an ultra high vacuum (UHV) chamber. The base pressure of the chamber is in order of 10^{-9} to 10^{-11} mbar, which gives a long mean free path for the molecules or atoms of source materials to travel from source to the heated substrate without interacting with each other in the path. Because of a slow growth process (1 μm/hour), it provides great control over dimensionality, composition and impurity incorporation. The major advantages of the MBE growth are [23, 25]:

i. MBE provides precise control of layer thickness, composition and dopant incorporation down to atomic scale.
ii. UHV environment in the growth chamber allows in-situ measurement techniques to study the growth process.
iii. Compared to other growth techniques, no complicated chemical reactions take places on the substrate surface.
iv. Toxic chemicals are contained within the vacuum chamber.

The MBE growth is governed by kinetic processes on the substrate surface unlike the conventional growth techniques (i.e. Liquid Phase Epitaxy) where the growth takes place under

near thermodynamic equilibrium conditions. In atomistic model (see Figure 3.1) the impinging atomic beam reaches the surface of the substrate where several surface processes occur. In addition to surface diffusion, the atoms can be incorporated into the lattice, initiate surface agglomerations, desorb from the surface or interdiffusion can play a role during the epitaxial film growth [23].

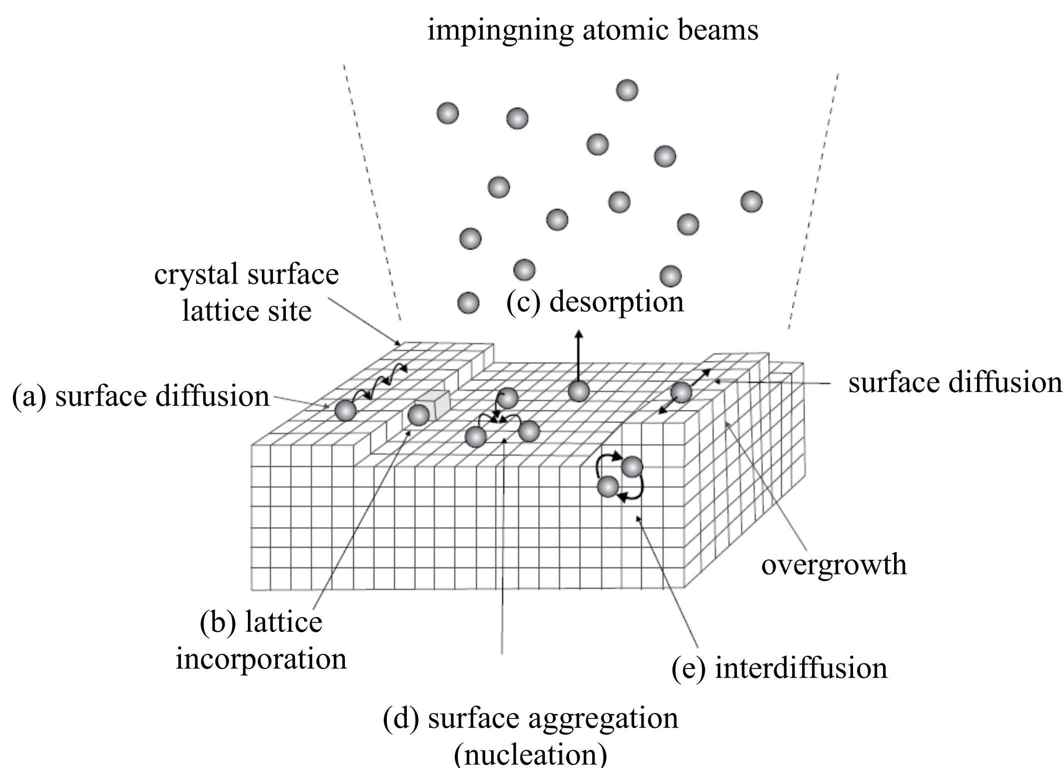

Figure 3.1: *Schematic illustration of surface processes occurring during film growth by MBE: (a) surface diffusion, (b) lattice incorporation, (c) desorption, (d) surface aggregation, and (e) interdiffusion, after* [23].

The growth stoichiometry of arsenide based III-V semiconductors is self-regulated over a large range of the substrate temperature (500°C-650°C) as long as excess group V elements is present on the surface. Normally, arsenide based III-V compound semiconductors are grown with two to ten times excess supply of the arsenic. This condition is called As-stabilized growth mode. The sticking coefficient of As is zero in the absence of the group III elements, so the arsenic contributes to growth when group III element is present on the surface. In contrast to the preceding so-called As-stabilized growth, there is Ga-stabilized growth which occurs when the flux ratio is approximately 1. An excess of Ga atoms is generally avoided, however, because they tend to cluster into molten droplets [26].

3.1.1 Molecular Beam Epitaxy System

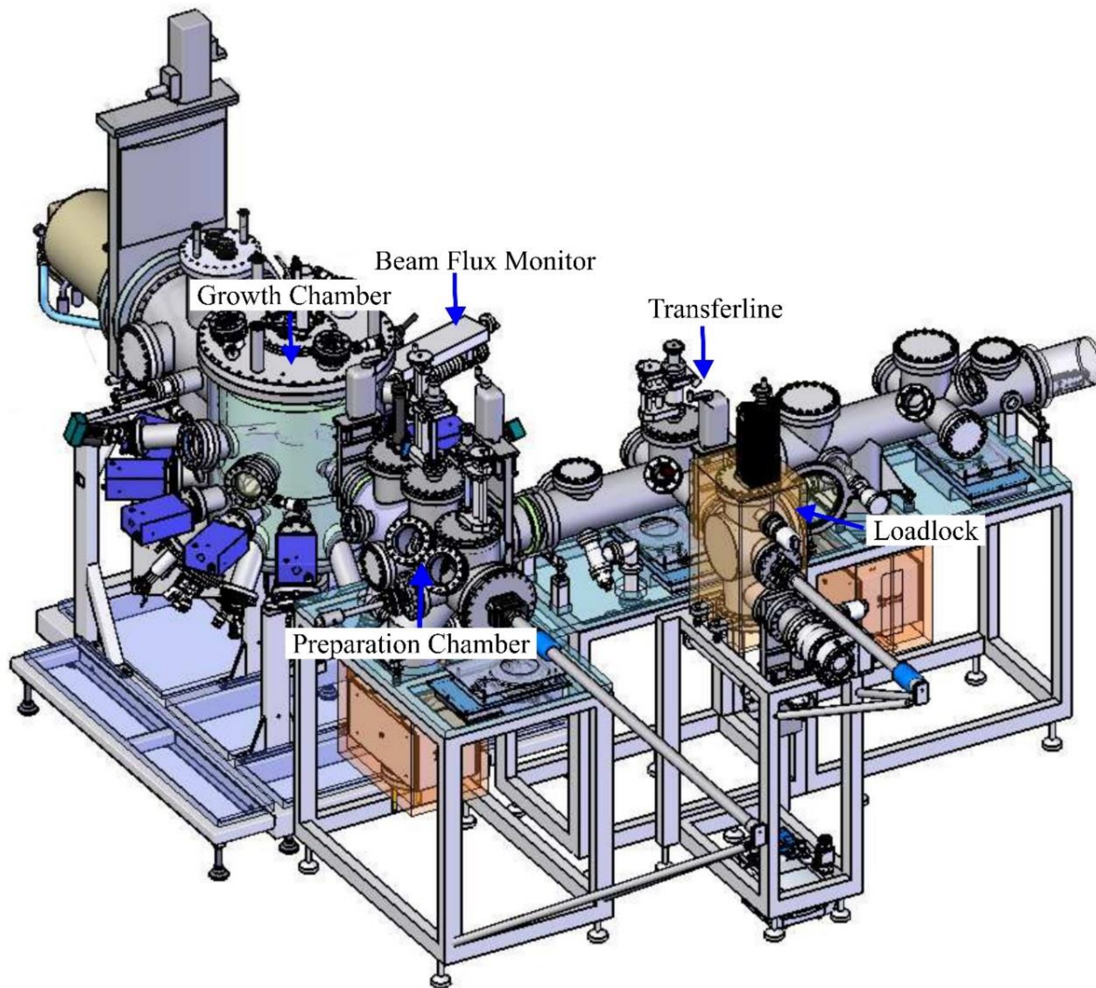

Figure 3.2: *Schematic of the III/V molecular beam epitaxy system (MBE Komponenten).*

In this work, an III/V semiconductor epitaxy system from MBE Komponenten is operated. The system is newly installed in our group. Figure 3.2 shows a schematic of the MBE system. This system is composed of four main chambers, (a) Growth chamber, (b) Preparation chamber, (c) Transfer chamber and (d) Loadlock. Except for loadlock, all three chambers have a base pressure of $< 10^{-10}$ mbar. The growth chamber is pumped with 3000 liters/sec closed-cycle helium cryopump, liquid nitrogen-cooled titanium sublimation pump, ion pump (600 liters/sec) and liquid nitrogen filled cryo shrouds surrounding the sample and source cells within the vacuum space. The film growth is monitored using RHEED. The substrate manipulator is attached to external water cooling to reduce thermal load. Additionally, cryogenic screening by a liquid nitrogen shroud around the substrate manipulator minimizes

the contamination from the wall of the chamber. Figure 3.3 shows a schematic of the growth chamber of the MBE system.

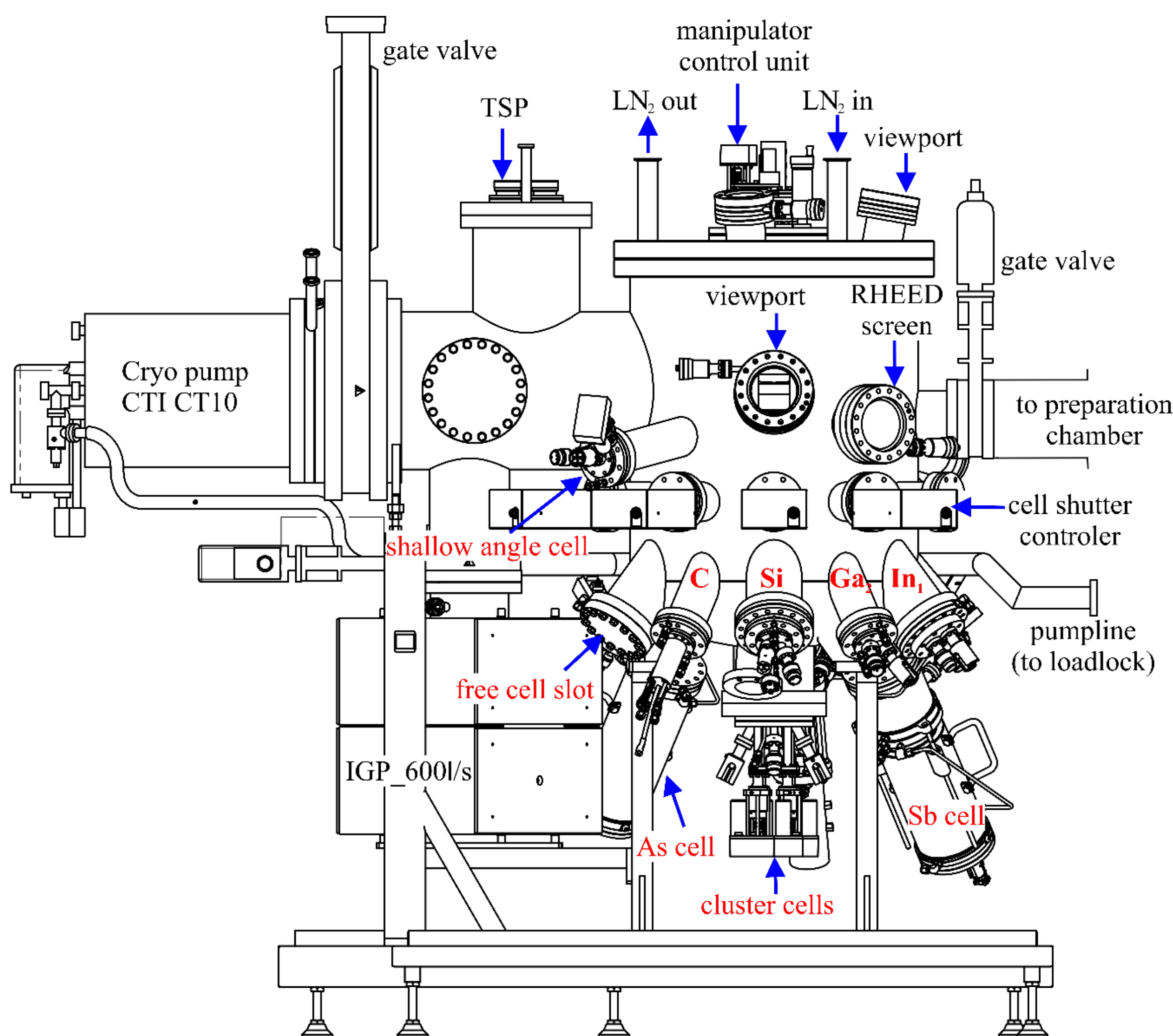

Figure 3.3: *Schematic sketch of the MBE growth chamber (MBE Komponenten).*

The preparation chamber is equipped with an atomic hydrogen cleaning unit and a heating station (substrate heater) which are used for substrate cleaning at low temperatures. The heating station is also used to degas substrates before loading into the main chamber. This chamber has a substrate magazine holder for storage of 8 samples. Additionally, this chamber is equipped with a preparation stage where mask can be attached and removed to a wafer in UHV. The chamber is pumped with an ion pump (300 liters/sec) and a liquid nitrogen cooled titanium sublimation pump. The transfer chamber is a long transfer line which is used to transfer the sample from loadlock to preparation chamber. The transfer chamber is also pumped with an ion pump (300 liters/sec), and a titanium sublimation pump. A pumping line provides valved

connections to each of the chambers and additionally to the cryopump. The pumping line can be pumped with the turbopump from the loadlock chamber. It also can be purged with i.e. nitrogen or argon from gas cylinders. The pumping line allows performing maintenance tasks such as regenerating the cryopump or venting/pumping down an individual chamber without affecting any separated part of the equipment. The load lock chamber is used to load the sample into and out of the vacuum environment without breaking the vacuum integrity of other chambers. This chamber has a substrate magazine holder for loading up to 6 samples. This chamber is pumped with a turbo pump which provides a base pressure of $< 2\times10^{-8}$ mbar. Each time after loading wafers, the chamber is pumped and degassed for 8 hours at 120°C before transferring the wafer to the transfer chamber. This minimizes carrying contaminations to the transfer chamber. After that, the sample is degassed at the heating station at 200°C in the preparation chamber. The steps for growing a sample in our MBE system are:

- loading wafers to loadlock chamber (3” or ¼ 3” wafer)
- degassing in loadlock for 8 hours at 120°C ($<1\times10^{-7}$ mbar)
- transferring wafer to preparation chamber via transfer chamber
- again degassing at 200°C at heating station in preparation chamber
- atomic hydrogen cleaning is performed in the case of patterned substrate
- transferring wafer to growth chamber
- substrate prepared and sample grown
- transfer grown sample to loadlock chamber and take it out from the system

The substrate preparation and buffer layer growth processes are discussed in next chapter.

Materials sources in the MBE system are loaded in the effusion cells which are made from non-reactive refractory material crucibles usually pyrolytic boron nitride (PBN). For group III materials, the main chamber is equipped with Aluminium (Al), Gallium(Ga) and Indium (In) source cells and for group V materials, the main chamber is equipped with Arsenic (As) and Antimony (Sb) source cells. For doping materials, Silicon (Si) is used as an n-type dopant and carbon (C) is used as a p-type dopant. Some cells are shown in the schematic sketch of the growth chamber in Figure 3.3. However, group V materials (AS, Sb) are loaded into cracker cells (valve controlled cells), in order to achieve III/V ratio for different layers without interrupting the growth process. In these cells, the materials stay in evaporating state and the flux is controlled through compatible valves. All cells have individual fast acting (<0.2 sec) mechanical shutters to block the molecular beams. All the cells are connected to external water

cooling lines to reduces the thermal load from the chamber. A total of 15 cells is attached to the growth chamber. In Table 3.1 all cells are listed and described briefly.

Cell No.	Source material	Capacity	Additional information
1	As source VACS (valved arsenic cracker source)	500 cm^3	source of As_4 and As_2 as group V material
2	Ga(I)	130 cm^3	standard Ga source
3	Al(I)	80 cm^3	standard Ga source
4	Sb source VCCS (valved corrosive cracker source)	420 cm^3	source of an antimony radical (Sb_x) molecular beam as group V material
5	Al(II)	80 cm^3	standard Al source
6	In(I)	130 cm^3	standard In source
7	Ga(II)	60 cm^3	standard Ga source
8	Si (doping)	2 filament	for n-type doping
9	C (doping)	filament	for p-type doping
10	In (shallow angle)	60 cm^3	10° angled cell for growth with high gradient in flux
11	Ga (shallow angle)	60 cm^3	10° angled cell for growth with high gradient in flux
12	Al cluster	10 cm^3	cluster cell unit, mounted to perpendicular to substrate manipulator, for growth through a mask
13	Si cluster	2 cm^3	
14	Ga cluster	10 cm^3	
15	In cluster	10 cm^3	

Table 3.1: *Different source cells with their description*

3.2 Reflection High Energy Electron Diffraction

Reflection high energy electron diffraction (RHEED) is perhaps the most useful surface analytical tool in the MBE growth technique for in-situ studies of surface crystallography and kinetics. RHEED is regularly used in the MBE system to monitor and control the growth process.

In RHEED, a collimated monoenergetic electron beam from the electron gun is directed towards the substrate surface at a grazing angle of 1° - 2°, as shown in Figure 3.4. The electron energy lies in the range of 5-40 kV, in this work 10 kV. The penetration depth of the electron on the surface is limited to few monolayers due to grazing angle incidence. Therefore, a smooth crystal surface acts as a two-dimensional grating which diffracts the incident electron beam. A fluorescent screen is mounted opposite the electron gun and records the diffraction pattern. In this configuration, the growing surface can be continuously monitored [25, 27].

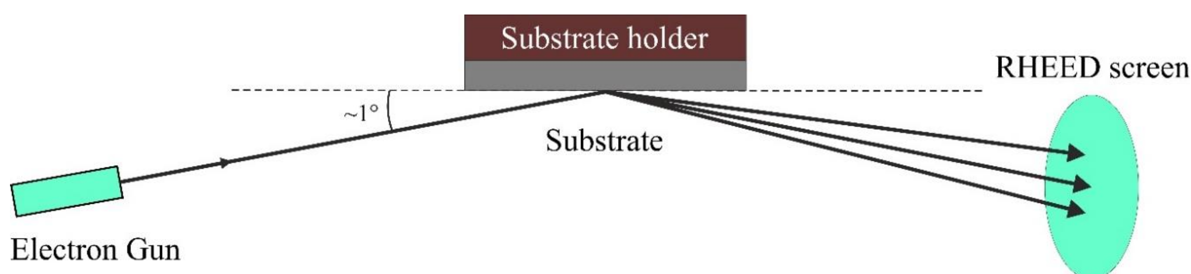

Figure 3.4 *Schematic diagram of RHEED arrangement*

3.2.1 Surface Morphology and Reconstruction

The diffracted beam seen on the RHEED screen shows patterns, which are characteristic of the surface morphology. In the case of an atomically smooth surface, the incident electron beam interacts with few MLs on the surface and diffraction occurs from a two-dimensional net of atoms from the surface whose reciprocal lattice consists parallel rods. Due to the high energy of electron beam, the Ewald sphere is so large that it interacts with several rods and excites Bragg reflections. Such a diffraction pattern consists of a set of streaks indicating smooth surface as shown in Figure 3.5(b). In case of a rough surface, electron beam penetrates the surface and gives diffraction from three-dimensional lattice. Therefore, RHEED pattern from a rough surface is spotty as shown in Figure 3.5(a).

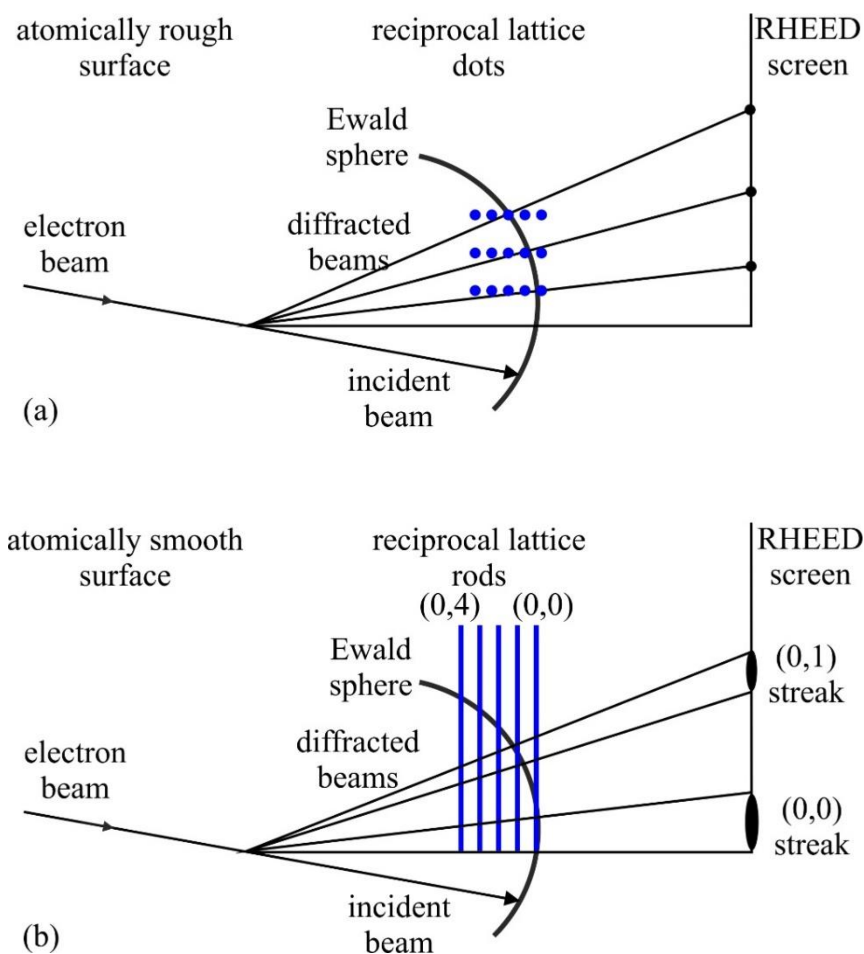

Figure 3.5: *Schematic representation of RHEED pattern: (a) from rough surface and (b). from atomically smooth surface. The intersection of Ewald sphere and reciprocal lattice defines the diffracted streaks and spots on RHEED screen* [24].

There are a lot of surface phenomena occurring during epitaxial growth like diffusion, surface reconstruction etc. Surface reconstruction is re-arrangement of atoms of the outermost atomic layers at the surface of the growing crystal resulting in a surface structure different from the bulk periodicity in a plane parallel to the surface plane. This occurred to minimize the surface energy. In Case of GaAs (100) growth, in this work, we use As-rich growth mode with appropriate substrate growth temperature where the (2×4) reconstruction is observed on RHEED screen. The diffraction pattern in Figure 3.6 shows streaks with spacing proportional to the inverse of the bulk atomic distances. The pattern for (011) and (01$\overline{1}$) exhibits ½ and ¼ order streaks respectively indicating that the presence of reconstructed surface structures with spacing two and four times as large as those of the bulk [28]. The GaAs(100)-c(4×4) surface reconstruction is also observed during cooling down a (2×4) reconstructed surface in an arsenic flux.

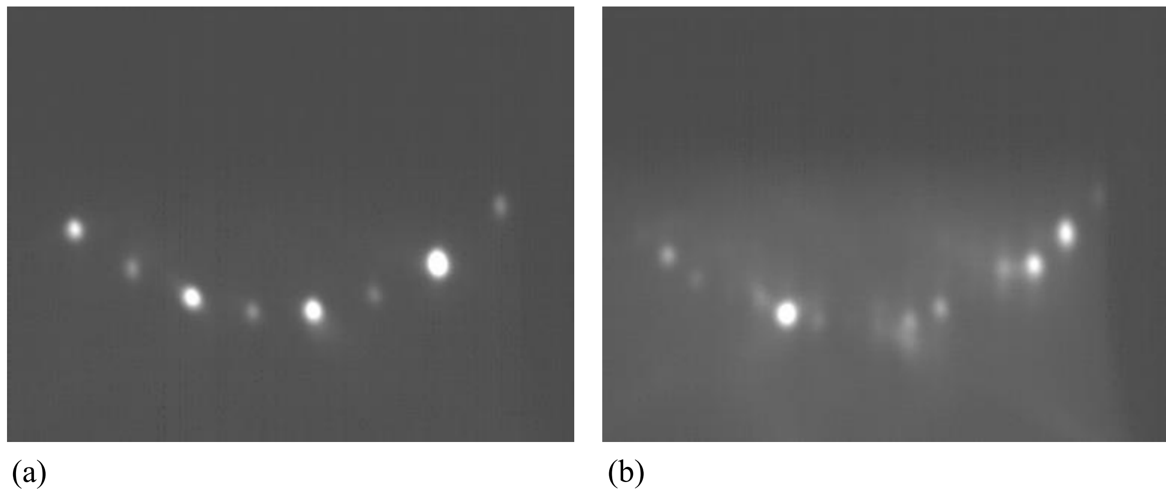

(a) (b)

Figure 3.6: *RHEED patterns observed along the* (011) *(a) and* $(01\bar{1})$ *(b) azimuths during the molecular beam epitaxy (MBE) growth of an epitaxial GaAs layer deposited on a GaAs(100) substrate; the surface reconstruction is the As-stabilized (2×4) one.*

3.2.2 RHEED Oscillations

RHEED oscillations correspond to the intensity oscillation of diffracted beam during layer by layer growth. In this growth, one layer is essentially completed before the following layer and this produces periodic oscillation of the surface morphology. Such periodic oscillations in surface morphology are the reason of the RHEED oscillation. The period of oscillation corresponds to the growth of one ML of GaAs layer, for GaAs (100) 1ML is 2.83Å. RHEED intensity oscillations during growth of GaAs are shown in Figure 3.7, where the growth rate for GaAs is 0.7ML/sec. This oscillation process is routinely used in MBE growth to calibrate beam fluxes, control alloy composition, the thickness of quantum wells and superlattice layers [23]. When the growth is terminated via closing Ga shutter, the intensity of the beam recovers. This is due to the recovery of the flatness of the surface. The RHEED intensity is measured via a CCD camera from iCube and the intensity profile is recorded by RHEED Vision software form STAIB instruments.

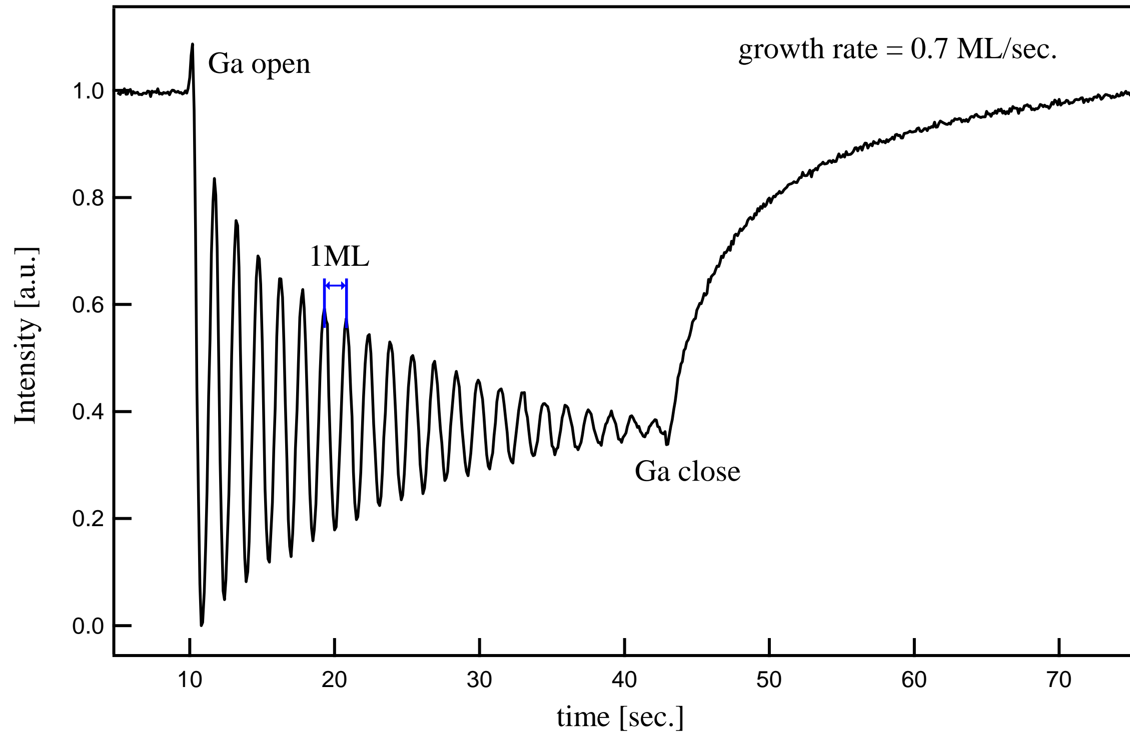

Figure. 3.7: *RHEED intensity oscillations during growth of GaAs on GaAs (100) substrate. The growth rate of GaAs is 0.7ML/sec.*

3.3 Atomic Force Microscopy

The atomic force microscopy (AFM) is a scanning probe microscopy technique to obtain information of the surface morphology, e.g. surface roughness on an atomic scale. Detailed information can be found in Ref. [29]
The operation principle of this method is shown in Figure 3.8(a). A nanometric sharp tip is mounted at the end of a flexible cantilever arm and scanned across the sample surface. When the tip approaches the sample surface, forces on the atomic scale interact between the tip and the surface due to the van-der-Waals attraction. A laser beam is reflected from the reverse side of the cantilever onto a position-sensitive 4 quadrant photodetector. Any deflection of the cantilever arm produces a change in the position of the reflected laser spot. The deflection changes can be monitored and used to collect relative height information of the surface topography.

In AFM imaging mode, the cantilever is usually scanned over the surface to get a three-dimensional image. There are different operating modes in AFM, like the tapping mode and the non-contact mode, but in this thesis, only the contact mode is used. Here, the probe remains in contact with the sample in a constant force mode during the measurement. A feedback mechanism keeps the deflection of the cantilever (hence the force) constant. As the cantilever arm is bent the z-height is altered to cause a return to the original starting point. A change in topography induces a bending of the cantilever, which can be used to create a topographical image. Such images can then be analyzed with regard to the root mean square (*rms*) roughness (S_q) of the surface, which is defined as

$$S_q = \sqrt{\frac{1}{n} \sum_{i=1}^{n} (z_i - \overline{z})^2}$$

where n is the total number of measurement points, z_i the height at every i measurement point and $\bar{z}$ the median value of the height [30]. Figure 3.8(b) shows an AFM image of single InAs QD at low density area. The surface is atomically smooth with roughness (S_q) of 0.42 nm.

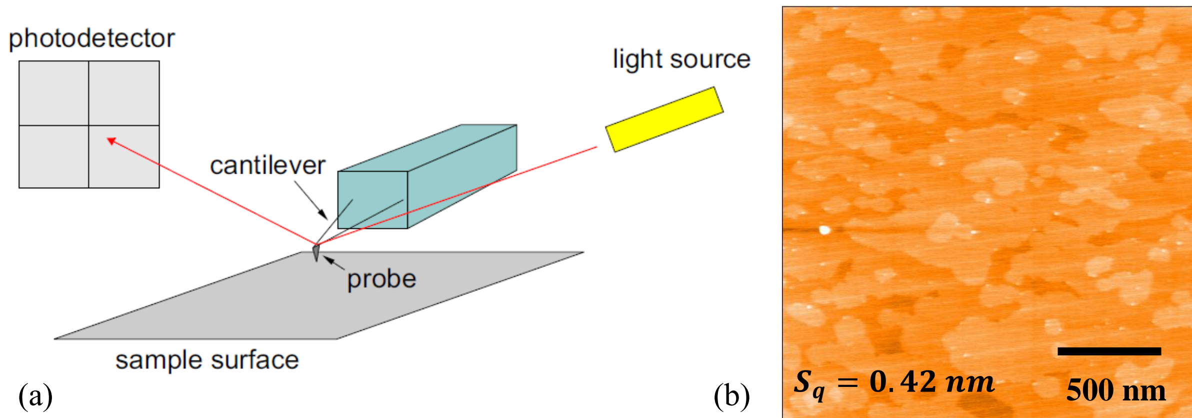

Figure 3.8: *(a) Schematic sketch of an AFM setup* [30], *(b) AFM image of single InAs quantum dots on GaAs(100) at low density area. The surface is atomically smooth and rms value of the roughness is 0.42 nm.*

The AFM technique is often used for ex-situ characterization of GaAs surface and InAs quantum dots. The analysis of quantum dot density, diameter and height distribution can also be achieved after sample deoxidation [31, 32]. In this thesis, all measurements have been performed with an AFM (type MobileS) from Nanosurf and tips from Nanosensors. The tip is used with force of 18 nano Newton and a nominal radius of curvature < 10 nm. AFM apparatus was placed on a damped table during the scanning to reduce the noise originating from vibrations in the environment. The maximum scan size is 10 µm × 10 µm.

3.4 Photoluminescence Spectroscopy

Photoluminescence (PL) spectroscopy is a simple and non-destructive optical technique which commonly used to characterize semiconductor materials. This technique provides information for both intrinsic and extrinsic semiconductors. In the case of extrinsic semiconductors, this technique provides the information about shallow donor and acceptor and some deep traps which affect the material quality and device performance [33].

In photoluminescence process charge carriers in the materials are excited by the incident light which has energy above the band gap of the material i.e. $E_{exe} > E_g$. The carriers (electron and holes) are relaxed via phonons to the corresponding band edges. The study of the energy of the photons emitted through radiative transition is the base of the photoluminescence. The basic idea behind PL process is sketched in Figure 3.9. Normally PL Spectroscopy is useful in quantifying: (1) optical emission energies, (2) composition of materials, (3) impurity content and (4) layer thickness, etc [34].

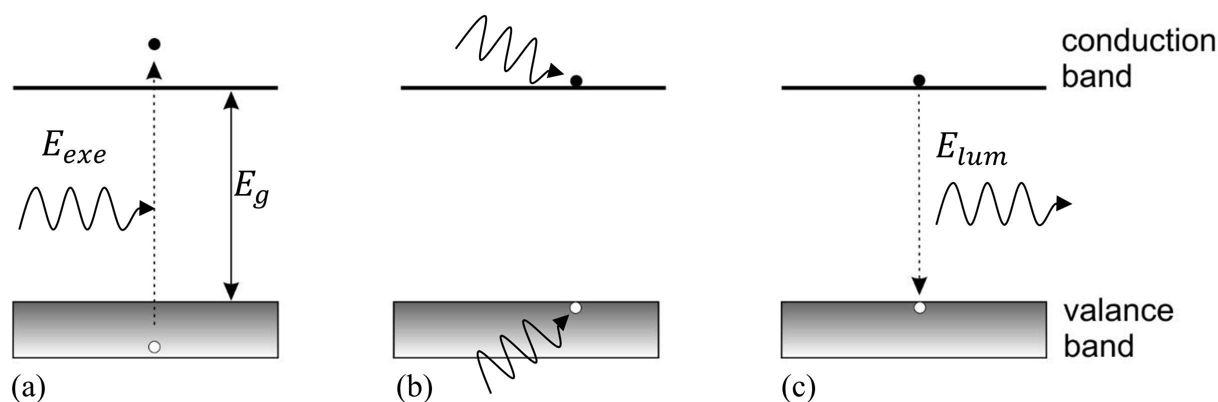

Figure 3.9: *Illustration of photoluminescence process (a) a photon excites an electron-hole pair in the material (b) the carriers thermalization and diffuse (c) a photon is emitted from recombination of electron-hole pair.*

Excitation of a non-equilibrium populations of electrons and holes is commonly achieved by using a semiconductor diode laser. The advantage of using a semiconductor laser is that its wavelength is well defined and the intensity can be controlled in a wide range. The PL is then collected from the same surface as the surface excited by the laser. The light is detected by a detector after being spectrally dispersed by a spectrometer.

In this work, the PL experiment is performed on ensemble on InAs QDs grown by Stranski-Krastanov (S-K) method. The ensemble consists of individual quantum dots with slightly different shape, size and composition such that the energy spectrum varies from dot to dot. This leads to inhomogeneous broadening ensemble properties. conventional PL experiment on quantum dots, the excitation photons are absorbed by the barrier material and electron-hole pairs are created. These photoinduced carriers relax to quantum dots and afterwards recombines radiatively and show luminescence. The schematic process of PL in InAs QD is shown in Figure 3.10a, where dots are buried in the GaAs matrix. These dots are grown by Stranski-Krastanov method. The lowest energy peak (E_0) corresponds to the ground state emission from the QD. The following, higher energy peaks form the excited states of the conduction band and the valance bands in the QD. With increasing excitation power, additional excited quantum dot states contribute to the luminescence. At very high excitation powers, luminance from InAs wetting layer at 1.34 eV (920 nm) and from bulk GaAs at 1.42 eV (870 nm) is also observed. A typical PL spectra of InAs QD ensemble is shown in Figure 3.10b

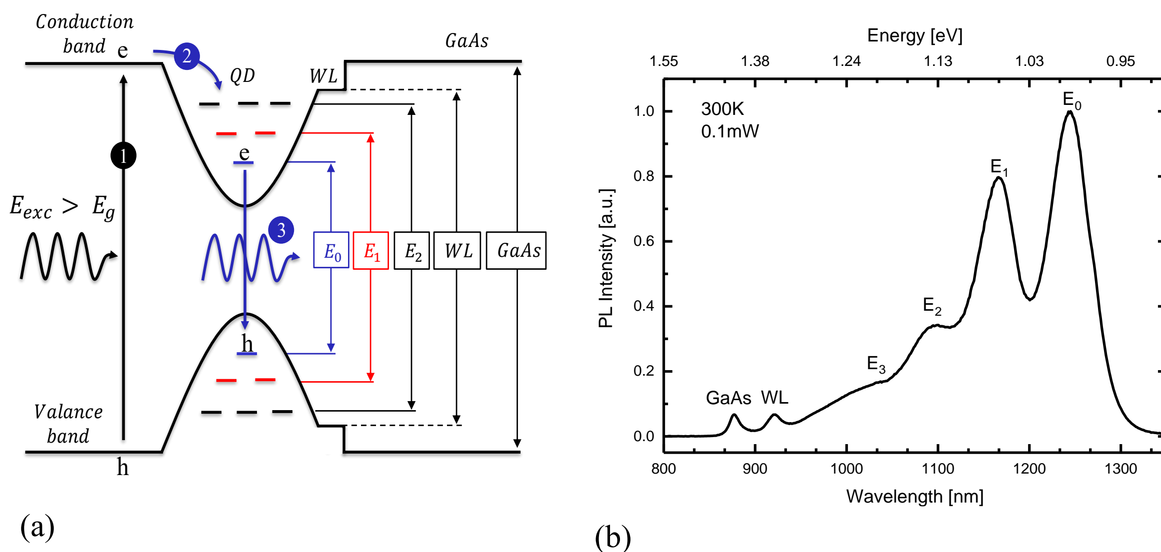

Figure 3.10: *(a) Schematic representation of PL process in InAs QD: (1) creation of electron-hole pairs in bulk GaAs by laser excitation; (2) capture in QD by phonon emission; (3) recombination and emission of photons from different states. (b) shows a room temperature PL spectrum of QD ensemble.*

PL Setup

The measurement setup used in the framework of this thesis is shown in the Figure 3.11. It consists of an excitation laser diode, cryostat, some focusing optics and a spectrometer. The laser operating at 635 nm (1.95 eV) above the bandgap of GaAs to excite the charge carriers in our samples with a maximum power of 4.5 mW. Natural density filter wheel is used to reduce the power density of laser. The sample is mounted in the cryostat which can be cooled by liquid nitrogen and liquid helium. The cryostat allowed temperature-dependent measurements in the range from T=8K….300K. The laser beam is focused on the sample by a microscope objective to a spot of about 3-4 µm. The same microscope objective is utilized to collect PL signals in backscattering mode. The collected PL signal is dispersed using a spectrometer equipped with a grating of 600 lines/mm and detected by InGaAs detector cooled to 65K.

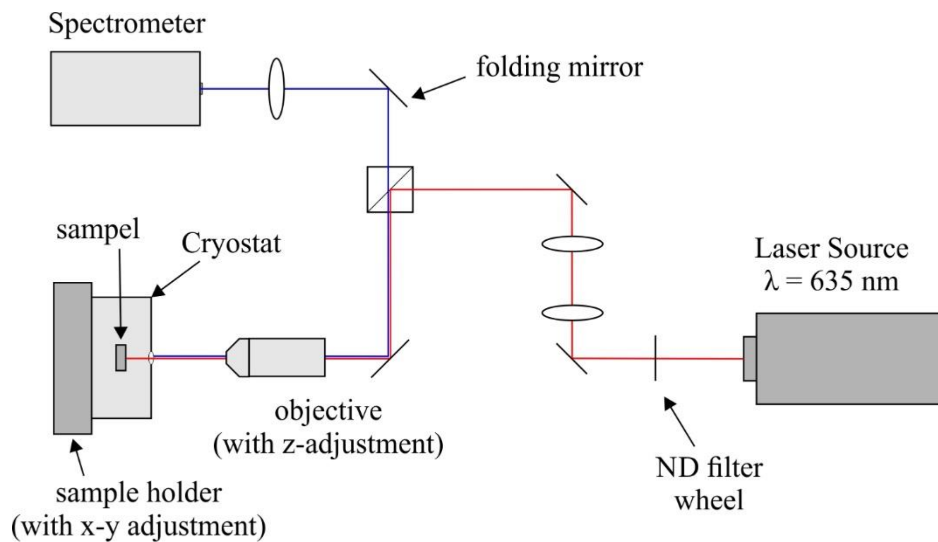

Figure 3.11: *Schematic sketch of the photoluminescence setup.*

3.5 Electron Beam Lithography

Electron beam lithography (EBL) is a high-resolution patterning method, in which a focused beam of electrons is used to cure the resist. The pattern is patterned on a dedicated resist according to the distribution of the incident electrons and transferred to the sample by etching. The high-resolution of this method is due to the small wavelength of the 10-50 keV electrons [35]. Factors which limits the resolution are scattering of the electrons in the resist and in the sample, and charge accumulation and various aberrations of electron optics [35]. The electron beam is controlled digitally, and computer-aided design makes this technique very flexible. However, systems comprising of several electron beams have been developed in order to increase the throughput of EBL [36].
In this work, the Raith Pioneer (Raith150_2 Series) system is used, it is an electron beam lithography system integrated with a scanning electron microscope (SEM). This allows users to analyse the structural properties of their nanostructures. This unit includes a laser interferometer translation stage which gives nanometre precision move to the sample during patterning. It also possesses two electron detectors: in-line and scattering. The maximum acceleration voltage for this system is 30 kV. The system is combinedly used for imaging and lithography purpose.

During this thesis work, 20 keV electron energy is used to define the pattern on a positive photoresist (PMMA 950K). The patterning process is discussed in next Chapter.
The resolution of EBL system is limited by diffraction. The main constraints of the resolutions are

(a) Scattering: The scattering of the electrons during the interactions of an electron with the resist and substrate broadens the diameter of the incident beam and provides an extra dose of electron exposure to resist.
(b) Aberrations: electron beam undergoes enhanced aberrations of the electron-optical lenses.

Chapter 4

4 Sample Preparation and Patterning Process

In general, smooth and clean surface during epitaxial growth is the basis for successful heterostructure preparation. In this chapter the preparation of the wafer/substrate will be described, which is necessary for every successful growth. First, the growth of smooth GaAs layer grown on GaAs(100) will be described. Then the patterning (via optical lithography and electron beam lithography) on pre-grown GaAs wafer for site controlled quantum dots will be described. Chemical cleaning and in-situ atomic hydrogen cleaning is used to clean the patterned substrate for regrowth technology, is described in the last section of the chapter.

4.1 Sample preparation

To produce high-quality heterostructures via MBE growth technique, atomically smooth layers with minimum defects is essential. The MBE system was new and the growth process for smooth layers is optimized. In this work 3“ or ¼ of a 3“ GaAs(100) semi-insulating wafers form Wafer Technology are used to grow semiconductors heterostructures. These wafers are epi-ready and they do not need any additional cleaning before loading to the loadlock chamber. The sample preparation before the growth of the heterostructure can be divided into two parts:

(a) Preparation before loading to growth chamber

(b) preparation in the growth chamber

(a) Preparation before loading to growth chamber

After cleaving the 3“ wafer in four parts, the wafers parts are loaded to loadlock. The cleaving of the wafer is done very carefully to make less crystalline particles from the wafer. Such particles adhere the surface and forms defects during growth [37]. These wafers are placed in highly pure molybdenum plate holders and loaded to loadlock chamber.These holders are designed in such way that the wafers are held by gravity. The loadlock chamber is pumped via turbopump in order of pressure of 10^{-7} to 10^{-8} mbar. After that the wafers are degassed at 120°C for 8 hours to remove water residuals and other impurities in load lock. Subsequently, the wafers are transferred to the preparation chamber where again degassing is performed at 200°C on heating station for at least 1 hour. Typically, the preparation chamber pressure incre-

-aes from 1×10^{-10} mbar to 5×10^{-8} mbar during degassing of GaAs (100) wafers and after 20-30 minutes pressure start to decreases. After 1 hour degassing the preparation chamber pressure has decreased to 5×10^{-10} mbar. After that the wafer is ready to transfer to the growth chamber.

After transferring the sample to growth chamber, first we measure metal fluxes (Gallium, Aluminium, Indium). This is done with ionization gauge, placing in front of the sample. After that As flux is measured at different valve opening and the ion gauge is removed from the position. The typical value of the fluxes of group III materials is shown in table 1. For group III cells, hot-lipped or two-temperature group III cell are used to reduce spitting of microdroplets, where the upper part of the cell is 100°C to 150°C hotter than the bottom of the cell. The effusion cells are independently heated until desired material flux is achieved. The change of the temperature of the source cell as small as 0.5°C will lead to flux changes on the order of one to two percent.

Source	Cell Temperature	Flux(mbar)	Flux (atoms/cm^2/sec)
Ga	1004°C/1154°C	1.5×10^{-6}	4.38×10^{14}
Al	1145°C	3.5×10^{-7}	2.19×10^{14}
In	750°C/850°C	1.1×10^{-7}	1.75×10^{13}

Table 4.1: *Temperature of group III cells and their fluxes.*

(b) Preparation in the growth chamber

In growth chamber, GaAs wafer is deoxidized in the presence of As_4 ($\approx 2.0^{-5} mbar$) via thermally heating up the substrate to 620°C prior to growth. However, the temperature of the substrate heater is measure by thermocouple which is attched to the backside of the heater but the actual themperature of the substrate is monitored by infrared pyrometer with an acuuracy of about ±5°C. The deoxidation of wafer occured around 600°C pyrometer temperature, this process is also observed in the RHEED pattern. During removal of the oxide from surface, the intensity of the specular spot on RHEED screen incresase rapidely within 2°C to 3°C range

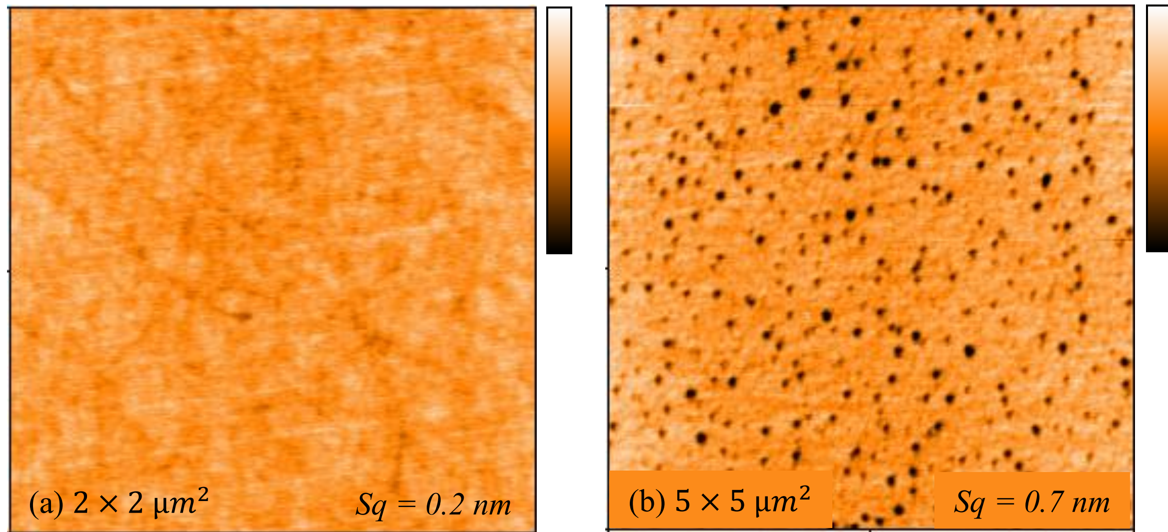

Figure 4.1: *AFM image of GaAs(100) wafer (a) before and (b) after thermal removal of the surface oxide. The pit density is around* $10^9/cm^2$*. The heightscale for (a) is 3 nm and for (b) is 6 nm.*

and surface becomes rough [38, 39, 40]. Due to oxide removal from the surface, surface pinned by small holes. In Figure 4.1(a), AFM image of epi-ready GaAs (100) wafer is shown, and in Figure 4.1(b), AFM image of GaAs (100) wafer after thremally remove of the native oxide in presesnce of arsenic is shown. The rms value of roughness of the surface increased from 0.2 nm (for epi-ready wafer) to 0.7 nm due to thermal desorbtion of the surface oxide.

After removal of oxide, the GaAs surface is annealed at 620°C pyrometer temperature, near to congruent sublimation temperature of GaAs [41] for 10 minutes to complete desorption of surface oxide and other impurities. After that substrate temperature is decreased to 610°C and 100 nm GaAs are grownand annealed for 5 minutes at that temperature. The annealing process improves the surface smoothness. The growth rate of GaAs, AlGaAs is also measured with the help of RHEED oscillation [42]. The III to V flux ratio is adjusted in such a way that 30 oscillations are easily observed. The substrate is typically rotated 10 rpm in order to maintain good growth and temperature uniformity across the wafer. After growth the samples are cooled down at the rate of 20°C/min with As_4 shutter open down to 300°C. For surface morphology study, the sample is transferred to load lock chamber and taken out. The AFM images are taken in contact mode. The vertical resolution is 0.1 nm and lateral resolution is 10 nm. The exposure to air leads to the formation of a thin oxide layer which does not impair the imagining of structure [31].

Here Figure 4.2 shows this process, where 4.2(a) shows AFM image of the bare wafer after thermal degassing and also the corresponding RHEED pattern. The AFM image shows the smooth oxidized GaAs substrate with some polishing lines and RHEED shows the diffusive spotty pattern due to the thin surface oxide layer [38]. Figure 4.2(b) shows AFM images of GaAs substrate surface after thermal deoxidation, there are large (0.2-0.5 nm) and deep (5 nm) holes with a lateral spacing of 0.2 to 1 µm are present as observed in [39, 40]. Corresponding spotty diffraction pattern also confirms that the surface is rough. However, after deposition of few monolayer GaAs a clear (2×4) reconstruction can be seen [43]. Figure 4.2(c) shows AFM image of smooth GaAs surface of 100 nm GaAs and corresponding RHEED shows streaky diffraction pattern. The rms vale of the surface is less than 0.2 nm and atomic steps are clearly visible.

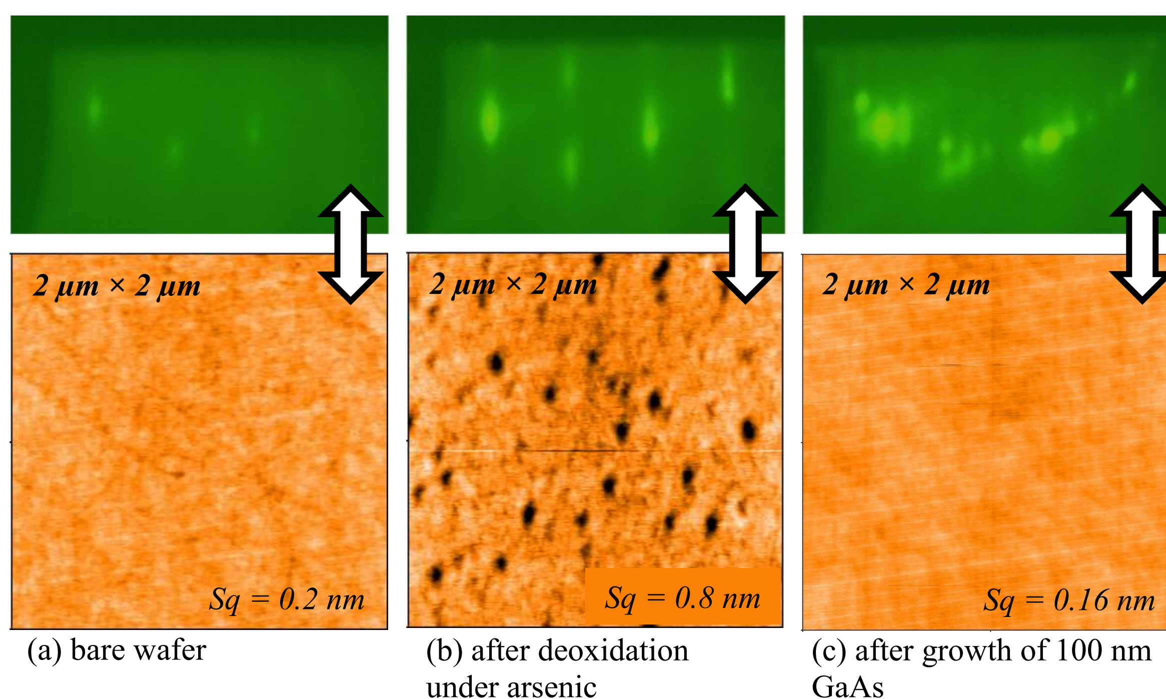

Figure 4.2: *AFM images and corresponding RHEED pattern of different types of GaAs surface. (a) shows an AFM image of epi-ready GaAs substrate after thermal degassing at 200°C in UHV and corresponding RHEED pattern, (b) shows an AFM image of GaAs surface after thermal removal of the surface oxide and corresponding RHEED pattern and (c) shows an AFM image of epitaxially grown smooth GaAs and corresponding RHEED pattern.*

The growth process of GaAs is optimized for best material quality and smooth surfaces to grow InAs quantum dots. There are a lot of samples have been grown to get such a smooth surface as shown in Figure 4.2(c). After growing few hundred nm GaAs (mostly 500 nm), the

samples are taken out from the chamber for ex-situ characterization. Here Figure 4.3 shows laser microscope images of different types of surface oval defects on the epitaxial grown GaAs in our system. These defects are directly related to the growth parameters, chamber impurities and source quality [44, 45, 46]. The surface density of oval defects varies from about 10^2 to 10^6 cm^{-2} with characteristic size in the range of 5-100 μm^2 [46]. Presence of these defects degraded the electrical and optical properties of semiconductor materials. A lot of factors decides the heterostructure quality, few main factors are listed here:

1. Bake out of the main chamber (20-30 days at 250°C), to minimize the chamber impurities

2. Elevated temperature degassing of source materials (1000 to 1250°C for group III materials and 400°C to 500°C for group V materials).

3. High quality source materials

4. Properly cleaned substrate holders

5. Growth parameters (arsenic pressure, substrate temperature, …)

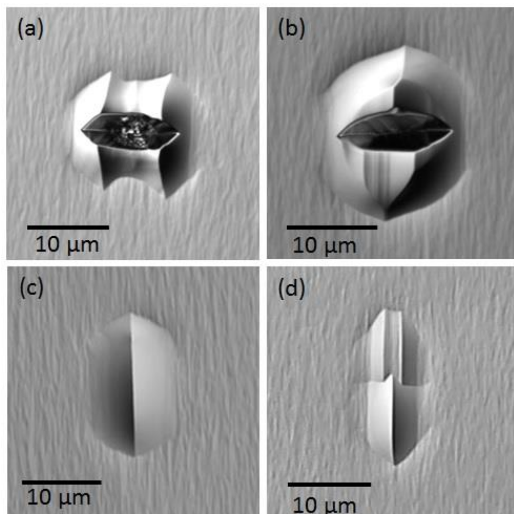

Figure 4.3: *Different types of oval defects on MBE grown GaAs Surface. (a) These type of oval defects are due to Ga spitting on surface , (b) oval defect with notch in the centre, these are defects are related to chamber impurities and (c) & (d) these oval defects are related to the arsenic flux in the chamber* [44, 45, 46, 47, 48]. *In optimized growth temeprature and As flux conditions, the defect density can be reduced to 20-30 defects/cm^2.*

In optimized growth conditions (substrate temperature and III/V flux ratio), the irregular hillocks and pits on GaAs surface are mainly due to gallium spitting from the effusion cell on

to the substrate [47, 48]. The substrate temperature and arsenic flux are main growth parameters which strongly affects the surface quality and oval defect density. In best growth conditions, these oval defects are reduced to 20-30 defects/cm^2 in our MBE system.

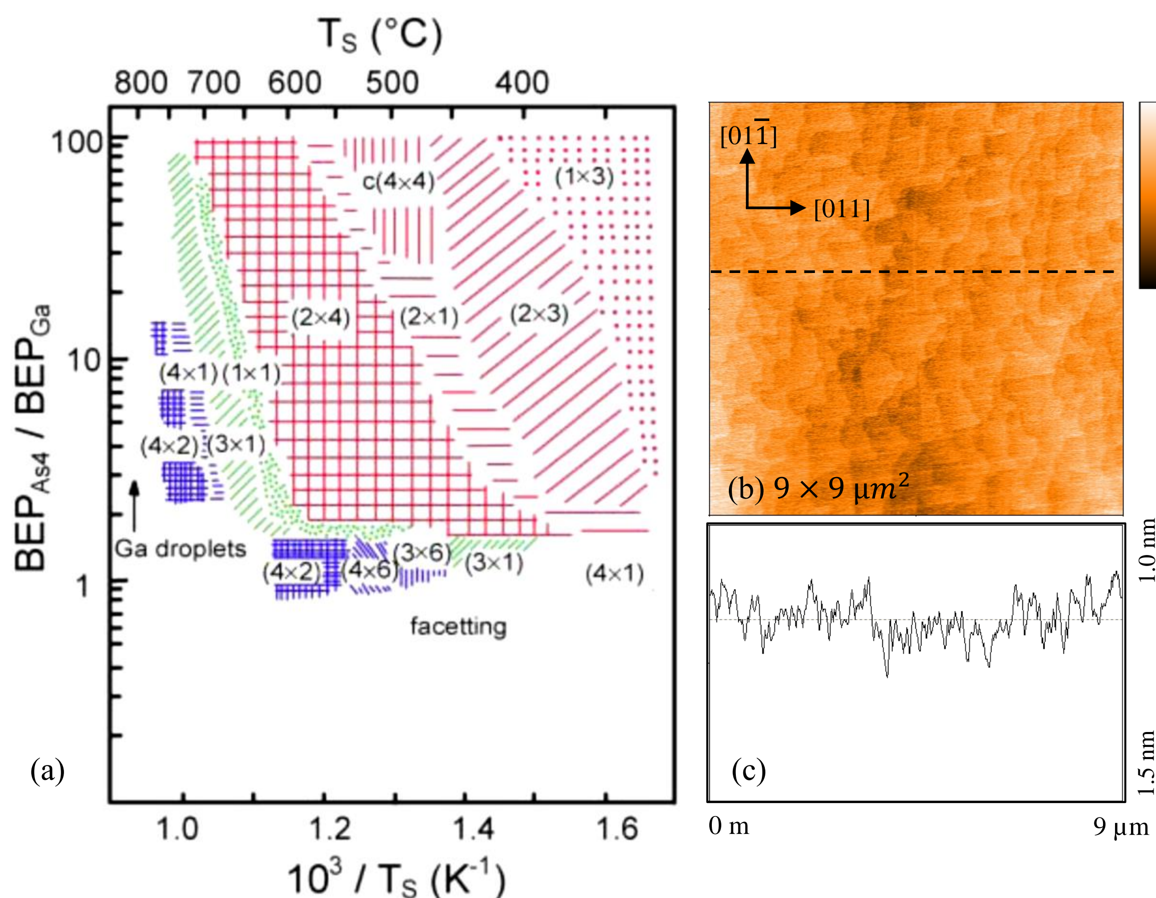

Figure 4.4: *(a) Surface phase diagram for the epitaxial growth of GaAs from Ga and As$_4$ beams on GaAs (100) substarte* [49], *(b) AFM image of epitaxial grown GaAs surface and (c) shows line scan of the surface along the dotted line in figure (b).*

As we have discussed earlier, the substrate temperature is used 10°C higher to thermal deoxidation temperature of GaAs for GaAs growth in normal growth conditions. The surface phase diagram of the epitaxial growth of GaAs from Ga And As$_4$ beams on GaAs (100) substrate is shown in Figure 4.4(a), where a wide range of substrate temperature window is possible to grow (2×4) reconstructed surface [49]. Figure 4.4(b) shows an AFM image of smooth, atomically flat GaAs surface, grown at 610°C substrate temperature and the Ga to As flux was around 18, the vertical scale is 3 nm and Figure 4.4(c) shows the line scan along the dotted line in the Figure 4.4(b). The sticking coefficient of As on As terminated GaAs(100)

surface is zero at such high temperature and therefore stops the growth of bulk arsenic. In such conditions, the incoming flux of Ga atoms decides the growth rate [50], which can be controlled by Ga cell temperature and stopped by cell shutter. So the sticking coefficient of Ga is unity in such condition This is valid for all group III elements (Ga, In and Al). The growth rate of GaAs is kept constant at around 0.7ML/sec or 0.71 μm/h during all the sample except in some special cases. Normally after growing 100 nm buffer layer,.a superlattice containing 20 pairs of 2 nm AlAs/2 nm GaAs are grown which prevent the propagation of dislocations [51]. On the otherhand small surface defects also emerge when superlattice is fabricated [51]. After that the further structure is grown. For the surface morphology analysis, 500 nm GaAs is grown.

Effect of Arsenic Pressure

Arsenic overpressure plays a key role in surface morphology. Low arsenic pressure enhances Ga cluster formation due to excess Ga and higher arsenic pressure suppress the diffusion process. In Figure 4.5, an AFM images of GaAs surface is shown for growth of GaAs in low arsenic pressure ($P_{As_4} = 1.5 \times 10^{-5}$), where the ratio of As to Ga flux is around 12. Such surfaces shows a lot of oval defects which are mainly due to excess Ga and their size is around 2μm to 4μm long along [01-1] and 0.5μm to 1μm wide along [011]. The elongation of defects is due to anisotropic surface diffusion of Ga [52, 53, 54]. Such oval defects provide the strain field to align the InAs quantum dots around them and degrade optical and electrical properties of the dots [55].

In case of high As pressure, the growth of GaAs is dominated by mounds growth due to suppression of Ga diffusion. The As to Ga flux ratio is around 30. The mounds do not disappear if a thicker layer (≈10 μm) is grown. This type of growth process represents the unstable growth [54]. Figure 4.6(a) Laser microscopy image of GaAs surface grown in high arsenic pressure, in centre of the image an oval defects is present due to high arsenic and Figure 4.6(b) shows An AFM image of such surface. Mounds are clearly visibl

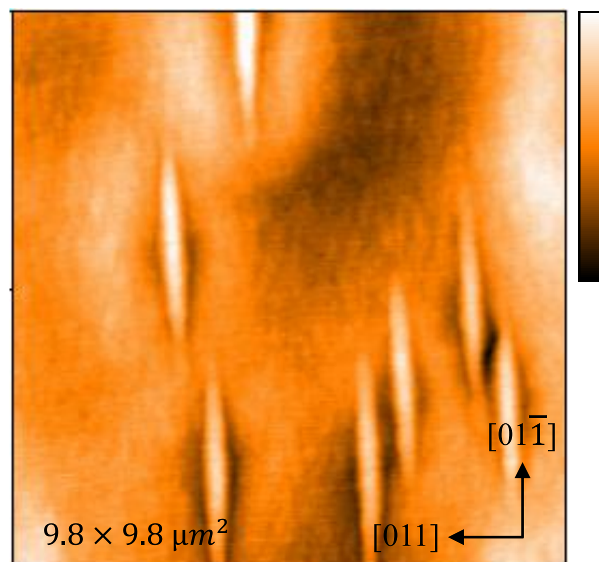

Figure: 4.5: *GaAs surface at low As pressure (P_{As_4} = 1.5 × 10^{-5} mbar) An AFM image of GaAs surface with surface defects. The vertical scale of AFM image is 7 nm.*

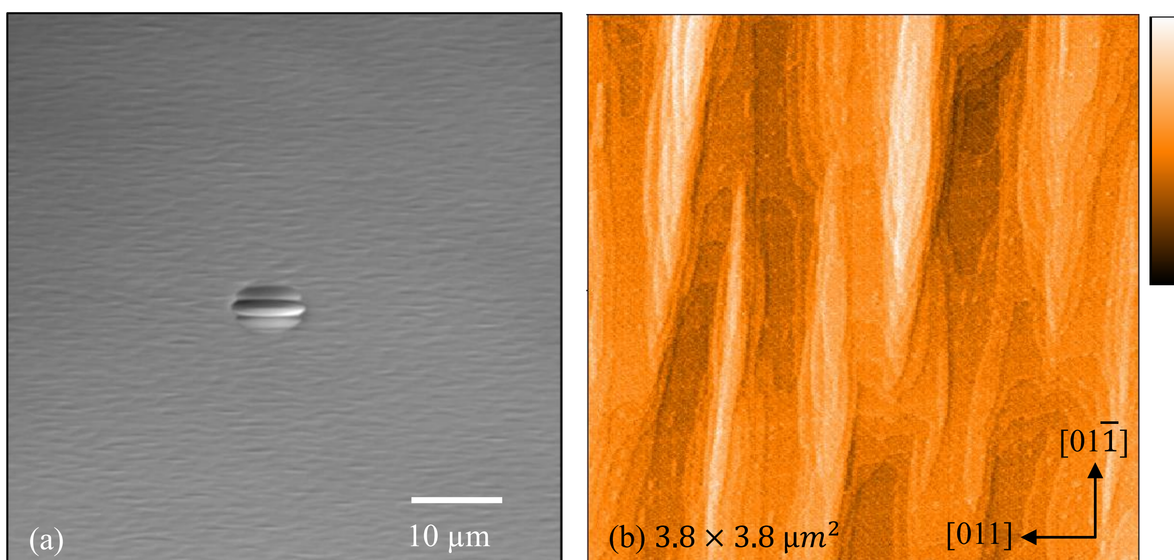

Figure 4.6: *GaAs surface at high As pressure (P_{As_4} = 3.5 × 10^{-5} mbar) (a) Laser microscopy image of GaAs surface with mound growth. (b) AFM shows mound traces with size of 1 μm to 2 μm. The vertical scale for AFM is 8 nm.*

4.2 Substrate Patterning

In this thesis work, patterning process is done to define the pattern which acts as nucleation sites for fabrication of site-controlled quantum dots. There are different patterning techniques used like optical lithography, nanoimprint lithography and electron beam lithography to define the pattern. In this work optical lithography is used to define large mesa structures and alignment marks and electron beam lithography is used to define nanohole arrays with different diameters and different pitches on GaAs(100) substrates. The pattern defined by optical lithography are above 100 µm in size which helps to locate the position for next patterning process. Both patterning processes are described in the following sections.

Before doing any lithography process, the smooth GaAs is grown by MBE on a 3” full wafer as discussed in section 4.1. After that the wafer is cleaved in four quarters and used for patterning process.

4.2.1 Optical Lithography

In the optical lithography process, the photoresists are exposed by ultraviolet light for the fabrication of the semiconductor devices. The ultraviolet light source is commonly a mercury lamp. (312, 335, 365, 405, 435 and 540nm). During the exposure, in the case of positive tone photoresist, UV light breaks the long chain chemical bonds to shorter and thus exposed resist becomes more soluble. In case of negative tone resist, UV lights cross links the polymer chains and the exposed resist become less soluble. The change in solubility allows the resist to selectively remove.

In optical lithography process, a ¼ 3” GaAs (100) wafer is patterned to define 300 × 300 μm^2 mesa structures and alignment marks. All the steps are sketched in Figure 4.7. The GaAs wafer is cleaned with acetone and isopropyl (IPA) and positive photoresist [ARP 3510 : AR 300-12 (1 : 1)] from *Allresist* is spin coated used at 300 rpm. The thickness of resist is in order of 1.8-2 µm and backed for 1 minute at 100°C on a hot plate. Photomask as shown in Figure 4.8(a) is used to exposed the resist to UV light. After exposure, the resist is developed in developer (AR 65-70:H_2O = 1:1) for 30 seconds. To stop developing, the wafer is rinsed with deionized (DI) water and blown dry with N_2 gas. Using sulphuric acid based etching solution (H_2SO_4 : H_2O_2 : H_2O ≈ 1 : 1 : 50), the pattern is transferred to GaAs wafer. The solution is gently stirred for uniform etching over the wafer. The etching rate of the solution is around 115 to 120 nm per minute. The etching process is stopped by merging the wafer in DI water and

rinsed for 30 seconds. Mesas are defined 400 nm to 500 nm in depth, which are clearly visible in the optical microscope. After transferring the pattern, chemical cleaning is performed to remove all resist residuals. After that the substrate is ready for e-beam lithography. The chemically cleaning process is discussed in Appendix I.

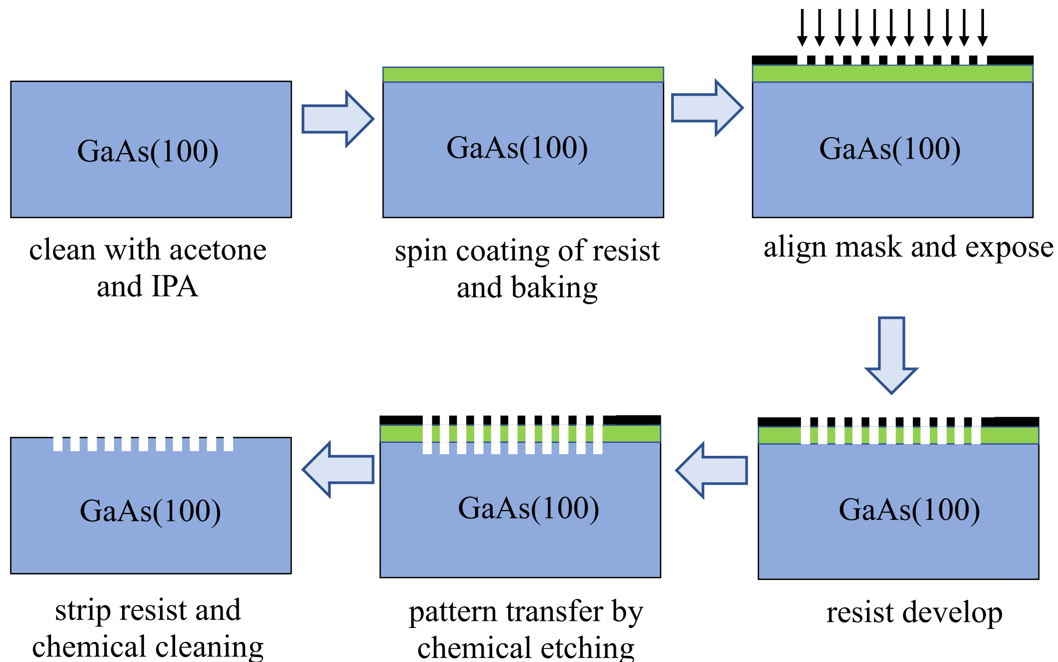

Figure 4.7: Schematic of the optical lithography process.

In Figure 4.8(a) schematic of ¼ 3" wafer is shown with optical lithography mask. The mask is an emulsion glass mask prepared at AFP group at the University of Bochum. Figure 4.8(b) shows the laser microscope image of patterned mesas and alignment marks. Afte each step, the mask is cleaned with acetone and IPA to remove any resist particles on the surface.

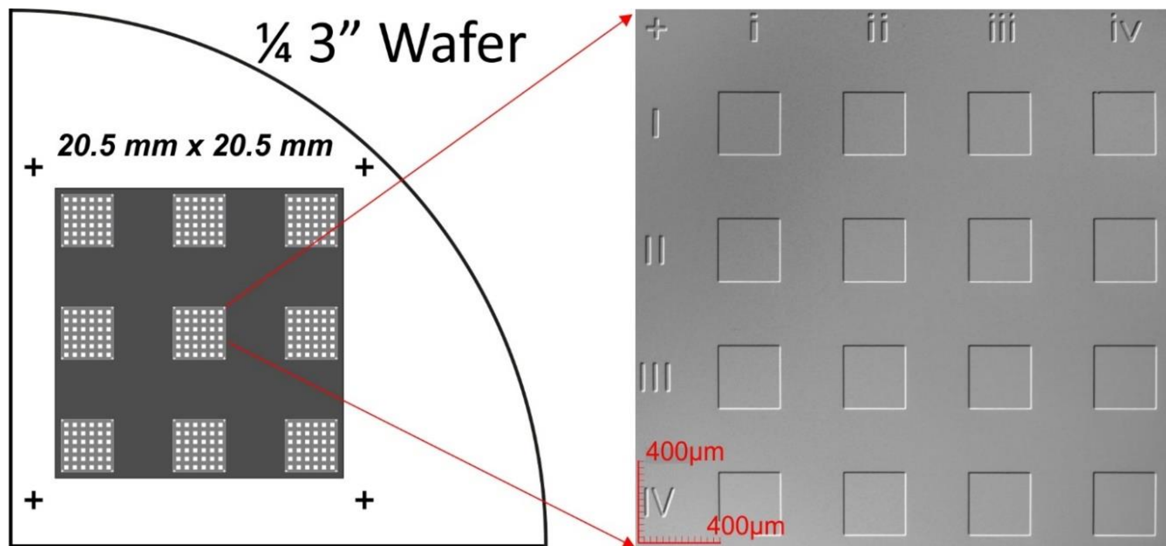

Figure 4.8: *(a) Schematic of a ¼ 3" GaAs (100) wafer with optical lithography mask and (b) Laser microscope image of the patterned mesa. The mesa size is 300 × 300 µm^2 and 400 nm deep etched.*

4.2.2 Electron-Beam Lithography

In electron-beam lithography (EBL) process the mesa structures are patterned with 2-dimensional hole array using a positive photo-resist poly methyl methacrylate (PMMA 950k). Via chemical etching the holes were transferred to the wafer. Each hole array (100μm × 100μm) is centred to the mesa as shown in the schematic Figure 4.9b. Holes with different size and spacing are defined. After etching the resist is removed by solvents such as trichloroethylene (TCE) and n-methyl pyridine (NMP). After that surface is cleaned with several ultrasonic baths of organic solvents. Hydrofluoric acid cleaning is used at end of all patterning and cleaning process to remove all residuals of resist and oxide from the surface.

After photolithography, on a cleaned ¼ 3" GaAs (100) substrate, diluted PMMA 950K (ARP671.02) is spin coated with 5500 rpm for 30 sec. The thickness of the spin PMMA is around 70-75 nm (which is measured by profilometer after patterning a step by EBL). The sample is backed for 90 seconds at 150°C on a hot plate. After this wafer is transferred to the EBL system.

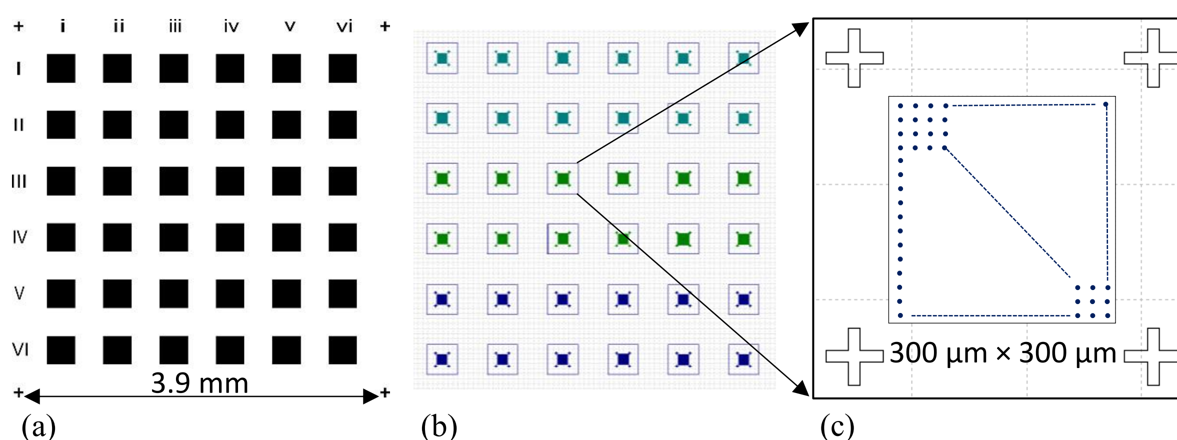

Figure 4.9: *Overview of the mask design, (a) Schematic of patterned mesa via optical lithography, (b) schematic of pattern mask for EBL, here different colours corresponds to different layers for patterning nanoholes and (c) shows an array of holes with alignment marks in the centre of the mesa.*

In EBL, process steps are listed in Table 1. The mask for EBL process is designed by Pioneer software from Raith GmbH as shown in Figure 4.9 (b) & (c). The mask for EBL is designed for each mesa with different pitch size (500 nm, 1 μm, 2 μm…) and different hole diameters. At first, the alignment of the sample with respect to the mask is done with the help

of marks and mesas patterned by optical lithography. After that electron beam is finely focused to 15-20 nm diameter spot for all the samples. The focusing quality is observed by burning a spot (exposing electron beam for 1-2 seconds). Initially different dose (200- 300 $\mu C/cm^2$) is tested exposing 20keV electron beam for optimum results. The dose $280 \mu C/cm^2$ is showing best results for patterning the nanoholes in PMMA.

After patterning, the pattern is developed via dipping the substrate in MIBK : IPA (1:3) solution for 30 seconds and stopped by dipping in IPA for 30 seconds. Acid based chemical etching process is used to transfer the pattern to the substrate. For that sulphuric acid based etching solution ($H_2SO_4 : H_2O_2 : H_2O \approx 1 : 8 : 800$) is used, the etching rate of this solution is around ~1 nm/sec. for GaAs (100). The etching process is stopped by rinsing with DI water and substrate is dried by dry nitrogen. After transferring the pattern to the substrate, resist is primarily removed by acetone and IPA. The wafer is examined under laser microscope to ensure complete development of the pattern over the wafer, attention is paid to bigger alignment features for the presence of nice sharp edges.

Substrate Preparation	Substrate should be perfectly clean and dry. Just before coating the substrate is flushed with acetone and isopropanol and dried with dry N_2
Spin	PMMA 950K 2% solution, 5500 rpm, 30sec.
Pre-bake	150°C for 90 sec. on a hot plate
Patterning	Raith Pioneer System, 20kV, dose: $280 \mu C/cm^2$,
Develop	MIBK : IPA (1:3), 30 second , 30 sec. in IPA for stopping
Transfer Pattern	via chemical etching in solution: ($H_2SO_4 : H_2O_2 : H_2O \approx 1 : 8 : 800$), etch rate = 1 nm/ sec, stopped by DI water
Strip	resist removed by acetone and IPA cleaning
Cleaning	Chemical cleaning is used to remove all resist residuals and other impurities (see Appendix I)

Table 4.2: *Process steps for nanohole patterning by an electron beam lithography process.*

4.3 Chemical Cleaning

A sophisticated chemical cleaning is processed before loading the samples into the loadlock chamber. After chemical cleaning, to check the surface quality and nanohole morphology, AFM is used. In chemical cleaning, ultrasonic bath at high frequency (135kHz) with organic chemicals (Acetone, IPA) is performed. Heated NMP (n-methyl pyridine) and TCE (trichloroethylene) are also used to remove any resist residuals. The steps of the cleaning process are described in Appendix I.

Here in Figure 4.10(a) shows an exemplary AFM image of nanoholes in GaAs(100) after removing PMMA via acetone and IPA. A lot of PMMA residuals are present on the surface. Figure 4.10 (b) shows the image after chemical cleaning. The hole diameter is around 70 nm and the spacing is 1 µm. Figure 4.11 shows different mesa with patterned nanoholes after chemical cleaning.

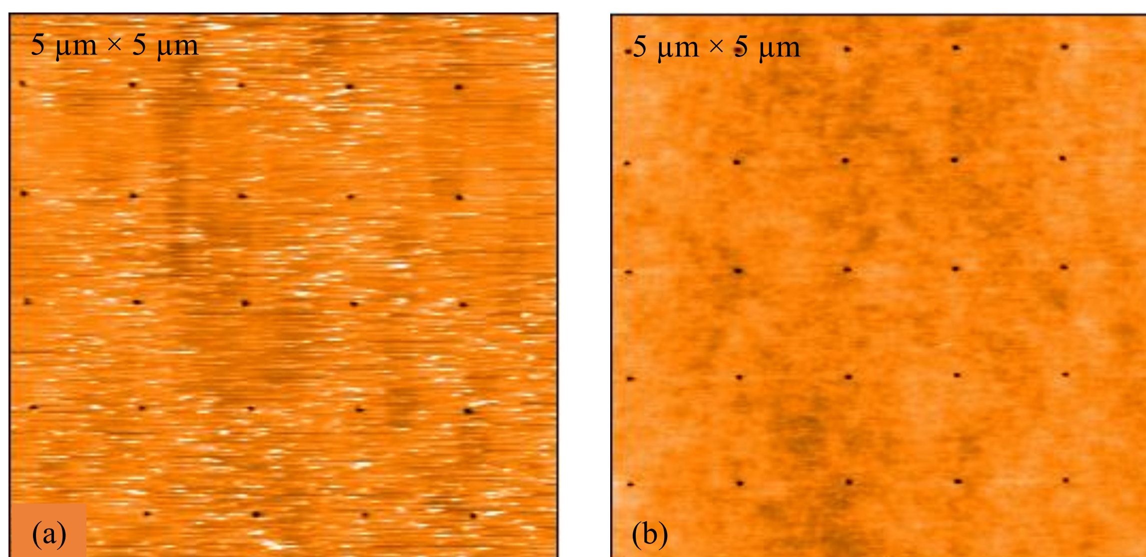

Figure 4.10: *AFM images of patterned nanoholes on GaAs (100), (a) after removing resist with acetone and IPA, (b) after chemical cleaning.*

After chemical cleaning, all the samples are cleaned by hydro fluoric (HF) acid based solution. The sample is placed in 50%HF + IPA (1:1) solution for 5 minutes. This solution removes all the remaining residuals and thin the surface oxide. After 5 minutes dipping in the solution, the sample is rinsed by Di water for 10 minutes. After that sample is loaded to the

loadlock without exposing to air for long time. This step is very crucial for the re-growth technology in GaAs based epitaxy where the surface oxide is not removed completely by atomic hydrogen cleaning process. Because the organic chemical treatment to GaAs wafer increases the oxide thickness which hinders the re-growth process. By this step the oxide layer is removed and very thin layer of oxide is formed during the transfer of the sample to loadlock, which is removed by atomic hydrogen cleaning in UHV conditions, prior to growth. The atomic hydrogen cleaning process is discussed in next section.

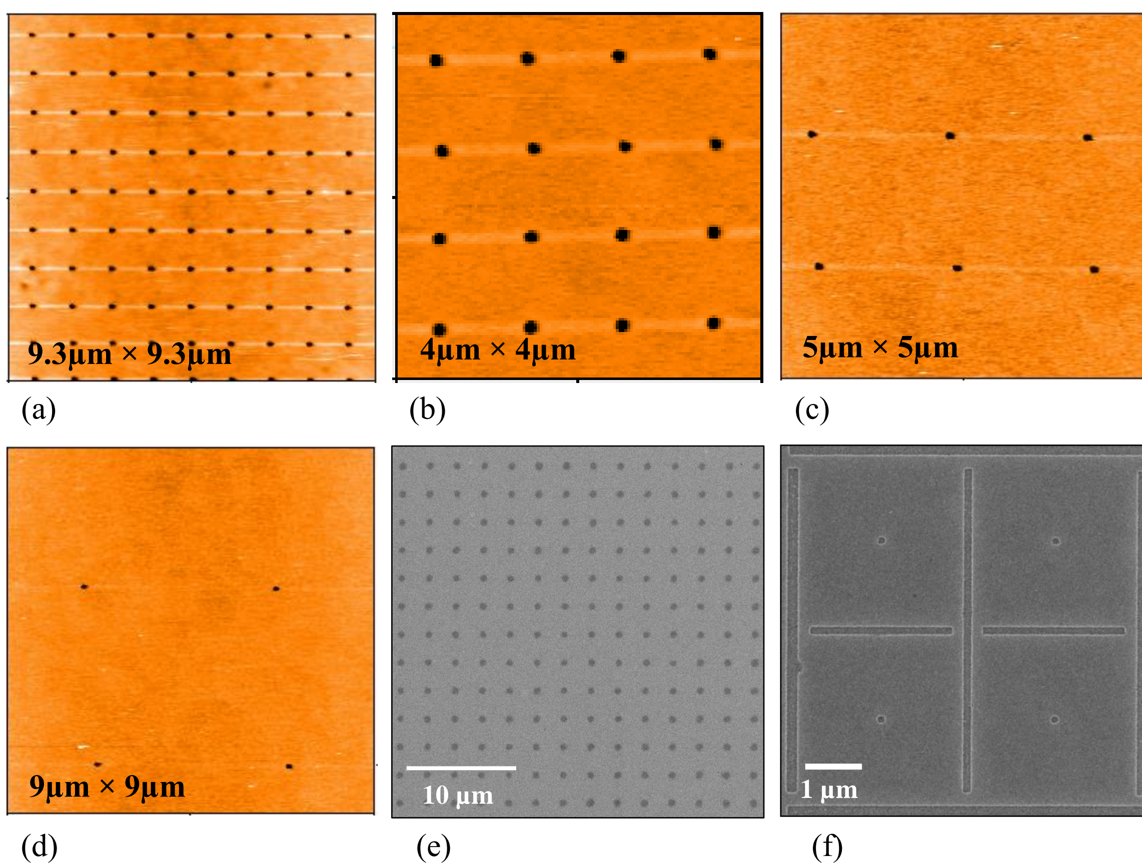

Figure 4.11: *Nanopatterned holes with different spacing. (a), (b), (c) and (d) shows AFM images at different mesa structures with patterned nanoholes. (e) and (f) shows SEM images of such nanoholes.*

4.4 Atomic Hydrogen Cleaning

It is highly desirable to have a cleaning process which can be used in an ultrahigh vacuum to remove oxide, resist residuals and other contaminations fr0m a patterned substrate without damaging the structure and substrate. Additionally it is also desired that the process should be done at low temperature (in case of GaAs- 300° to 400°C) to avoid any thermal degradation of the surface. Atomic hydrogen (AH) cleaning meets all of the criteria and is very effective method for preparing clean GaAs (100) surfaces for re-growth technology in epitaxy.

Thermally activated hydrogen atoms react with the GaAs surface, where it forms volatile hydride compounds. These hydrides can be removed thermally. It is also conveniently found that hydrogen is much more reactive with amorphous surface bonds such as As-O and Ga-O than the GaAs crystal bonds. Initially the hydrogen reacts with arsenic oxide and releases molecular arsenic and later it reacts with non-volatile Ga_2O_3 oxide and forms volatile Ga_2O [56, 57]. Hydrogen atoms also react with carbon and after that thermally can be removed [58]. The hydrogen atoms reactions also take place at much lower temperatures than those required for efficient thermal desorption via heating only. Cleaning at lower temperatures is therefore possible and will reduce the amount of thermal desorption via etching of the substrate, segregation of dopants, and the diffusion of both component atoms and impurities into the wafer.

For realising the site-controlled QDs, atomic hydrogen cleaning process is necessary prior to regrowth on a patterned substrate. In this thesis work, a commercial hydrogen atom beam source (HABS) from MBE Komponenten GmbH is used to generate atomic hydrogen via thermal cracking of hydrogen molecules in a heated long tungsten capillary. The tungsten capillary is heated with DC feeded surrounding W-filament. Operation temperatures up to 1800°C is used for an efficient thermal cracking ($\geq$ 70%) of H_2 molecules within the capillary. Higher temperature up to of 2000°C are also achievable but this might affect the filament lifetime. The high purity W-tube is directly contacted to the hydrogen gas and forms a narrow angle gas beam ejected from the HABS [59, 60]. It provides high flux rates at the sample position while keeping the H_2 background pressure of the chamber low. The HABS unit is connected to water cooling line to reduce the thermal load to the chamber. Figure 4.12 shows the photograph of the HABS unit.

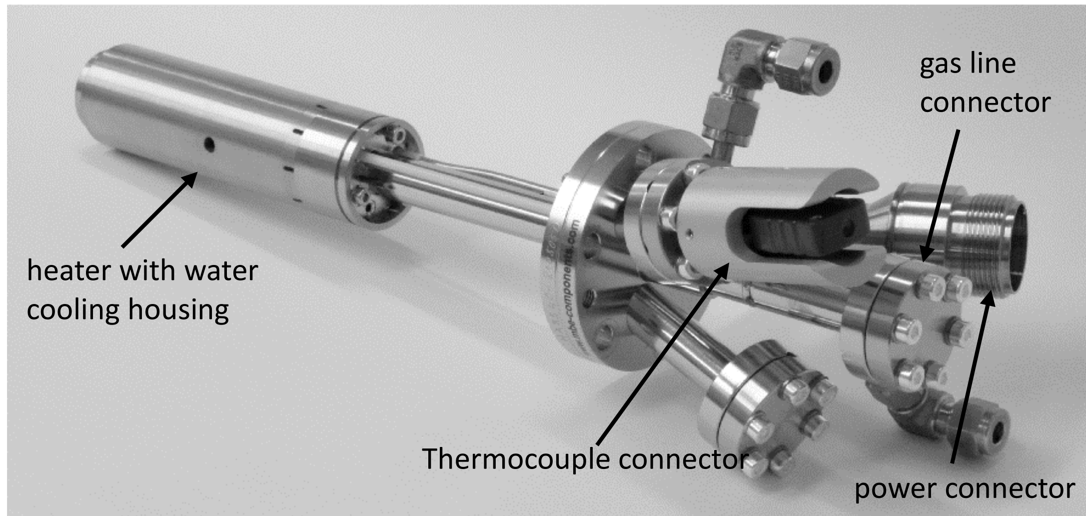

Figure 4.12: *Photograph of the hydrogen atom beam source (HABS) unit (MBE Komponenten).*

The HABS unit is connected to the preparation chamber and mounted towards the heating station. The H_2 gas line is connected to the HABS via UHV compatible leak valve. For ultra-pure operation, H_2 gas purifier form SAES (0.003µm filter) is placed before the leak valve. The hydrogen flow used during cleaning of the substrate is controlled by leak valve opening and monitored through the chamber pressure. The sketch of the atomic hydrogen cleaning unit is shown in Figure 4 13. The chamber is pumped with ion pump and titanium sublimation pump which keeps the base pressure in the chamber around 5×10^{-11} mbar. Additionally, liquid nitrogen shroud surrounds the TSP which enhances pumping speed for hydrogen and other gases.

The AH cleaning process had to be established within the framework of the thesis. As a first step, AH cleaning process is optimized to clean native oxide from GaAs(100) wafers. First, the substrate is degassed at 200°C substrate temperature in the base pressure of 10^{-10} mbar. The appropriate substrate temperature for cleaning of GaAs (100) is around 350°C and hydrogen exposure time is around 30 minutes at base pressure of 5×10^{-6} mbar of the chamber. Such a low substrate temperature does not desorb the As from GaAs surface. A pre-grown GaAs(100) sample which is exposed to air for few days is used to test the AH cleaning process. After cleaning, the substrate temperature is decreased to 200°C and hydrogen leak valve is closed. The temperature of the HABS unit is decreased to 200°C. After that sample is transferred to the MBE growth chamber when preparation chamber pressure is decreased to

5×10^{-9} mbar. A lot of efforts are put to realize the AH cleaning process. Here the different steps are listed:

(a) AH cleaning setup is newly installed so a lot of test samples are used to figure out the appropriate substrate temperature and the hydrogen pressure.

(b) For each sample, *in-situ* RHEED and *ex-situ* AFM are performed to analyse the surface.

(d) GaAs buffer layer (10-15 nm) are grown and Analysed by AFM

(c) QD samples are grown on AH cleaned surface to realize the complete removal of the surface oxide and compared their optical quality.

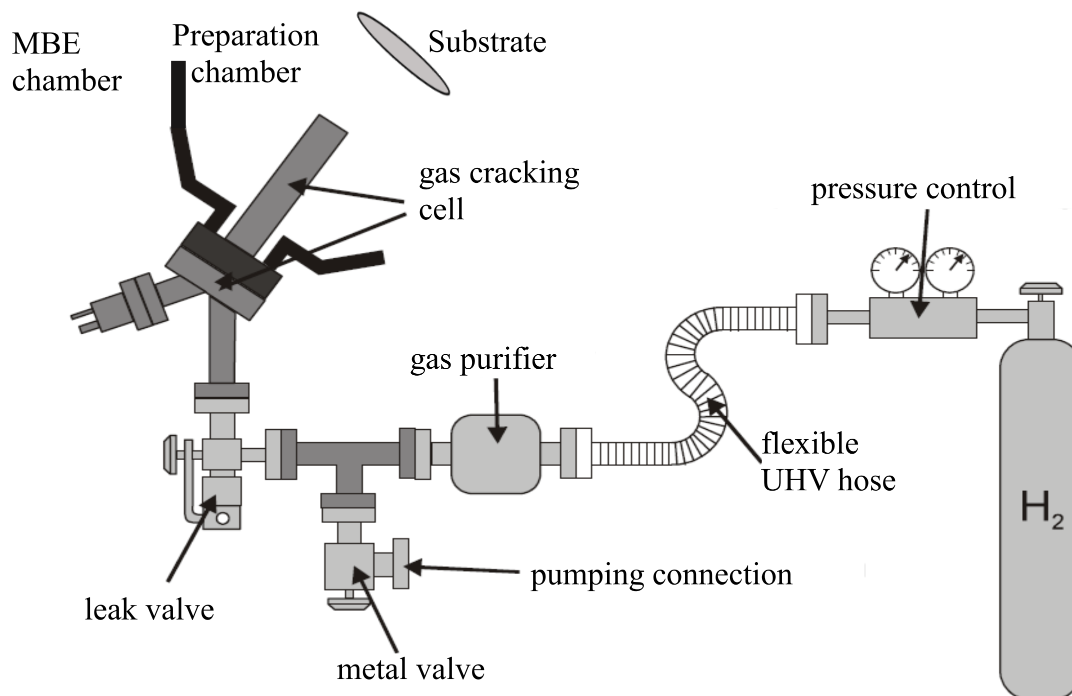

Figure 4.13: *Schematic sketch of the atomic hydrogen cleaning unit*

AH cleaned surface is investigated in-situ via RHEED in MBE chamber and ex-situ via AFM. RHEED patterned is recorded of GaAs surface before AH cleaning and after AH cleaning process. Figure 4.14(a) shows a diffusive spotty RHEED pattern before atomic hydrogen cleaning due to the presence of a thin oxide layer and 4.14(b) shows sharp RHEED pattern after atomic hydrogen clean which confirms the removal of oxide [61, 62].

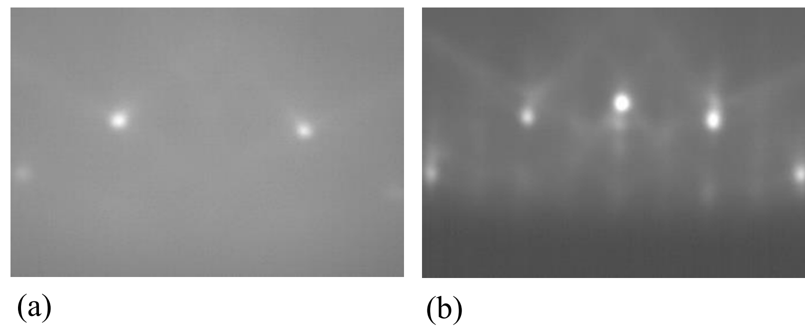

Figure 4.14: *(a) shows the diffusive spotty pattern on RHEED screen before AH cleaning and, (b) after removal of oxide shows the sharp pattern* on the RHEED screen.

After AH cleaning and RHEED investigations, the substrate is taken out from the MBE system and investigated under AFM. Figure 4.15(a) shows an AFM image of GaAs surface after removal of the surface oxide by thermal desorption in arsenic overpressure in MBE chamber and Figure 4.15(b) shows an AFM image of the same sample after AH cleaning. As we see that the thermal cleaning creates surface pits with 2-3 nm deep and rms value of surface roughness is increased. In case of hydrogen cleaning no surface damage is observed in the AFM measurement.

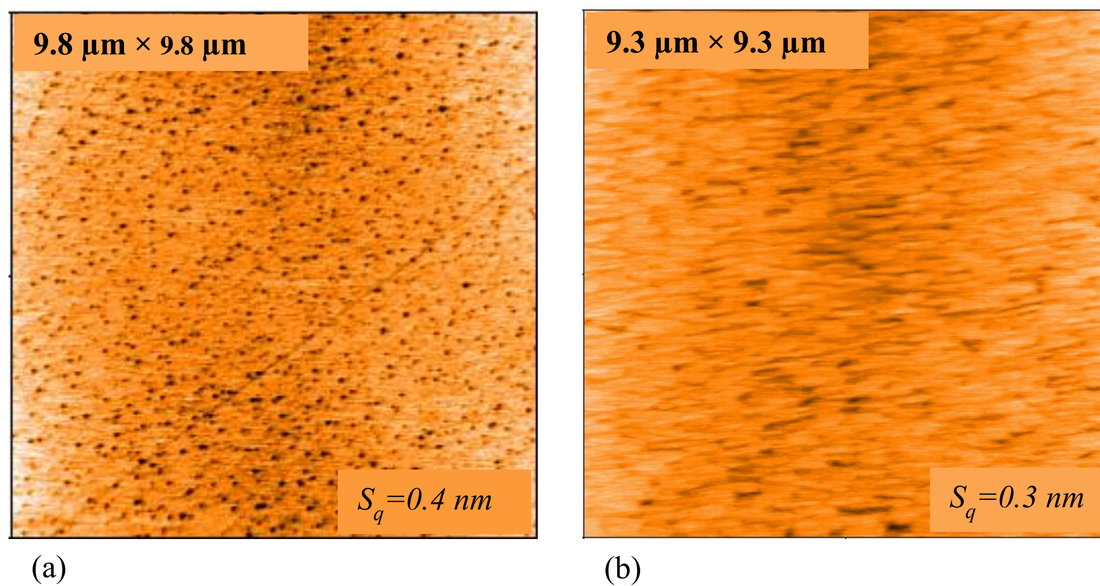

Figure 4.15: *AH cleaning: (a) AFM image of thermally cleaned GaAs surface, and (b) shows AFM image of GaAs surface after AH cleaning.*

In similar way, on another sample, after AH cleaning InAs QDs are grown at 510°C substrate temperature. The growth process of QDs is discussed in Chapter 5. Figure 4.16 (a) shows AFM of InAs QDs grown on as grown GaAs(100) surface and 4.16 (b) shows InAs QDs grown on AH cleaned GaAs (100) surface. In case of AH cleaned surface, the size inhomogeneity of QDs increased, which is suggested due to surface defects and surface pitting.

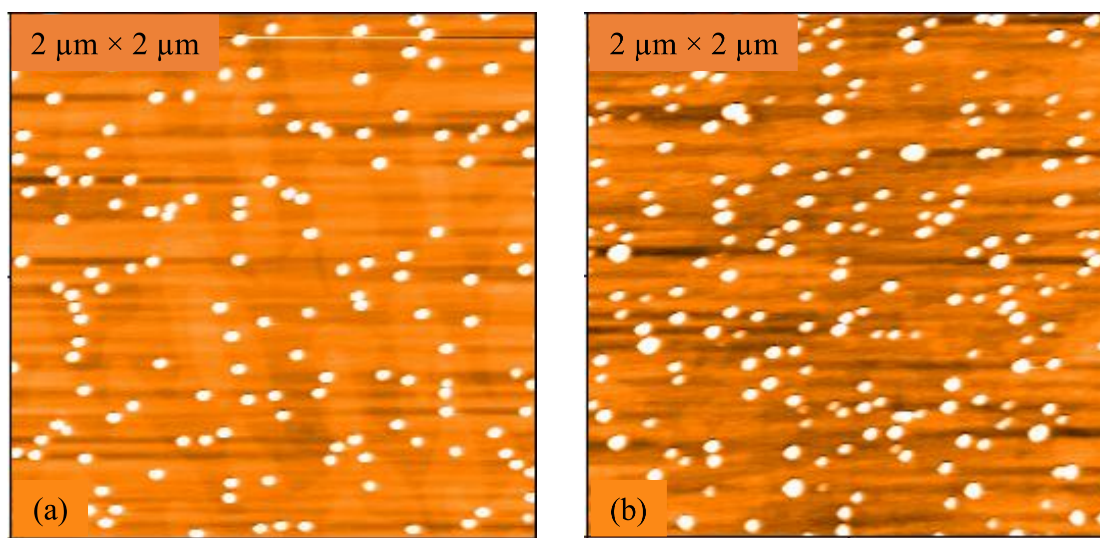

Figure 4.16: AFM image of InAs QDs (a) on as grown GaAs surrface and (b) on atomic hydrogen cleaned surface on GaAs (100) substrate.

To see the effect on optical quality of InAs QDs on AH cleaned substrate after all lithography process and chemical treatment, InAs QDs are grown and capped with GaAs. In Figure 4.17, PL spectra of InAs QDs of different samples at 77K are shown. Spectra (a) represent the PL spectra of InAs QDs grown on as grown GaAs surface (AH cleaning and no air exposure). This is a reference sample. The FWHM of the ground state for the QDs is 30.4 meV which is due to size and composition inhomogeneity in the QDs. Spectra (b) represents the PL spectra of InAs QDs grown on AH cleaned surface where 15 nm GaAs buffer layer is grown at 510°C substrate temperature. The FWHM of the ground state for the QDs is 22.8 meV, which indicate the narrow size distribution of the QDs. Spectra (c) corresponds to the Ahcleaned surface where InAs QDs are grown without buffer layer growth. Due to defects at-

the interface, the PL intensity of these QDs is very low. These defects contribute to the non-radiative recombination processes. The FWHM of the ground state for dots is increased due to increase in size inhomogeneity.

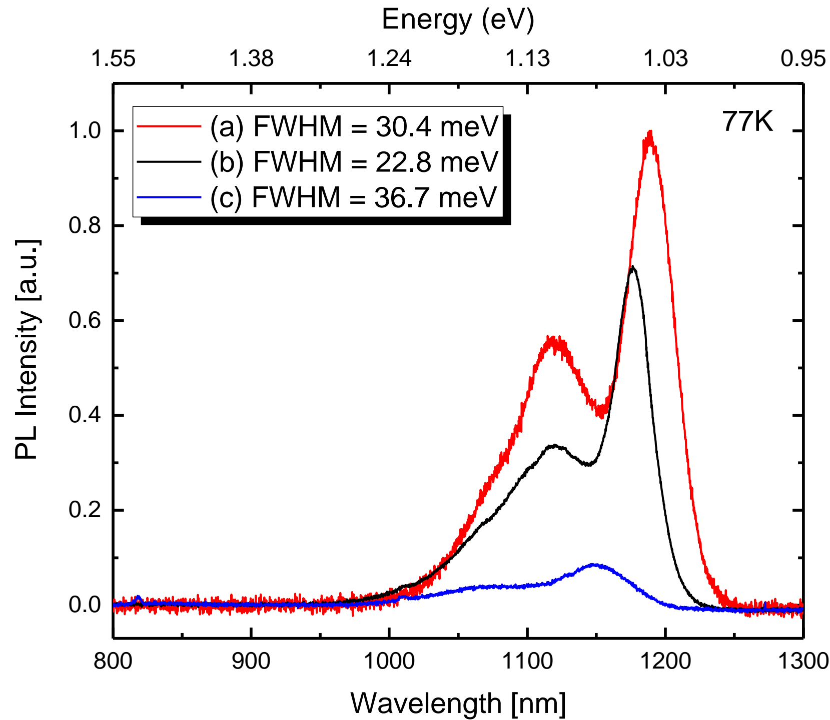

Figure 4.17: *PL spectra of InAs QDs at different surfaces where (a) belongs to the reference sample, (b) atomic hydrogen cleaned sample and (c) chemical cleaning + atomic hydrogen cleaned and 15 nm GaAs buffer layer. In all cases QDs are optically active. The FWHM for the ground state also shown for each sample.*

The aim of AH cleaning in the thesis work is to grow site-controlled QDs on a patterned substrate, which is realized in Chapter 7. In Chapter 7, growth of site-controlled QDs is discussed.

This page has been intentionally left blank.

Chapter 5

5 Growth of Self-Assembled (In,Ga)As QDs on GaAs(100)

(In,Ga)As/GaAs based self-assembled quantum dots (SAQDs) have unique optical and electrical properties, therefore have been under intense research in the past two decades. This chapter briefly describes the growth process of InAs quantum dots (QDs) on GaAs(100) substrate as well as their structural and optical properties. The density control of the dots can be achieved in diverse ways such as In-gradient technique, annealing approach, and pre-patterning process. In this chapter, In-gradient approach will be discussed. To tune the emission energy of QDs different approaches used, which are described in the last section of the chapter.

5.1 Introduction

In homoepitaxy (GaAs growth on GaAs) or in nearly lattice matched systems (i.e. AlAs growth on GaAs), one material can be epitaxially grown on another with minimum strain energy in the crystal. If this is not the case, the lattice mismatch between the substrate and deposited material forces different growth dynamics in the growing films and typically leads to the island formation after few monolayers growth [63, 64]. There are multiple examples of such semiconductor systems, including InAs/GaAs, InAs/InP, InP/GaAs, Ge/Si, CdSe/ZnSe and GaN/AlGaN. Among those, the InAs/GaAs system is the most studied due to its interesting properties. InAs has a 7% larger lattice constant than GaAs. Initially, in epitaxial growth, InAs grows on GaAs as layer by layer due to lower surface energy [65] but after a critical thickness (θ_c), the growing layer could not sustain the strain and InAs islands forms. This island formation process is accompanied by a wetting layer [66, 67]. This process is known as Stranski-Krastanov (S-K) growth method. The critical thickness (θ_c) for island formation in InAs/GaAs system is in the range of 1.5 ML to 3 ML and depends on the substrate temperature and In-flux [68]. These islands are coherently strained and defect free and are known as self-assembled quantum dots (SAQDs). Up to a certain InAs amount, strain relaxation is elastic and dislocation free, this leads to coherent QDs formation. If this InAs amount is exceeded, dislocation formation starts in the material and degrades the QD quality [69].

The size, shape and density of QDs can be controlled by growth parameters, mainly substrate temperature, In amount, and As to In flux ratio. Typically, the height and diameter of these dots are in the range of 5-8 nm and 20-30 nm respectively. The total number of atoms in such a dot is $\approx 10^4$-10^5. For carrier confinement, generally InAs QDs are buried in a GaAs matrix.

The band structure of InAs QDs embedded in a GaAs matrix forms a type-I heterostructure. This means that the GaAs matrix provides three-dimensional confinement for electrons and holes. Due to three-dimensional confinement, these dots show discrete energy levels for electrons and holes and are often referred as "artificial atoms". The ability to tune the confined energy states of such QDs via controlling their size and composition is one of the main potential that has been realised for both optical and electrical devices. In QDs, confined electrons and holes form excitons and that is the key aspect of modern quantum information technology.

In this work, the QDs are grown by strain driven MBE in Stranski-Krastanov growth mode. Precise control of the QDs growth provides desired optical and electrical properties. A lot of efforts are put into optimizing the growth of InAs and $In_xGa_{1-x}As$ QDs on GaAs (100) for good optical and electrical properties.

5.2 Quantum Dots Growth

Epitaxial growth of GaAs and AlAs on GaAs(100) substrate in MBE system can be performed in a wide range of substrate temperatures [49]. Normally in our MBE system, GaAs and AlAs are grown at 600°C substrate temperature (measured by Pyrometer) on a semi-insulating GaAs(100) substrate. The In has a low sticking probability on GaAs at such high substrate temperature due to its low congruent vaporization temperature. Due to this, the growth of InAs is done at lower substrate temperatures. As discussed in section 4.1, after growing a smooth GaAs buffer layer at 600°C, the substrate temperature is lowered to 510°C to grow InAs. Also, the arsenic flux is slightly reduced from 2.0×10^{-5} mbar to 1.5×10^{-5} mbar. The slightly lower arsenic pressure enhances the In diffusion and provides a smooth surface. The As to In flux ratio is kept high (>100) to suppress the Ga intermixing in InAs QDs.

The growth rate measurement of InAs on GaAs (100) is critical due to the formation of InAs islands after 1.7 ML deposition. So the growth rate of InAs is calibrated via RHEED oscillations while growing $In_xGa_{1-x}As$ layers. Table 5.1 shows the flux of In cell and growth rate of InAs at two different In cell temperatures. In most of the cases, QDs have been grown using 750°C In cell temperature. Figure 5.1(left) shows an AFM image of pseudomorphically grown InAs (1.6 ML) on GaAs(100) and Figure 5.1(right) shows an AFM image of pseudo morphically grown InGaAs (4 ML) layers at 510°C substrate temperature. The surfaces are atomically smooth with roughness value of 0.2 nm. Also, the growth rate is verified by observing the 2D to 3D transition on RHEED screen during deposition of InAs on GaAs. The transition occurs after 1.7 ML deposition of InAs.

In cell temperature(T_B/T_P)	Flux (mbar)	Growth rate (ML/sec.)	Growth rate (µm/hour)
750°C/850°C	8.9×10^{-8}	0.03	0.0306
780°C/880°C	1.9×10^{-7}	0.052	0.053

Table 5.1: *In flux and corresponding growth rate of InAs at different In cell temperatures. The growth rate of InAs is measured by RHEED oscillations while growing $In_xGa_{1-x}As$ layers at 510°C. Here T_B and T_P correspond to the temperature of the cell at the bottom and the top part of the cell.*

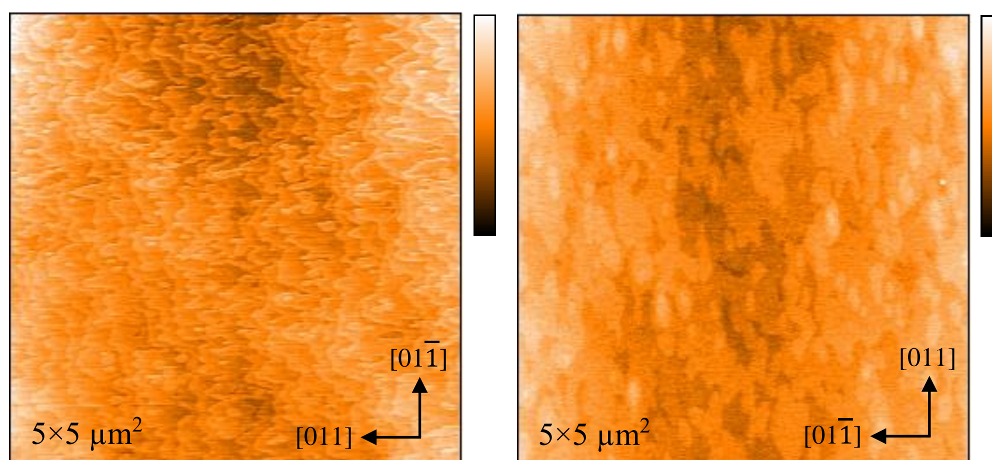

Figure 5.1: *(Left) shows AFM images of 1.6ML of InAs grown on GaAs(100) at 510°C substrate temperature where atomic steps are visible and (right) shows AFM images of 4ML of $In_{0.5}Ga_{0.5}As$ grown on GaAs (100) at 510°C substrate temperature. The colour scale for AFM images is 4 nm.*

In this work, InAs QDs are grown by the growth interruption method. InAs is deposited in cycles where the In cell shutter is opened for 4 seconds and closed for 4 seconds in the presence of excess arsenic. The interruption of 4 seconds enhances the migration of InAs on the surface [70]. We need 16 cycles to deposit around 1.7 ML ($>\theta_c$) of InAs at 750°C In cell temperature for QD formation. The transition from 2D growth mode to 3D mode (island formation) is monitored by RHEED. The slow growth rate decreases the size fluctuations in QDs [71] and provides better control over growth.

After growing a GaAs buffer layer, the substrate rotation is paused and the [011] direction is aligned along the electron beam of the RHEED gun to observe the surface reconstructions and monitor the growth of InAs QDs. In the next step, the substrate temperature is lowered down to 510°C. During the temperature decrease, the GaAs surface reconstruction transforms from (2×4) to c (4×4) as shown in Figures 5.2(a) and (b). It is observed that such surface reconstruction is suitable for the growth of dislocation free InAs islands [72]. Figure 5.2(c) shows the RHEED pattern after deposition of 5 cycles (0.6ML) of InAs, the reconstruction pattern disappears and several spots appear on the RHEED screen. Figure 5.2(d) shows a 3D spotty pattern due to the formation of QDs after depositing 16 cycles (1.73 ML) of InAs. These QDs can be desorbed via heating the substrate to 600°C. Normal QD samples are grown with substrate rotation.

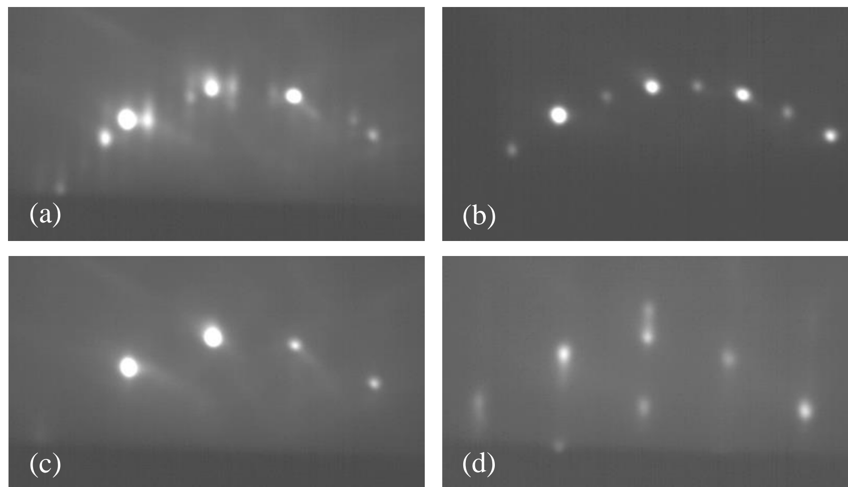

Figure 5.2: *RHEED patterns at different stage of the growth process: (a) after growth of a GaAs buffer layer at 600°C substrate - a (2×4) reconstructed surface, (b) after cooling down the substrate to 510°C – a c(4×4) reconstructed surface, (c) after deposition of 5 cycles of InAs (0.6 ML), and (d) after deposition of 16 cycles of InAs (1.73ML) – a spotty pattern due to 2D-3D growth transition.*

After growth of QDs, a 30-second break is provided while keeping the substrate at 510°C to anneal the sample. This reduces the inhomogeneous size broadening of the QDs via the Ostwald ripening process [73, 74]. Then the substrate temperature is rapidly lowered down to 485°C and 8 nm thick GaAs capping layer is grown. The temperature is lowered to avoid In desorption and to suppress the interdiffusion [10, 75]. Alloying is present at these growth temperatures (>400°C) [72, 76, 77] with non-homogeneous alloy composition and an In concentration gradient present from the apex of the QD to its base [78]. This happens due to In surface segregation and In-Ga intermixing. The GaAs cap layer isolates the QDs from the electronic surface states. In next step, the substrate temperature and As flux are increased to normal growth parameters. At the end of the growth process, uncapped surface QDs are grown in a similar way for structural analysis. After growth of QDs, the substrate temperature is lowered down to 300°C and sample is transferred from the main chamber to the preparation chamber. A schematic sketch of the growth process is shown in Figure 5.3. The buried InAs QDs are used for optical characterization and surface QDs are used for structural characterization. The surface QDs do not contribute to the optical emission due to a large number of surface states present at the surface.

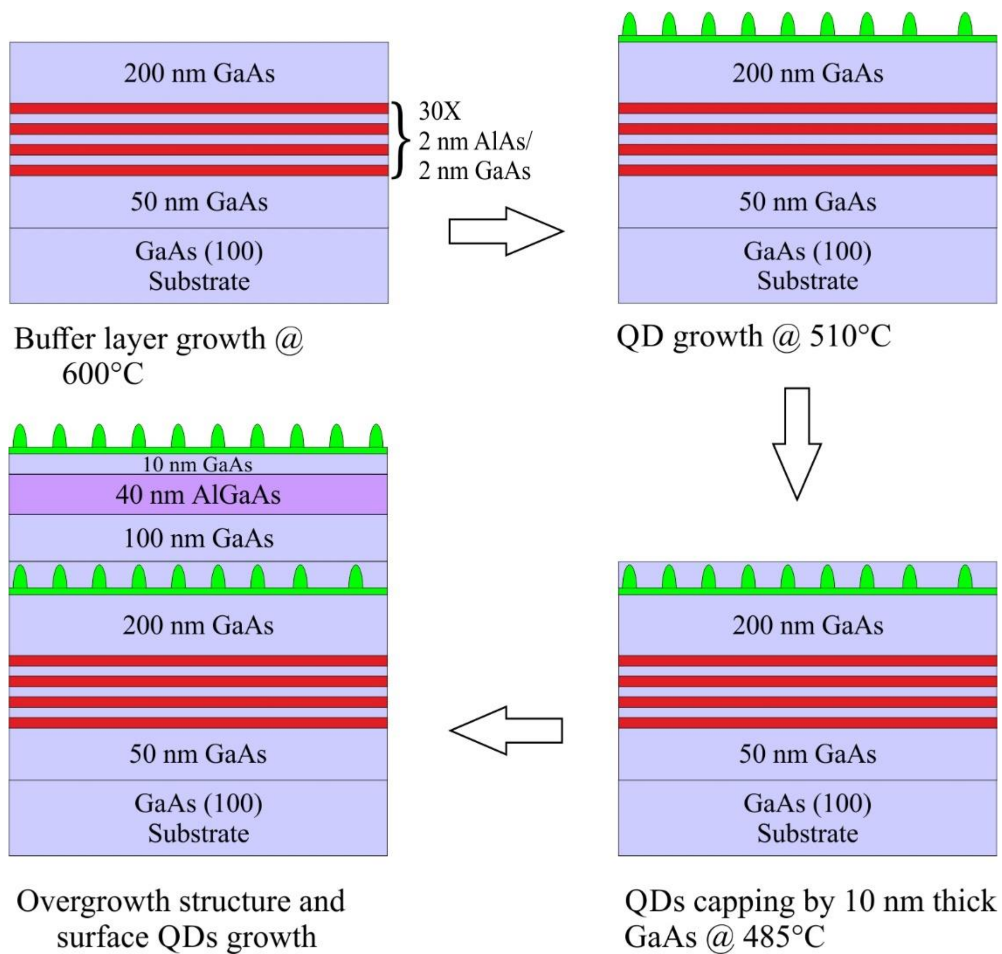

Figure 5.3: *Schematic process of InAs QDs growth on GaAs(100) substrate.*

5.3 Quantum Dots Characterization

QDs are morphologically and optically characterized by atomic force microscopy (AFM) and photoluminescence (PL) spectroscopy. In morphological characterization QDs density, size and height distribution are measured. In optical characterization PL spectra of QDs are measured.

5.3.1 Morphological Characterization

In this section, the morphological characterization of InAs QDs is summarized. The density of QDs for 1.73 ML InAs deposition with the growth parameters used in this work is around 4.0-5.0×10^9 QDs / cm^2 and it varies sample to sample in the range of 10% due to growth temperature and flux fluctuations. In this growth temperature range, the desorption of Indium fluctuates exponentially. The height of QDs is in the range of 6-8 nm.

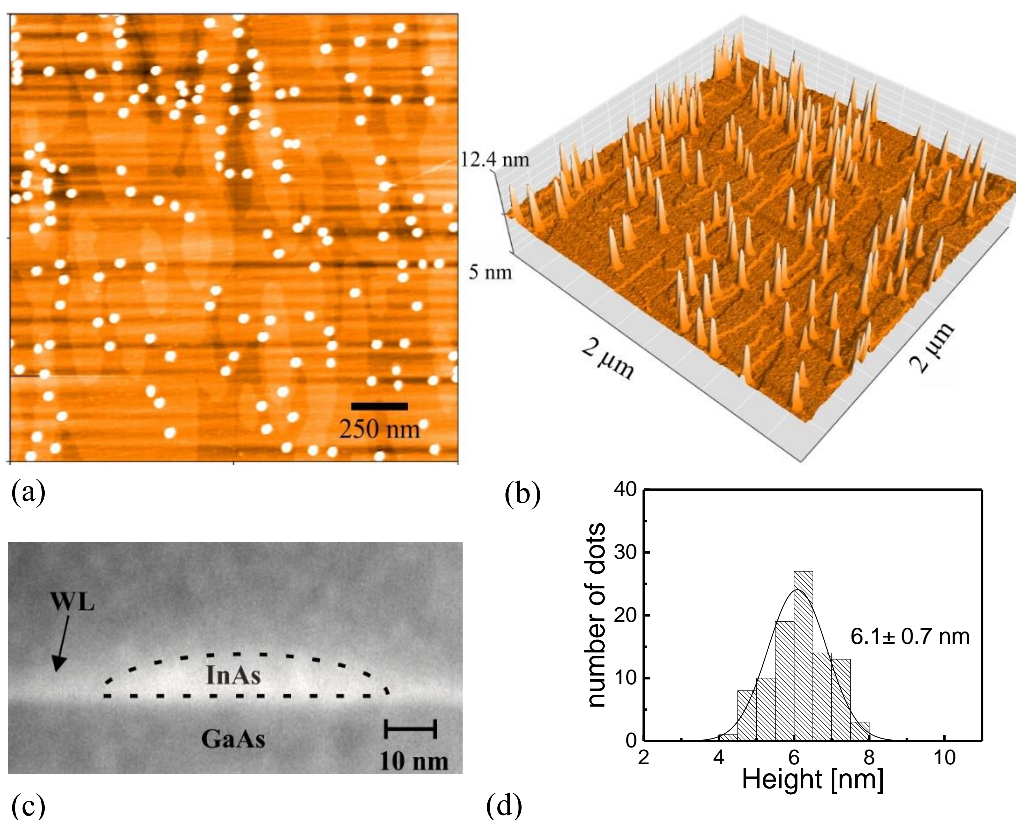

Figure 5.4: *(a) shows a 2D AFM view of surface QDs, the density of QDs is 4.0×10^9QDs/cm^2, (b) shows a 3D AFM view of the dots, and (c) TEM image of a single InAs QD and (d) shows the height distribution of these QDs, the average height of the dots is 6.1 nm*

Figure 5.4(a) shows a 2D AFM image of InAs QDs grown on GaAs(100). The scanned area is 2×2 μm^2. The density of QDs is 3.5±1×10^9 QDs / cm^2 and it may vary slightly from sample to sample in the range of ±10%. Figure 5.4(c) shows TEM image of a single QD buried in GaAs matrix. The InAs QDs are lens shaped and have a base diameter in the range of 25-35 nm. Figure 5.4(d) shows height distribution of these QDs. The mean height of the uncapped QDs is 6.1 ± 0.7 nm. Typical size distribution widths are in the range of 5-10 % of the mean QD size. The low growth rate (0.027ML/sec) and growth interruption method provide better size homogeneity. The volume of QDs is higher than the deposited additional InAs material after WL which indicates the migration and In-Ga intermixing [77, 79]. The WL thickness also increased during overgrowth process.

The growth of InAs QDs is also very sensitive to the GaAs surface quality. Surface with surface defects or mounds (long terraces on the surface with a height of 10-20 nm) would not allow random distribution of QDs on the surface. The QDs nucleate around the defects or along the mounds due to high surface energy. Figure 5.5(left) shows an AFM images of InAs QDs clustered around oval defects on GaAs(100). These oval defects are mainly due to chamber impurities or excess gallium. Figure 5.5(right) shows AFM image of 2 × 2 μm^2 area where oval defects are marked with red color ovals.

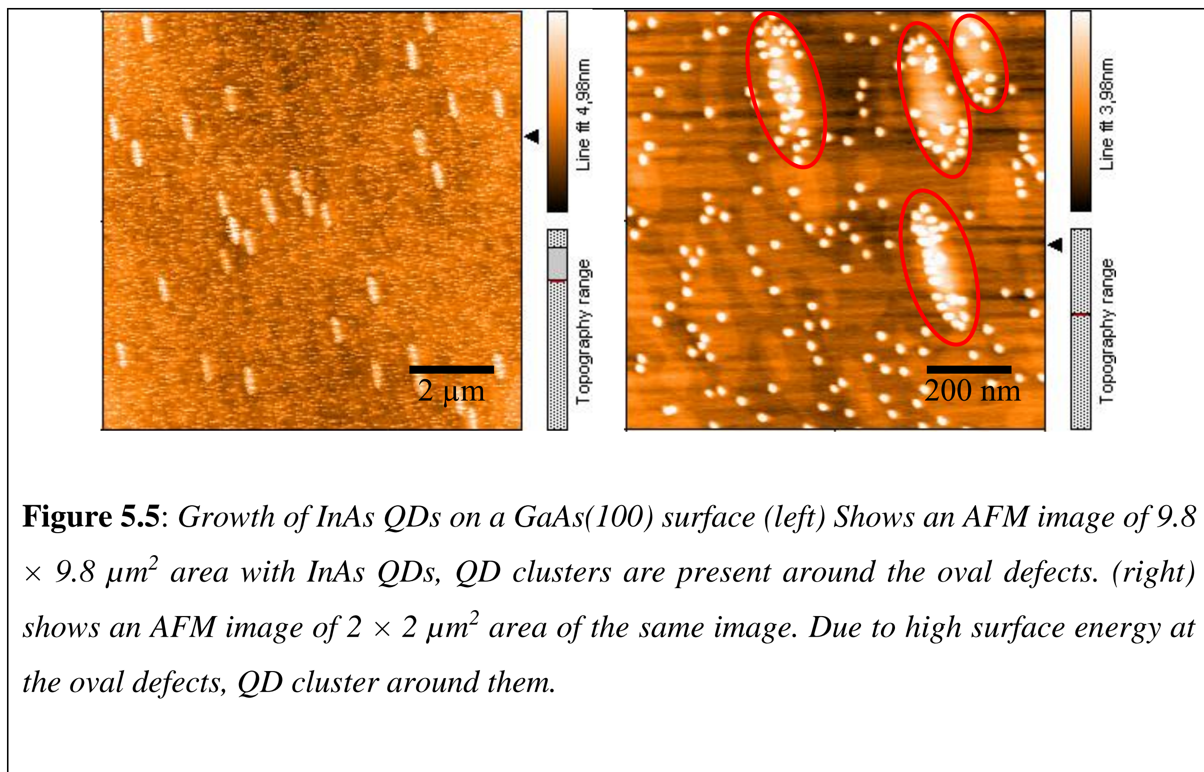

Figure 5.5: *Growth of InAs QDs on a GaAs(100) surface (left) Shows an AFM image of 9.8 × 9.8 μm^2 area with InAs QDs, QD clusters are present around the oval defects. (right) shows an AFM image of 2 × 2 μm^2 area of the same image. Due to high surface energy at the oval defects, QD cluster around them.*

The density and size of QDs depend on different growth parameters such as growth temperature, In amount and As to In flux ratio. In amount is one important parameter for QD density control. In order to see the effect of In amount on QD density, different samples have been grown with different cycle numbers. The quantum dot density increases rapidly with increasing In amount. At a very high In amount (> 3ML), large coalesced islands form on the expanses of QDs [80]. In our MBE system, the dot density changes one order of magnitude within 0.1 ML above the critical thickness. Figure 5.6(a-e) shows AFM images of surface QDs grown with different In amount. At a very high amount of In (4 ML), large InAs islands are formed as shown in Figure 5.7(a). The height of such islands is around 20 nm. At 17 cycles (1.84 ML) the dot density is around $2.0\times10^{10}/cm^2$ while at 16 cycles (1.73 ML) the dot density is around $4.3\times10^{9}/cm^2$. At 15.5 cycles (1.68 ML) the density is around is below $1.0\times10^{9}/cm^2$

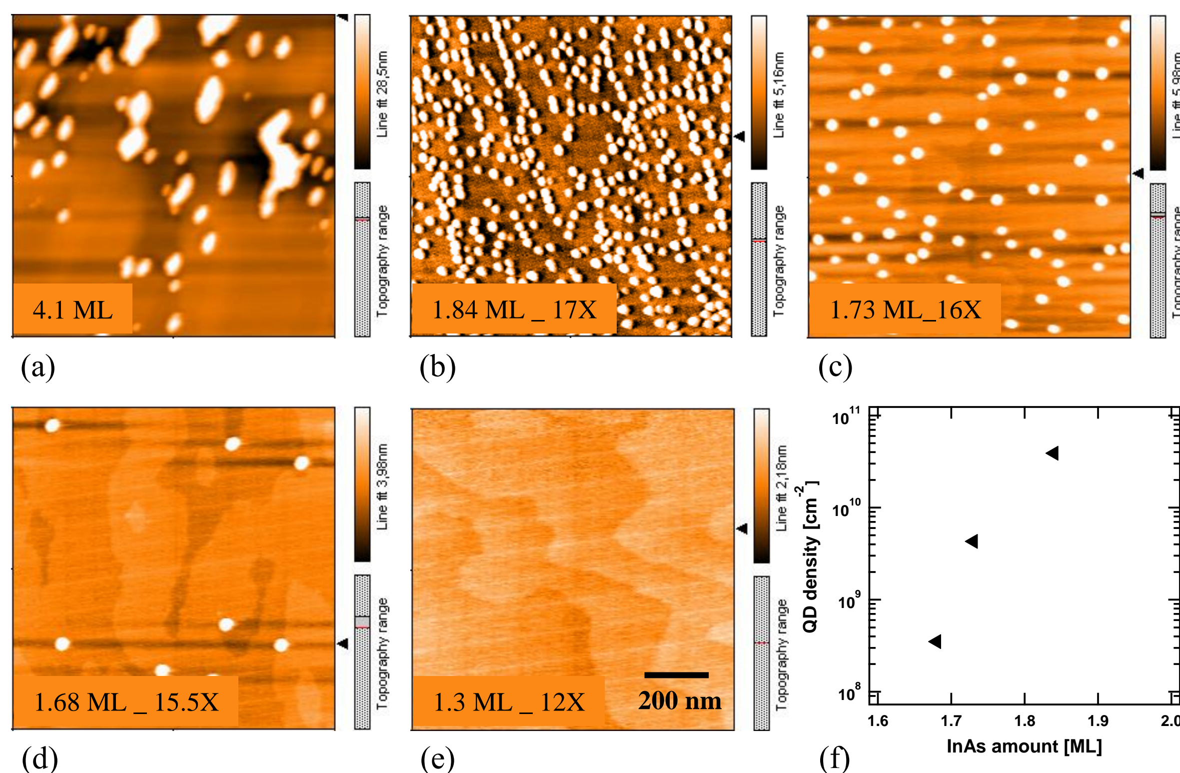

Figure 5.6: (a-e) *AFM images (1×1 μm^2) of InAs QDs grown on GaAs(100) substrate with different In amount, (a) grown with 4 ML; QDs coalesced and large island forms, (b) grown with 1.84 ML(17 cycles); QD density is 4.2×10^{10}, (c) grown with 1.73 ML (16 cycles); QD density is 6.8×10^{9}, and (d) grown with 1.62 ML; QD density is 1.0×10^{9}, and (e) grown with 1.30 ML (12 cycles); no QDs growth, and (f) shows density of QDs as a function of InAs amount deposited.*

as shown in Figure 5.6(c) and at 12 cycles (1.30 ML) flat InAs surface is observed as seen in Figure 5.6(e). It has been concluded that the critical thickness is around 1.7 ML for InAs on GaAs(100) substrate at 510°C in our MBE system. Figure 5.6(f) shows the density of QDs as a function of InAs amount. For single dot spectroscopy experiments, low density QDs ($\leq 10^8/cm^2$) is desired. In section 5.4, growth of low density QDs has been described.

5.3.2 Optical Characterization

The optical properties of the dots are characterized by PL spectroscopy. The measurements are performed in the confocal PL setup, described in Chapter 3. The QD excitation is done by semiconductor laser source of a wavelength of 635 nm (1.95 eV).

The room-temperature (RT) and low-temperature (8K) PL spectra of a normal QDs sample are shown in Figure 5.7. Due to relatively high QD density, multiple QDs are excited (10^2-10^3 QDs), because of that we observe the luminescence of a QD ensemble. Even though the electronic transitions in the single QD are very sharp (typicall<10 μeV FWHM). The QD size, shape and composition varies from dot to dot. Thus every dot emits at a slightly different

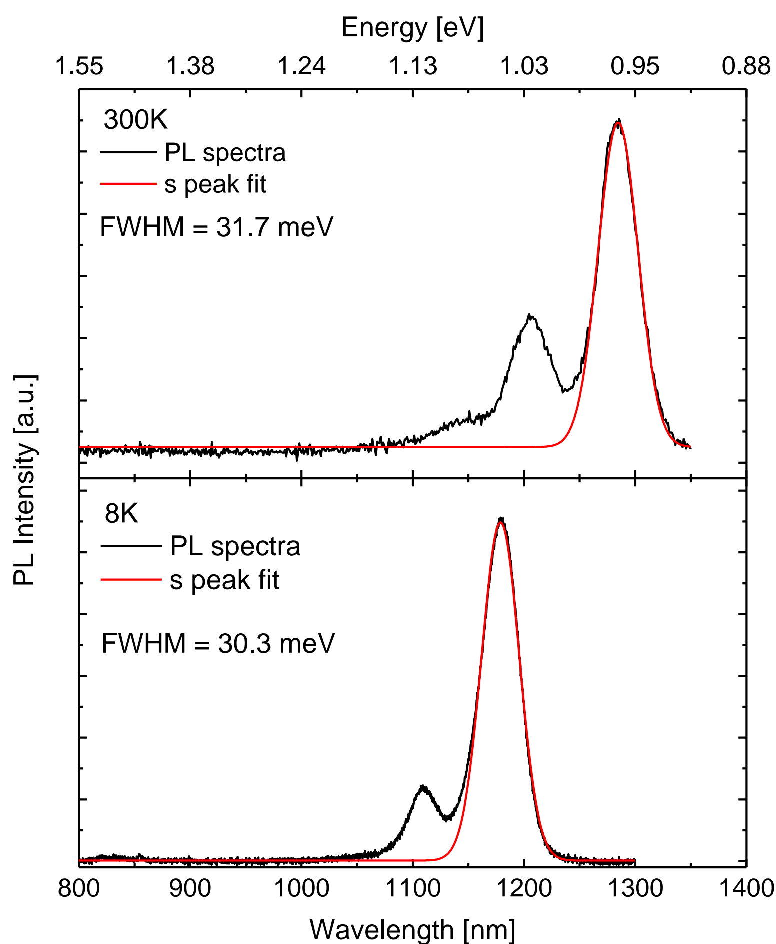

Figure 5.7: *PL spectra of an InAs QD ensemble embedded in a GaAs matrix at 0.045mW laser power. The QDs show ground state emission at 1284.65 nm (0.965 eV) with FWHM of 31.7 meV at RT. At 8K, the ground state emission is at 1178.88 nm (1.053 eV) with FWHM of 30.3 meV.*

.

wavelength which leads to the broadening of the PL spectra when the ensemble is measured. This effect is known as inhomogeneous broadening. At room temperature, the ground state emission (s-peak) appear at 1284.65 nm with an emission linewidth with a full width at half maxima (FWHM) of 31.7 meV as shown in the upper part of Figure 5.7. At low temperature (8 K), the ground state emission appears at 1178.88 nm with FWHM of 30.3meV as shown in the lower part of Figure 5.7. The peak position is shifted as expected from the temperature dependence of the band gap of InAs [14]. Due to the high quality of grown material, the FWHM does not change much after cooling down the sample.

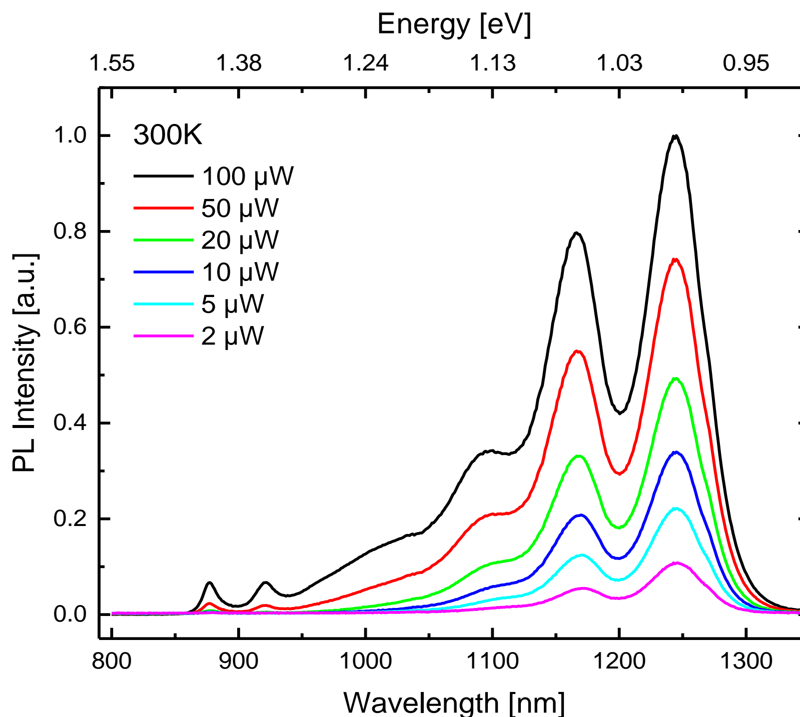

Figure 5.8: *Photoluminescence spectra of a self-assembled InAs QD ensemble at room temperature for different excitation powers. High laser excitation power stimulates emission of the higher order confined states.*

Figure 5.8 shows the excitation power dependent PL spectra of an InAs QD ensemble (#A0071), where different shells can be excited by increasing the power of the laser. At low optical excitation power, a few electron-hole pairs are created, which relax into ground state and first excited state so the only emission from ground state and first excited state is observed. With increasing excitation power, emission from higher quantized states (up to the 4th state) is observed due to state filling. At very high power, also emission from the bulk GaAs and InAs

wetting layer (WL) is observed. The lateral quantization of QDs electronic states provides multiple different shells (s, p, d, f, ...), with a nearly constant energy separation between them. In such an ensemble, an inhomogeneous broadening due to shape, size and composition is smaller than the lateral quantization energy i.e. an emission line width for ground state is smaller than the interlevel energy spacing.

The optical properties of QDs are also very sensitive to the growth parameters such as growth temperature, As to In flux ratio and growth rate of InAs etc. Figure 5.9 shows the effect of As to In flux ratio on the PL spectra of a QD ensemble. At lower As to In flux ratio (As/In≈115), the PL spectrum a QD ensemble is shifted towards the higher energy, which is attributed to stronger intermixing of Ga in InAs [71].

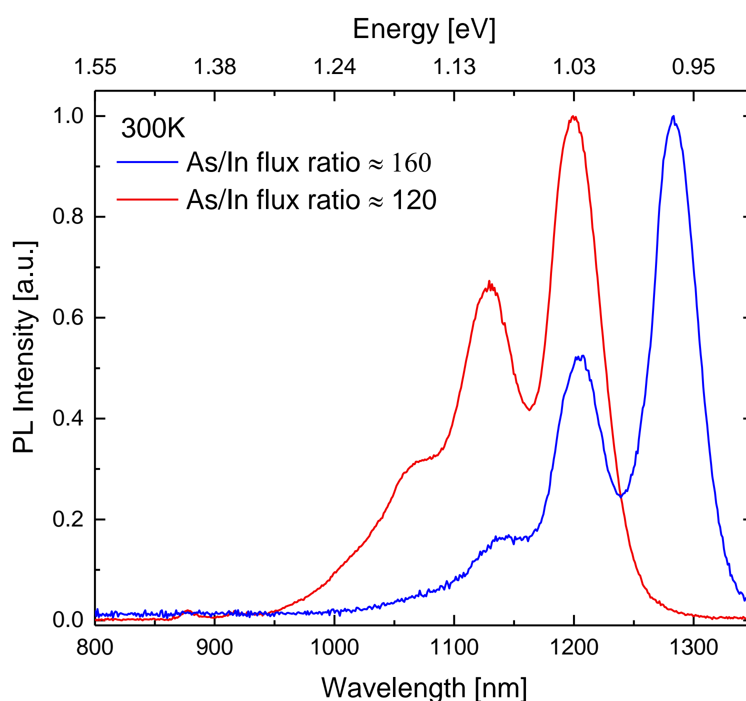

Figure 5.9*: Room temperature PL spectra of QD ensemble of two different samples grown at different As(Arsenic) to In (Indium) flux ratio.*

At higher growth rates of InAs, the QDs show a large shift in PL spectra towards higher energies, which is attributed to the smaller size of QDs and In-Ga intermixing [81]. In this case the inhomogeneous broadening of the QD ensemble is so large that the different excited states can not be resolved in PL spectrum. In Figure 5.10(left), the room temperature PL spectra of

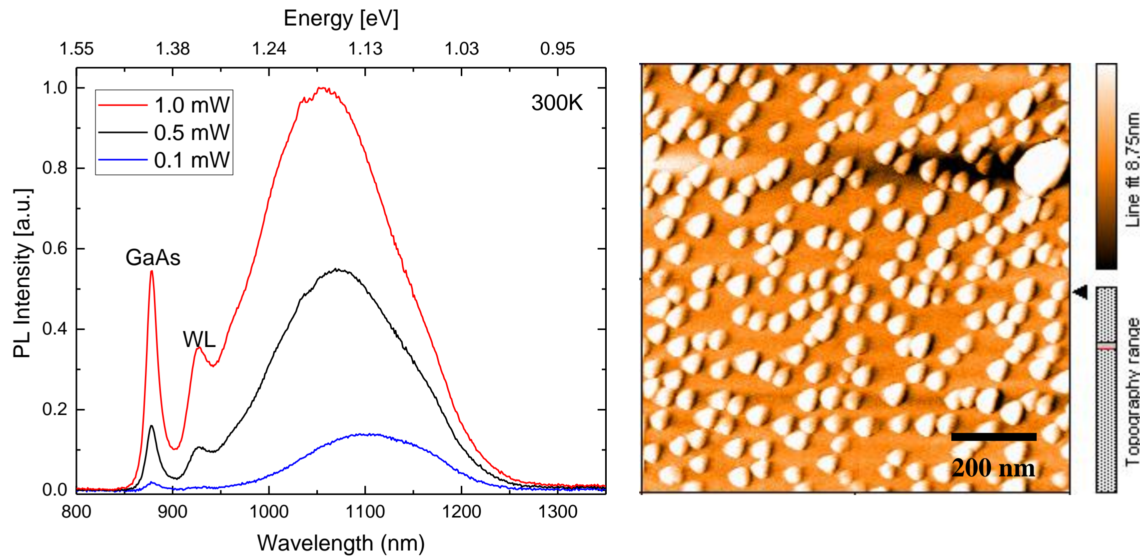

Figure 5.10: *(left) A normalized room temperature PL spectra of InAs QD ensemble at different excitation power, (right) AFM image of surface QDs. The scanned area is 1×1 μm^2. The average height of such QDs is 5.5±.5 nm and diameter is 35±2 nm. The triangular shape of the dots is due to tip art effects.*

InAs QD ensemble measured at different excitation powers are shown. These QDs are grown 25% higher growth rate (0.0375ML/sec.) than the normal growth rate (0.027ML/sec.) of InAs. The QDs are grown by growth interruption method where 12 cycles are needed to deposit 1.8 ML of InAs. In Figure 5.10 (right), an AFM image of such QDs is shown. The average height of such QDs is 5.5±0.5 nm and average diameter is 35±2 nm. These QDs are smaller due to the high growth rate which reduces the In surface diffusion. At higher growth rate, large coalesced island is also observed as shown in the top right corner of the Figure 5.10(right).

5.4 Growth of Low Density QDs

The electrical and optical properties of single QDs have attracted strong interest in the field of quantum information technology [69]. For that low density QDs (≤ 10^8/cm^2) are desirable in single dot based different optical and electrical experiments where a dot does not interact with the nearby dots. It is desirable to grow samples with low QD densities (≤10^8/cm^2) rather than using lithography techniques for defining small mesa structures (≤ 0.2 µm) or shadow mask process [82] which may introduce defects during the post-growth process in the structures. In the case of InAs QDs growth on GaAs(100) by Stranski-Krastanov growth method, the QD density increases from 0 to 10^{10} /cm^2 at the critical point for the transition from 2D to 3D growth mode. In such a growth process, the density can be controlled by substrate temperature or by InAs amount in the range of 10^{11}-10^9 /cm^2 but not lower than that. The formation of self-assembled InAs QDs is a first order phase transition like process. Due to this, to grow low density QD sample is difficult [66]. There are different approaches to grow low density quantum dots, i.e. In(Indium)-gradient approach [17, 18], temperature gradient approach [83], annealing approach [19, 20, 21], droplet phase epitaxy [84] and pre-patterning approach. In this thesis work, to achieve reproducible low density QDs In-gradient approach and pre-patterning approach are used. The pre-patterning approach is discussed in Chapter 7.

5.4.1 In-gradient Approach: Growth

In our MBE system, most of the effusion source cells are radially arranged (tilted by an angle of 40° from the perpendicular substrate axis). For such positioned effusion cells, the Mote Carlo simulation of flux distribution is shown in Figure 5.11a (from MBE Komponenten GmbH) over the substrate during stationary condition. In this figure each circle represents 10% change in the flux and red circle in the centre indicates the area covered by 3” substrate. Figure 5.11b shows the flux distribution at the 3” substrate. For a ¼ 3” wafer as shown in Figure 5.11b, approximately 10% of the flux difference is present between point A to point B. This produce a gradient in the growth rate at the substrate surface. This gradient during growth of heterostructure can be compensated by rotating the substrate with constant angular velocity. This standard gradient growth process can be utilized to grow low density QDs.

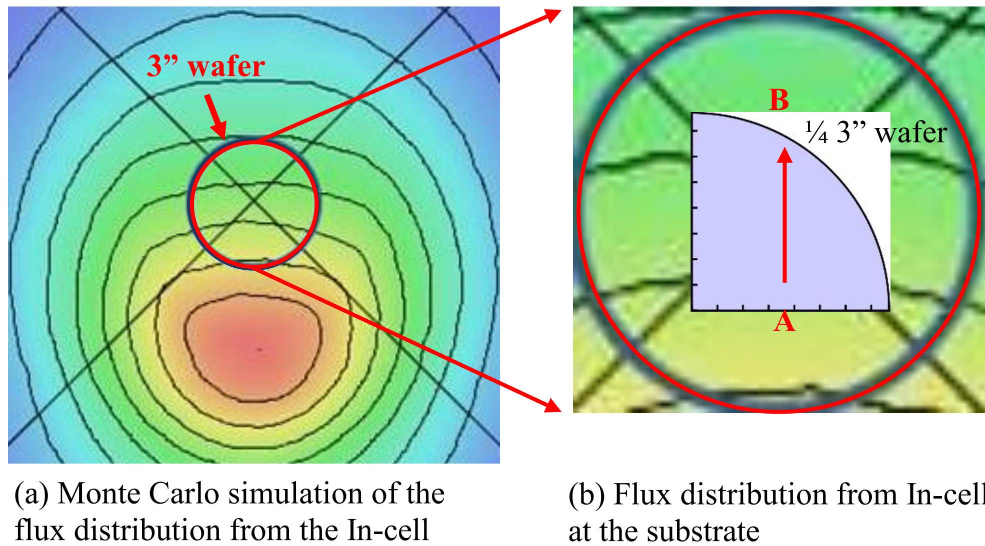

(a) Monte Carlo simulation of the flux distribution from the In-cell

(b) Flux distribution from In-cell at the substrate

Figure 5.11: *(a) Monte Carlo simulations of the flux distribution on a stationary substrate from the In-cell. Each black circle indicates 10% change in the flux and the red circle in the centre shows the position of the substrate. (b) shows the flux distribution over the substrate. A schematic of ¼ 3" substrate is shown in the centre of the image.*

In this approach, the substrate rotation is paused during deposition of InAs which results in an inhomogeneous deposition of Indium across the substrate. Figure 5.12(a) shows the In cell alignment in our MBE growth chamber and Figure 5.12(b) shows schematic of InAs coverage during substrate rotation growth (top) and without substrate rotation growth (bottom). Due to inhomogeneous deposition of In without substrate rotation, there is an InAs QDs density gradient over the substrate. By controlling the In amount, the position of the low density region on a quarter wafer can be adjusted.

After growing the buffer layer, the substrate temperature is lowered down to 510°C and substrate rotation is paused. The substrate is aligned to the [011] direction along the In-cell gradient. In contrast to the normal QDs growth process, described previously in this chapter, the substrate position remains fixed during the entire process of In deposition. After that, substrate rotation is started and the remaining structure is grown. Again, on the top of the surface, surface QDs are grown, similarly as discussed above for structural analysis. The major advantage of this process is that there is no additional *ex-situ* processing (lithography, etching and cleaning) required which may degrade the quality of QDs. The limitations of this process is that only a small fraction of wafer can be used for the single dot experiments.

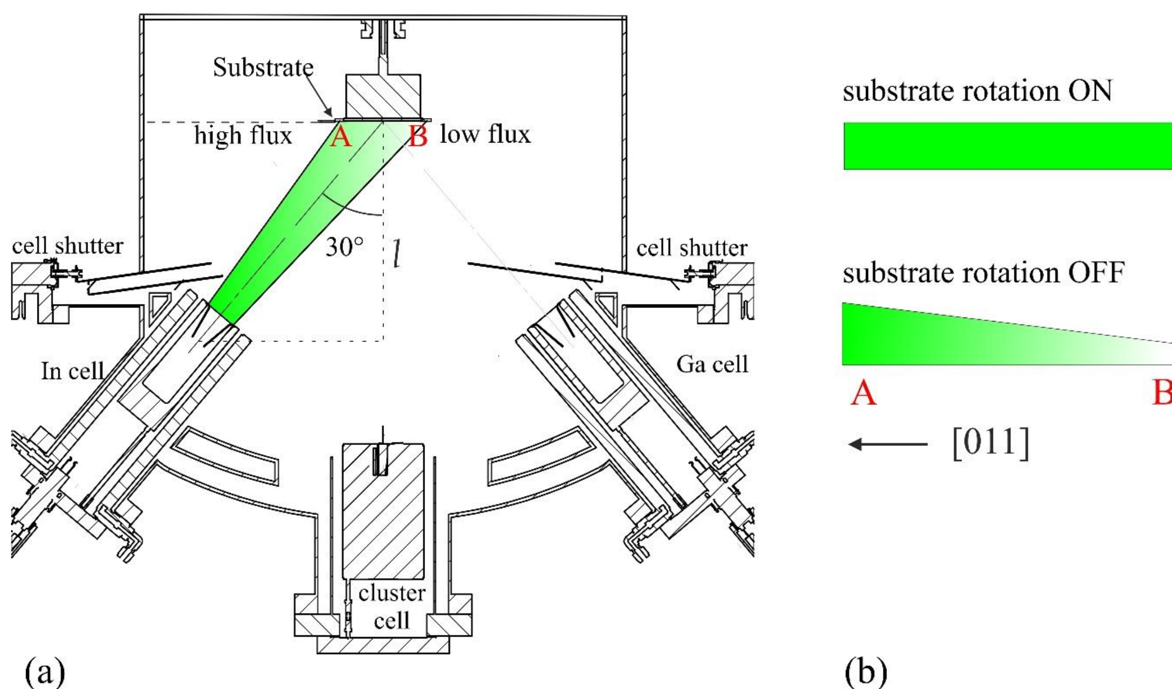

Figure 5.12: *(a) Schematic sketch of MBE growth chamber with In cell geometry for In-gradient approach to grow low density QDs, (b) schematic of InAs thickness profile with substrate rotation and without substrate rotation deposition*

5.4.2 In-gradient Approach: Characterization

After growing the QD sample with gradient approach, *ex-situ* AFM and PL spectroscopy are employed to characterize the QDs structurally and optically, respectively. AFM is employed to see the QDs density variation on the sample along the gradient axis.

In Figure 5.13, we see the schematic of the sample structure, wafer sketch and AFM images. On the wafer sketch, different positions are marked with black squares where AFM is performed. Figure 5.13(a) and (b) are corresponding to the high-density area where the density of QDs is in the range of 10^{09}-10^{10}/cm^2. The density at high density positions varies by 20% from sample to sample. In Figure 5.13(c), the density of QDs is around 5.5×10^8/cm^2 or less, this is the transition area. In Figure 5.13(d), only a smooth InAs WL is present. The region between image (c) and (d) is the low-density region and suitable for the single dot spectroscopy. The position of the low density area is reproducible within 2-3 mm from growth run to growth run. The height of QDs also increased along the gradient direction. At high density site the height of QDs is 6 nm and at low density site it is 10 nm.

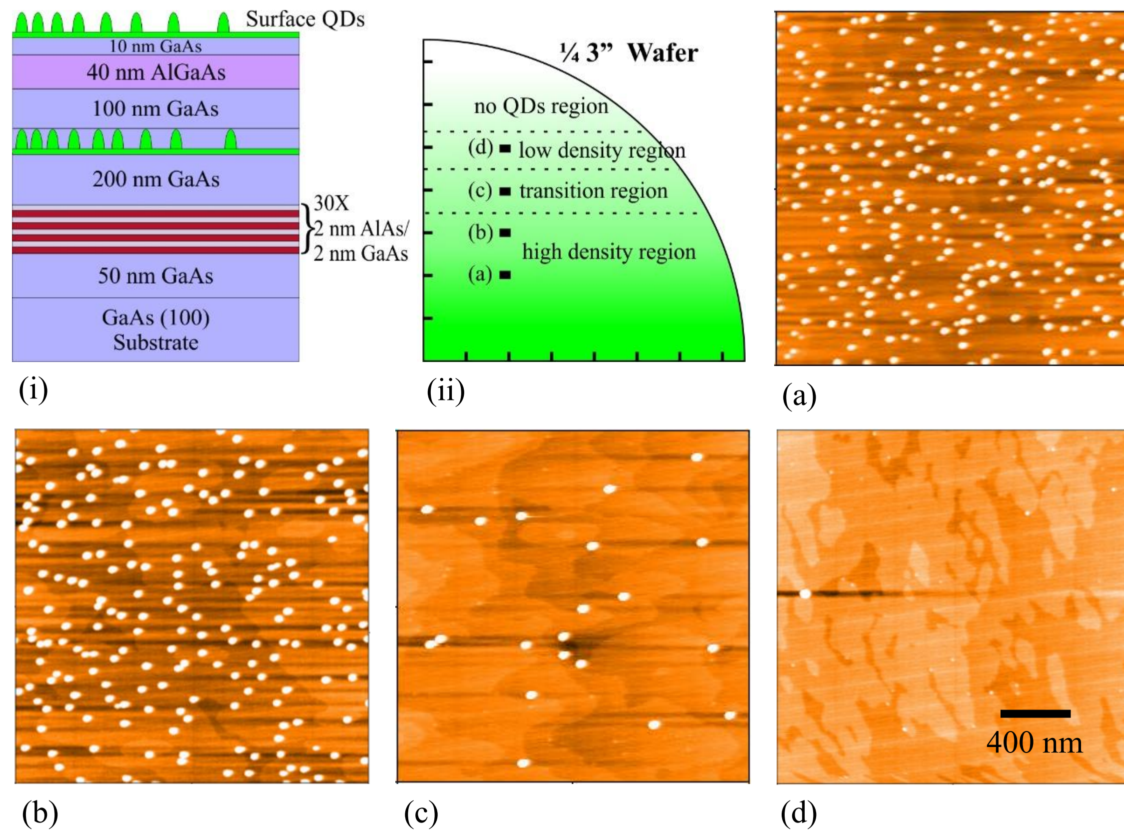

Figure 5.13: *(i) Schematic of a sample structure for low density approach and (ii) ¼ 3" wafer sketch with marked positions where AFM measurements are performed, (a) & (b) shows the AFM image of surface QDs at high density site (6-4 × 10^9/cm^2), (c) shows AFM image at transition region where density is 5.5 × 10^8/cm^2, and (d) shows AFM image at low density region (2.5 × 10^7/cm^2).*

PL spectra of the buried QDs grown with gradient approach are shown in the Fig. 5.14. PL measurements are performed at various positions on the sample along the In-gradient axis. The positions a, b,c, and d corresponds to Figure 5.13(ii).The ground state emission of these QDs is around 1250 nm at room temperature. The ground state peak intensity of the QDs is approximately proportional to the QD density which decreases along the gradient direction and vanishes at the detection limit due to very low density (< 10^8 /cm^2). As the density decreases, the PL signals from WL and GaAs increases. At low density area, the density of QDs is not enough to recombine all the carries in the QDs so the carries tunnel to WL and GaAs and recombine there. At very low density QDs area, only WL and GaAs peaks are observed because maybe we are not sensitive through to see QDs at density 1×10^8/cm^2 or lower. The area between point (c) and (d) is suitable for single dot based experiments.

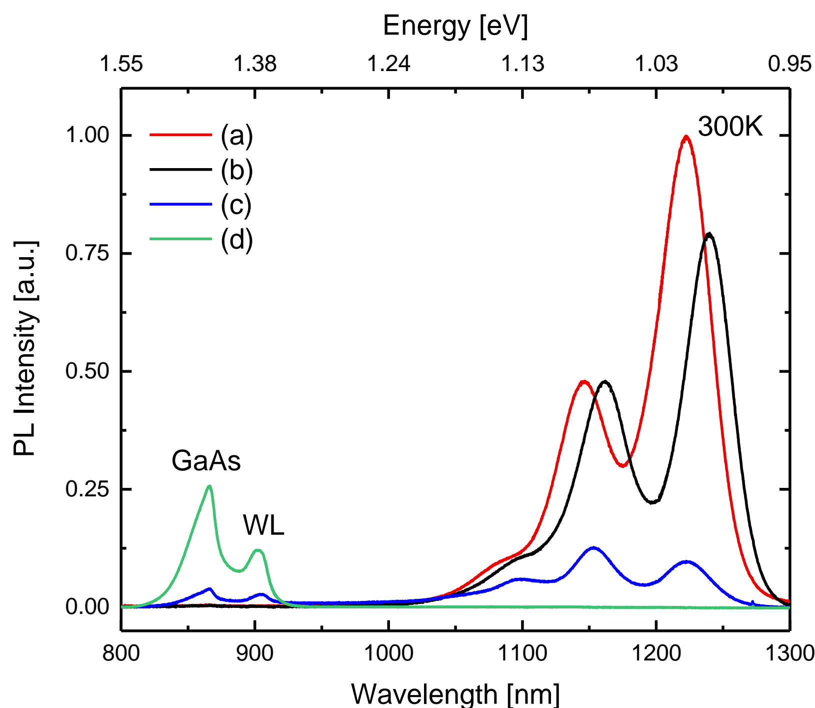

Figure 5.14: *PL spectra of InAs QD ensemble embedded in a GaAs matrix on GaAs (100) substrate at room temperature. QDs are grown with gradient (rotation of substrate paused). Positions a, b, c, and d corresponds to Figure 5.13ii.*

Figure 5.15 shows PL spectra of QDs grown with gradient approach with 17 cycles. PL spectrum at various positions along the gradient axis is measured. Inset shows the schematic of wafer sketch with marked positions where PL measurements are performed. The position of the low density QDs shifts towards the edge of the sample due to higher amount of InAs. The red shift in the PL specta along the In-gradient axis is attributed due to the QDs height. Along the In-gradient axis, the QDs height increases from 6 nm at high density area to 10 nm at low desnity area as observed by AFM measurements for uncapped QDs. Similar effect also assumed for the embedded QDs.

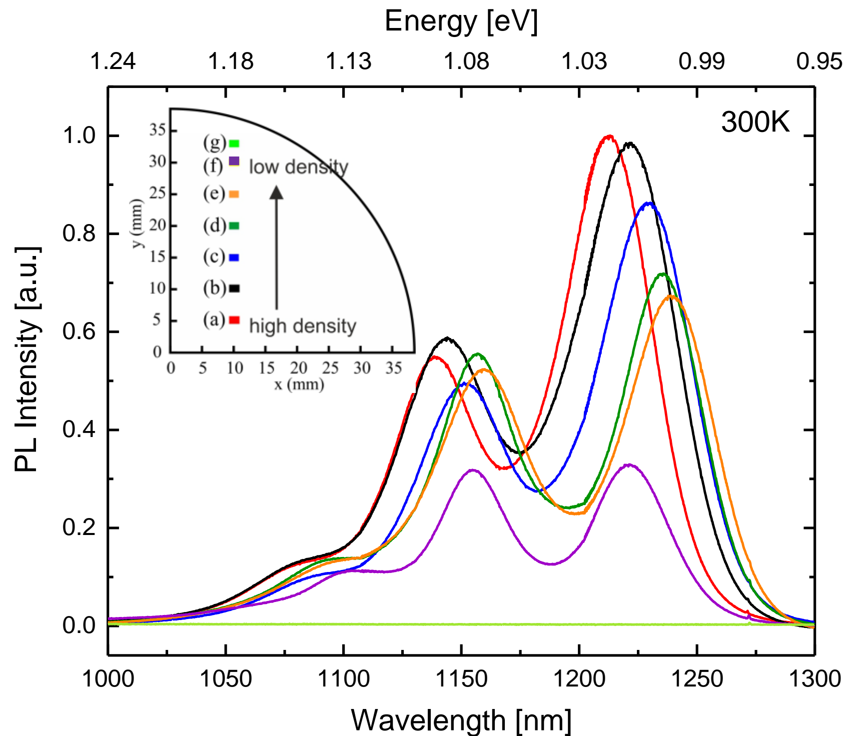

Figure 5.15: *PL spectra of InAs QDs at room temperature grown with gradient approach. The PL spectra show redshift along the gradient direction due to the presence of slightly high arsenic pressure. The inset shows a sketch of ¼ 3" wafer with marked positions where PL spectra are recorded.*

In summary, the In-gradient technique is used to grown low density QDs (≈1 × 10^8/cm^2). AFM and PL techniques are used to find the low density position on the sample. In this approach only small area (5-8 mm slice on the substrate) is covered with low density, the remaining area is covered with high density QDs or no QDs. For single dot based experiments, QDs have been grown in desired heterostructures and delivered to the different research groups for further investigations. The limitation of this method is that only a small fraction of the wafer is useful for single dot experiments.

5.5 Emission Energy Tunning

The optical and electrical properties of QDs depends on their size, shape and composition. By modifying these properties, one can modify their optical and electrical properties. The ground state emission (s-peak) of one as-grown InAs QDs are around in the range of 1250-1300 nm at room temperature. The Si-based efficient photo-detection technique loses their sensitivity above 1100 nm, to overcome this issue the emission from QDs is desired in the range of 900-1000 nm. To tune the emission energy of QDs, different approaches are used such as In-flush technique [85, 86, 87], Ga-intermixing in InAs [22], by strain layer incorporation in the structure [88, 89] and rapid thermal annealing [90, 91]. In this thesis work In-flush technique and Ga-intermixing approaches are used to tune the emission range of QDs.

5.5.1 In-flush Technique

The optical properties of SAQDs can be tuned by adjusting their height. By altering the height, the quantization potential changes and so as the energy states. The height of QDs is defined by GaAs capping layer thickness (d_{QD}). In normal QD growth process, d_{QD} is approximately 8 nm. In this process the QDs are partially capped (d_{QD} < 8 nm) and uncapped part is desorbed from the surface by heating the substrate in presence of excess arsenic. In this way the height of QDs is finely tuned. This process is known as In-flush technique. This process is also known as partial capping and annealing (PCA) technique [92]. Previously, this technique is developed to obtain homogeneous QDs height for narrower emission for fabrication of QD lasers [86].

The In-flushing technique can be described in four steps as shown in Figure 5.16. After growth of QDs at 510°C, the substrate temperature is rapidly lowered by ≈ 25°C to avoid any In desorption and GaAs capping layer of defined thickness d_{QD} is grown as shown in Figure 5.16(a). The step is known as partial capping of QDs. In next step, the uncapped part of QD is flushed by increasing the substrate temperature to 600°C within 2 minutes. Arsenic is also increased from 1.5×10^{-5} *mbar* to 2.0×10^{-5} *mbar*.to avoid any damage to GaAs surface. This step is shown in Figure 5.16(b). Because at high temperatures, InAs QDs are not stable and uncapped part is desorbed. During this step, In-Ga intermixing happens and due to that the QDs lateral dimensions also changed. The thickening of WL is also observed due to In-Ga intermixing. After that at the final step, GaAs or remaining heterostructure is grown as shown in Figure 5.16(d)

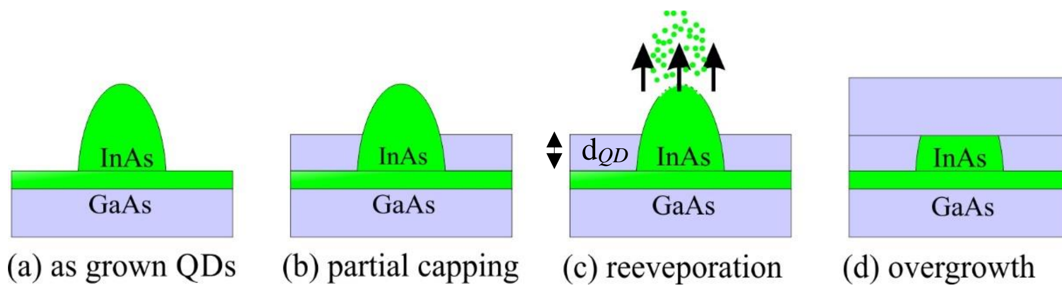

Figure 5.16: *Schematic of In-flush technique (a) a self-assembled InAs QD, (b) partially capping of the QD by defined GaAs thickness, (c) reevaporation of uncapped part of QDs by heating the substrate to 600°C and (d) overgrowth after flushing.*

The confinement in the growth direction becomes stronger when the QD height is decreased. This results in a large change in the band gap energy of In-flushed QDs and shifts the transition energy to higher energy. Furthermore, during the flushing step, the In-Ga intermixing occurred, which also result in even more shift in transition energy. The schematic of the confinement potential for normal and In-flushed QDs is shown in Figure 5.17, where conduction and valance band energies are drawn for in-plane and in growth direction [93].

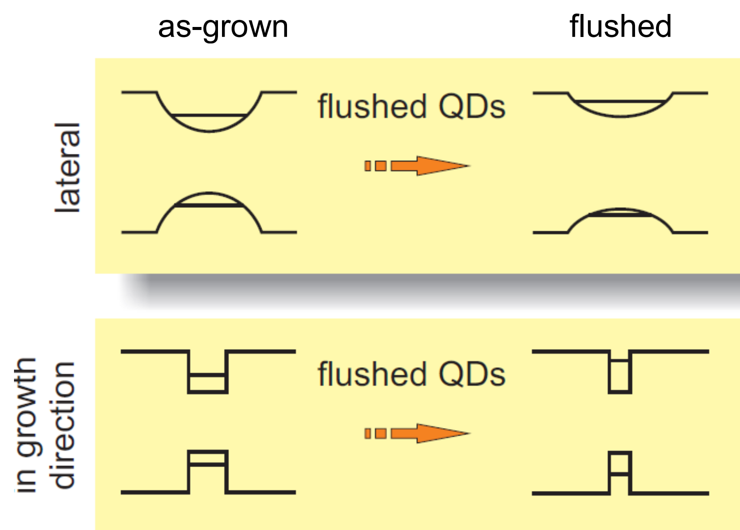

Figure 5.17: *Change in QD confinement potential induced by In-flush technique. Lateral and in-growth direction are depicted after* [93].

Figure 5.18(left) shows an AFM image of 2.3 nm flushed QDs which are overgrown with 4 nm of GaAs after flushing process. Due to the strain field from the QDs, a hump is observed on the GaAs surface during AFM measurement. The average diameter of such disks is 40 nm. Figure 5.18(right), the upper part shows cross-sectional HRTEM images of as grown QD and the lower part shows 5 nm flushed QD in GaAs matrix. The In-Ga intermixing observed at the interface of QDs and GaAs.

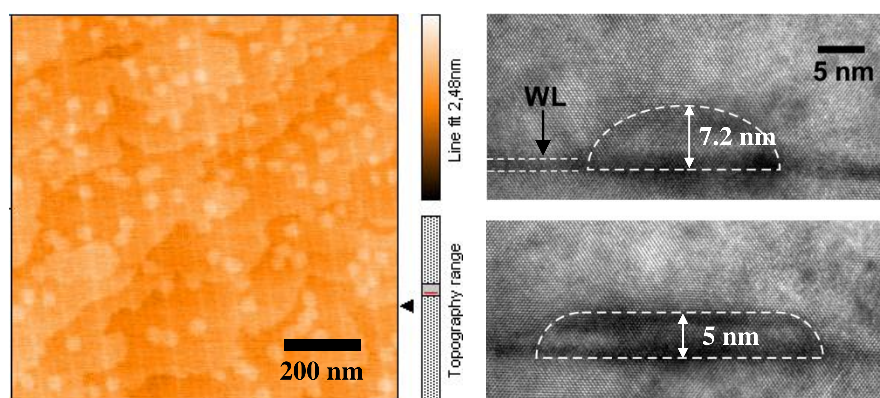

Figure 5.18*: (left) An AFM image (2 × 2 μm^2) of 2.3 nm flushed QDs capped with 4 nm GaAs. Underneath the GaAs, flushed QDs are disk shaped with average diameter of 40 nm.(right) HRTEM images of as grown QD and 5 nm flushed QD.*

The optical properties of the In-flushed sample are investigated by PL spectroscopy at room temperature. Figure 5.19 shows normalized room temperature PL spectra of InAs QDs with different capping layer thickness. A strong blue shift is observed when the capping layer thickness is decreased. At room temperature, the ground state emission of as grown QDs with 8 nm of GaAs capping layer appears at 1285 nm and with 1.8 nm of GaAs capping layer thickness appears at 950. For 2.1 nm flushed QDs, the ground state emission appears at 990 nm at room temperature, which is suitable for low temperature PL measurement using efficient Si based detection technology. It was also observed that the WL signal appears at 920 nm for as grown QDs and it shifts to 905 nm for 1.8 nm flushed QDs, which indicates the In-Ga intermixing during flushing step.

For single dot spectroscopy and to use efficient Si detection technology, In-gradient technique and In-flush technique is used. Figure 5.20 shows room temperature PL spectra of 2.5 nm flushed QDs grown with a density gradient. Inset show schematic of ¼ 3” wafer with marked positions along the gradient axis where PL measurement are performed. The low density position is present at the middle of the wafer. In the case of flushed QDs, the emission from WL and GaAs also appears at low excitation powers. This is may be due to a less deeper confining potential which allows the carriers to escape from QDs and recombine in WL and GaAs matrix.

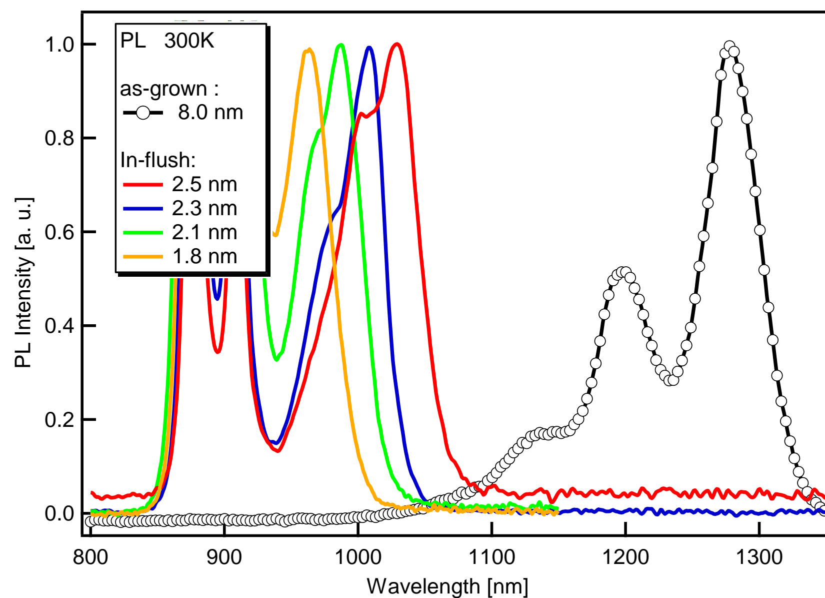

Figure 5.19: *PL spectra of InAs QD ensemble grown with different capping layer thickness (d_{QD}) at room temperature. For each sample, the spectra is normalised for ground state emission. Spectra shows blue shift with decreasing d_{QD}.*

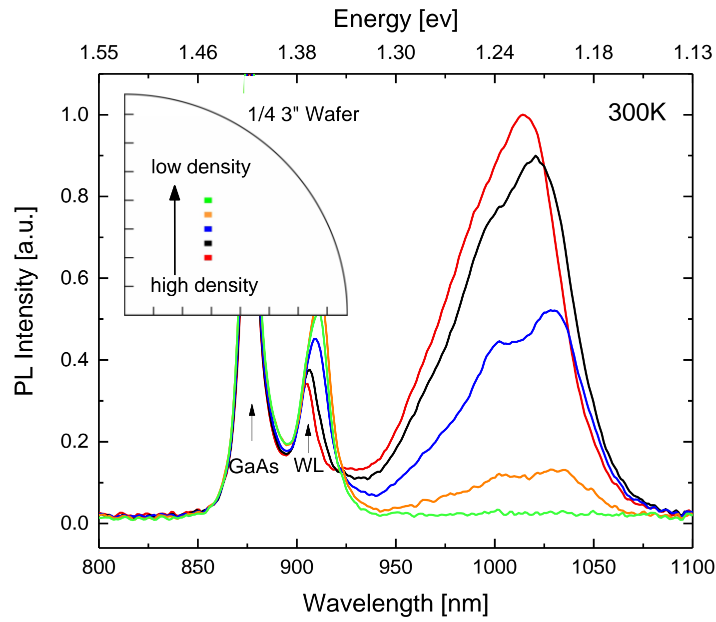

Figure 5.20*: PL spectra of 2.5 nm flushed InAs QDs at room temperature grown with In-gradient approach. Inset show schematic of ¼ 3" wafer with marked positions along the gradient axis where PL measurement are performed.*

5.5.2 Growth of InGaAs QDs

In addition to In-flush technique, the emission of InAs QDs also can be tuned by intermixing Ga into them. Such QDs are known as InGaAs QDs. These QDs are also grown to use efficient detection technology. For that, the emission of these dots should be in the range of 900-1000 nm at low temperatures. Approximately 50% of Ga incorporation in InAs QDs, shifts their ground state emission from 1285 nm to 1000 nm. Normally we can tune the emission of these dots from 1200 nm to 900 nm by varying the Ga incorporation.

The morphology and composition of QDs define their confinement potential and their electronic states. The incorporation of Ga in InAs QDs increases their effective band gap and shifts their transition energies to high energies. The main contributing factors can be addressed as:

- Ga incorporation reduces the stain in the QD
- GaAs matrix provides less deep confining potential to InGaAs QDs compared to InAs QDs
- InGaAs QDs will have larger effective band gap compared to InAs QDs
- InGaAs QDs are smaller than InAs QDs
- Decrease the electronic level spacing

5.5.3 InGaAs QDs: Growth Procedure

After growing first part of the heterostructure, the substrate temperature is decreased to 510°C and InGaAs QDs are grown. These dots also are grown by growth interruption method where for 4 seconds In and Ga is deposited and for 4 seconds interruption. The growth rate of Ga is also kept equal to In (0.027ML/sec) for QDs growth. For that another Ga source (Ga cluster cell*) is used which is mounted perpendicular to the substrate axis. The Ga incorporation during InAs growth decreases the strain in the growing film and increased the critical thickness for QD formation. For 50% Ga incorporation in InAs QDs, we need around 19 cycles for QD formation which is around 4.6 ML. So the critical thickness is increased from 1.73 ML for InAs QDs to 4.6 ML for InGaAs QDs. The transition from 2D to 3D growth is observed *in-situ* by RHEED.

The InGaAs QDs are grown for low density applications, so In-gradient approach as discussed in section 5.4 is applied during QDs growth. The schematic of the growth chamber with In cell and Ga cluster cell is shown in figure 5.21(a). During growth of InGaAs QDs, the substrate rotation is stopped and aligned [011] direction along the In cell. As seen in Figure 5.21(a), there is also composition gradient with the density gradient along the [011] direction. The aim is to grow low density quantum dot in the centre of the wafer with an emission wavelength of 930-950 nm which is achieved by adjusting In amount and Ga amount simultaneously. Figure 5.21(b) shows thickness profile of InGaAs with substrate rotation and without substrate rotation. After growth of the QDs, a 200 nm thick GaAs layer is grown at 510°C. Generally these QDs are grown in Schottky diode structure (see Appendix II) where emission of QDs can be controlled by applying external filed. At the end of the sample growth, surface QDs are also grown for morphology characterization. To avoid impurities contributions during cleaving step, final samples are grown on 3" full wafers.

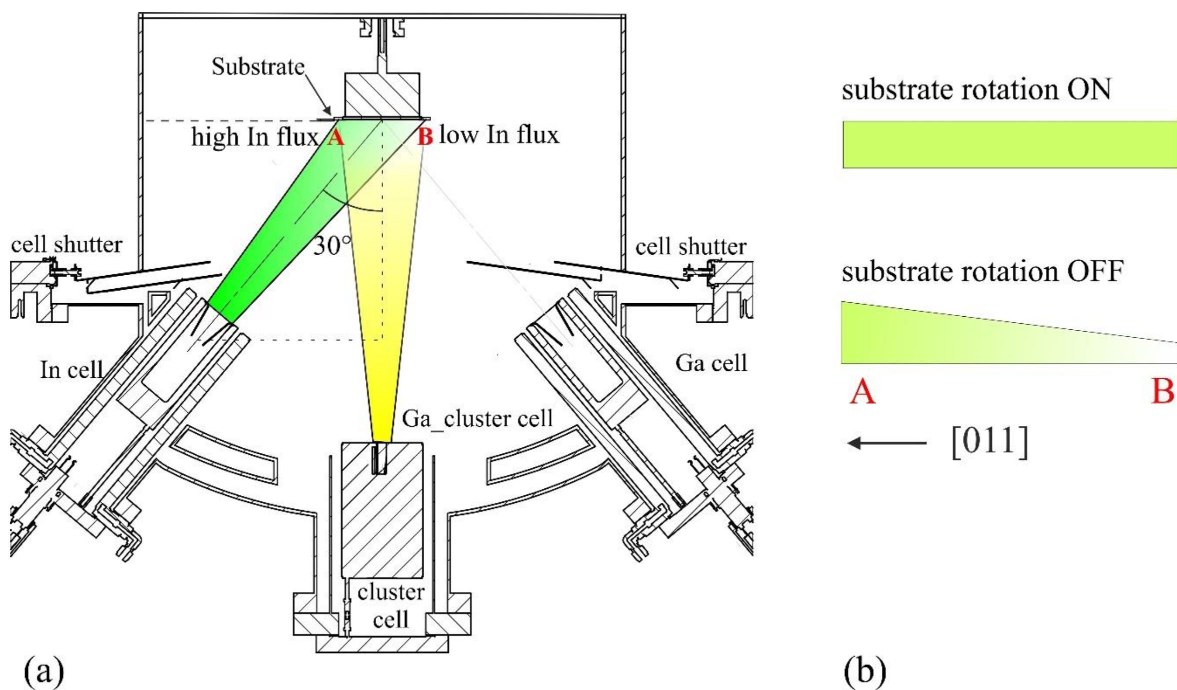

Figure 5.21: *(a) Schematic sketch of MBE growth chamber with In cell and Ga cluster cell geometry for low density InGaAs QDs growth, (b) schematic of InGaAs thickness profile with substrate rotation and without substrate rotation deposition.*

5.5.4 InGaAs QDs: Characterization

Surface QDs are also grown for morphology characterization. Figure 5.22(a-c) shows AFM images of InGaAs QDs grown with gradient approach on a 3” GaAs(100) substrate, (a) shows high density area, (b) shows low density, and (c) shows no QD area. Similar to InAs QDs, the low density position on the sample can be adjusted by varying the In and Ga amount. InGaAs QDs are smaller in height compare to InAs QDs. Figure 5.22(d) shows height histogram of InGaAs QDs. The average height of InGaAs QDs (5.0 +0.5) is smaller than InAs QDs (6.1+0.1) for high density area. Similar to the InAs QDs, InGaAs height also increases along the gradient direction.

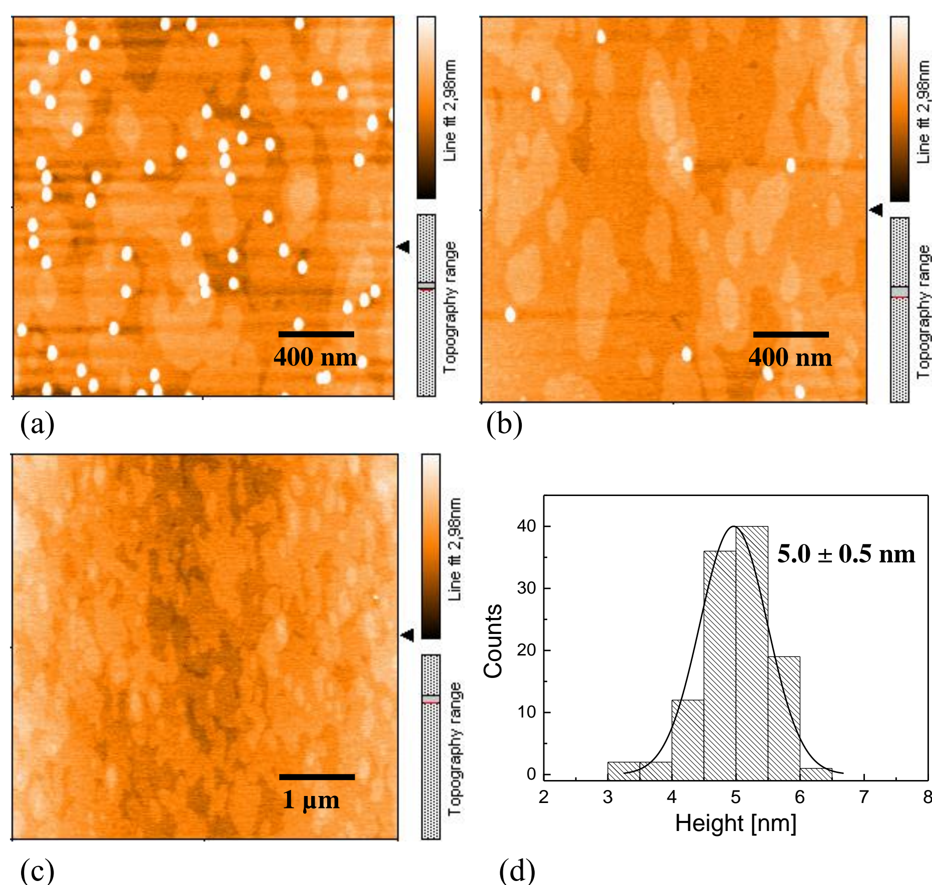

Figure 5.22: *(a-c) AFM images of $In_xGa_{1-x}As$ QDs grown with gradient approach. (a) shows QDs at high density area, (b) shows QDs at low density area, (c) shows only WL at no QDs area, and (d) shows the height histogram of InGaAs QDs at high density region.*

The optical properties of InGaAs QDs have been measured employing PL measurements at room temperature. Figure 5.23 show PL spectra of InGaAs QDs at various positions along the gradient axis. Here we see that along the gradient axis PL spectra shifts towards higher energy. This is due to the presence of In gradient. The Ga cell (used during QDs growth) is perpendicular to the substrate and does not provide a Ga-gradient during QDs growth as shown in figure 5.21(a). As we move towards the lower density sites, the Ga incorporation in the QDs increases which shifts the spectra towards higher energy. At low density area (10^8 QDs/cm^2), the Ga incorporation in InAs QDs is around 50%. Such low density $In_{0.5}Ga_{0.5}As$ QDs shows emission around 1000 nm at room temperature. In this way using a compositional gradient, we have grown low-density QDs which emits around 930 nm at low temperatures (suitable for Si-based detection technology).

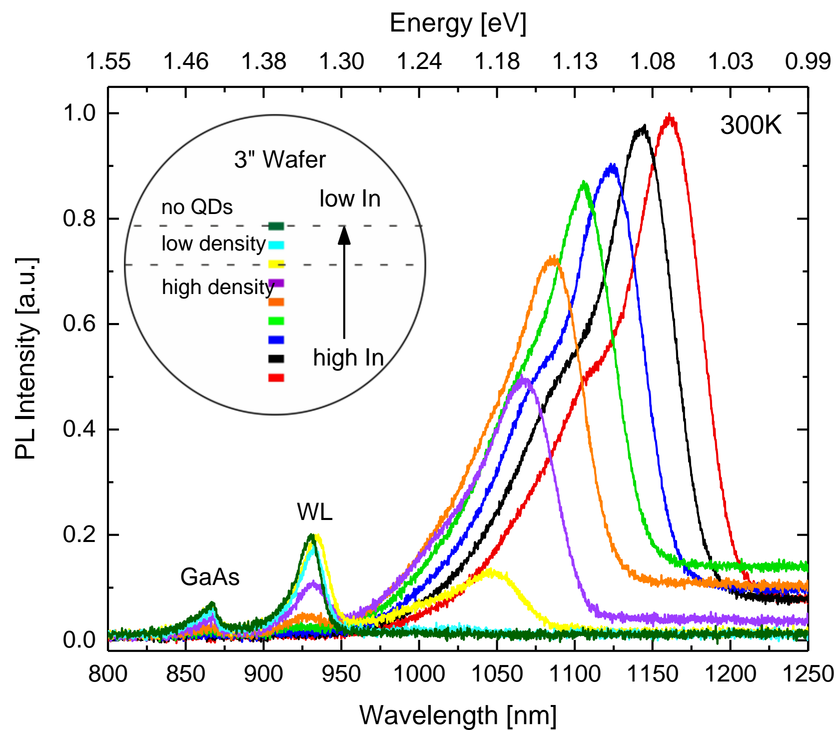

Figure 5.23: *Room temperature PL spectra of InGaAs QDs along the In-gradient axis. The inset shows wafer sketch with positions marked along the In-gradient axis. The inset (top left) shows the wafer sketch with mark positions along the gradient direction where PL measurement is performed.*

This page has been intentionally left blank.

Chapter 6

6 Quantum Dot Molecules

This chapter describes the fabrication of low-density InAs quantum dot molecules (QDMs) on GaAs(100) substrate. A modified gradient approach is established to ensure the vertical alignment of QDs. In-flush technique for emission energy tuning and In-gradient approach for low density are used. *Ex-situ* AFM and PL spectroscopy are employed to characterize the samples.

6.1 Introduction

Vertically stacked InAs quantum dots (QDs), which are electronically coupled, so-called quantum dot molecules (QDMs), are attractive candidates for solid state based quantum communication technology [94, 95]. The atom-like properties of the individual QDs can be engineered through modern nanofabrication and crystal growth technique, whereas the coupling can be controlled via the thickness of the GaAs barrier separating the two QD layers [11, 9]. Unlike to real molecules, the energy levels in each QD and degree of coupling can be tuned. In QDMs, QDs can be arranged in vertical or lateral alignment according to desired device properties [11]. Vertically stacked QDs have been in the research for more than two decades [9, 96, 97] where investigations are mainly concentrated on high QDMs densities. In such QDMs precise control of the interdot barrier is allowed by growth process which is crucial for the quantum coupling. Regarding the fabrication of QDMs, the pairing probability as a function of the interdot barrier thickness [9] and the QD size and shape in the bottom layer [96] have been studied. It has been suggested that the strain field of the bottom QD layer provides nucleation sites for top QDs. Quantitative models to describe the influence of the strain field have been proposed by several groups [9, 96, 97]. The bottom QDs influence the shape and size of the QDs in the top layer, too. They differ from those of QDs grown as a single layer employing the same growth parameters. This kind of stacked QD structures also observed in other system like InP/GaInP [98], SiGe/Si [97].

The optical and electronic properties of the InAs QDs can be defined via modifying their shape, size and composition. In case of QDMs, the optical and electrical properties of the two dot layers can be defined independently using In-flush technique [99]. In recent years, InAs

QDMs with low densities have been fabricated and studied by single QDM spectroscopy [100, 101].

Low density QDMs ($\leq 10^8/cm^2$) are required for single molecule spectroscopy. As described in Chapter 5, to grow low density QDs homogeneously over the whole substrate is extremely challenging and also the reproducibility is very low. To reproducibly grow such low QD densities employing an In-gradient across the substrate was proposed [66, 18]. The In-gradient provides a non-homogeneous deposition of InAs which results in a density gradient over the substrate. This provides an area on the wafer surface with the desired low QD densities. A corresponding approach can be used to realize low QDM densities. Bottom and top QDs can be grown using the In-gradient technique. This chapter will describe an alternative approach, in which only in the bottom QD layer a gradient is employed. For the top layer, spatial homogeneous In-deposition is used. It is shown that also with this deposition sequence a density gradient in the top-layer can be realized. We will discuss the influence of the In-amount deposited for the top QD layer on the resulting QD density gradient. The effect of interdot barrier thickness on the growth of top QD layer is also discussed. The emission energy of both dot layers is tuned using In-flush [99] technique. The optical properties of the QDMs are discussed in the last section of this chapter.

6.2 QDMs: Growth Process

The growth process of the QDMs starts with the preparation of the substrate as discussed in Chapter 4. All QDMs samples are grown on GaAs(100) semi-insulating substrate. After growing a buffer layer followed by 30 pairs of 2 nm AlAs /2 nm GaAs short period superlattice, an n-type back contact of 300 nm GaAs doped with Si (2.0×10^{18}) is grown at 610°C substrate temperature. A 40 nm GaAs layer as a tunnel barrier is grown before QDs growth step. Then the substrate temperature is lowered to 510°C and substrate rotation is paused. In next step, the bottom QD layer is grown with the In-gradient approach as discussed in Chapter 5 to achieve QD density gradient along the easy cleave direction of the wafer. The bottom QD layer is grown depositing 1.73 ML of InAs using 16 cycles (4s In + 4s break). The schematic of this step is shown in Figure 6.1a. The emission energy of bottom QD layer is defined employing In-flush technique (see Chapter 5, section 5.4) as shown in Figure 6.1b. After that, the substrate rotation is started and a GaAs interdot barrier of thickness d_B is grown at 610°C (Figure 6.1c). This step is followed by top QD layer growth with substrate rotation, i.e. homogeneous InAs deposition at 510°C.

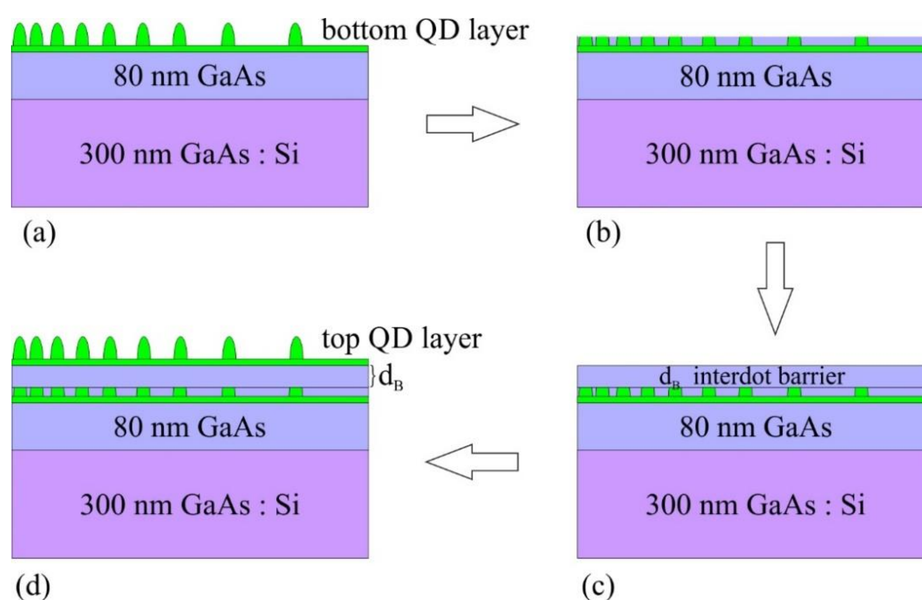

Figure 6.1: *Schematic of QDMs growth process (a) growth of bottom QD layer at 510°C with the In-gradient approach. In this step substrate rotation is paused and InAs QDs are grown with a density gradient along [011] direction, (b) In-flush process to define the height of QDs to tune emission energy, (c) interdot barrier growth at 610°C, and (d) top QD layer growth with homogeneous InAs deposition.*

For the top QD layer, various amount of InAs is deposited to study vertical alignment of QDs. After the top QD layer growth, the substrate temperature is lowered to 300°C and the sample is transferred to the loadlock for *ex-situ* AFM measurements or the QDs are overgrown by the desired heterostructure.

Two sets of samples have been grown to study the vertical alignment of QDs via *ex-situ* AFM. In both sets, the bottom QDs height is 2.2 nm defined by In-flush technique. In the first set of the samples, the InAs amount for the top QD layer is varied to see the effect of gradient from bottom QD layer to the top QD layer. In the next set of the samples, different interdot barrier thickness d_B (6 nm, 12 nm and 18 nm) is used to investigate the influence of this parameter on the growth of top QD layer.

Samples for optical characterization, after top QD growth In-flush technique is again employed to define the height of top QD layer for emission energy tuning. In next step, 280 nm GaAs layer is grown at 610°C followed by 10x 3nm AlAs/1nm GaAs short period superlattice. A 10 nm GaAs cap layer is deposited at the end. The complete sample structure of QDMs is shown in Figure 6.2. This is a typical Schottky diode structure where an electric field can be applied along the growth direction and charge state of QDM and relative position of the energy levels of the two QDs can be controlled by an external gate voltage [102].

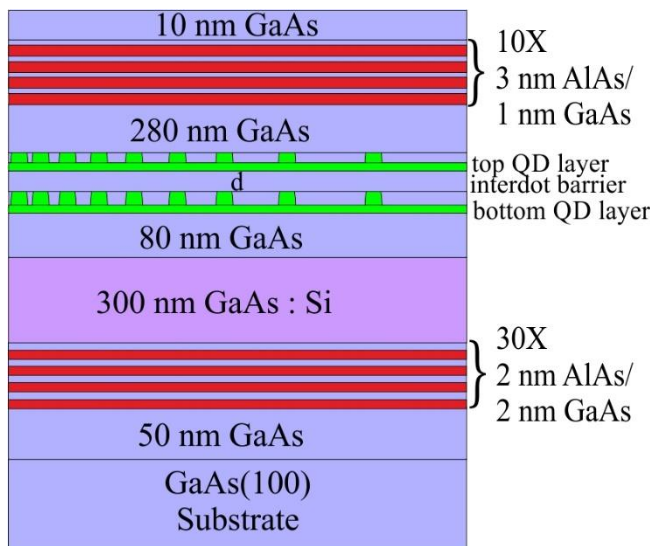

Figure 6.2: *Schematic of the sample structure of quantum dot molecules for optical investigations.*

6.3 QDMs: Characterization

For a density gradient reference sample on a ¼ 3" wafer, a surface QD sample is fabricated depositing 1.73 ML of InAs using 16 cycles (4s In + 4s break) at same growth conditions as used for bottom QD layer. The process of QDs with density gradient is discussed in Chapter 5 (section 5.4). The Figure 6.3(i) & (ii) shows the sample structure and wafer sketch, respectively and Figure 6.3 (a-d) shows AFM images at various positions along the density gradient axis. Positions (a) and (b) represents the high density QD region, (c) represents the transition region ($\approx 5.0 \times 10^8$ / cm^2) and (d) represents the low density region ($\leq 1.0 \times 10^8$ / cm^2). The position of the low density QDs area on the sample with respect to the wafer edge can be reproduced within 2-3 mm for sample to sample. The height of QDs also changes along the gradient axis, the average height at high density site is 6 nm and at low density site is 10 nm. Similarly, in QDM growth process, the QD density gradient should be present in the bottom QD layer. The overgrowth process only changes shape and composition but not the density of the dots.

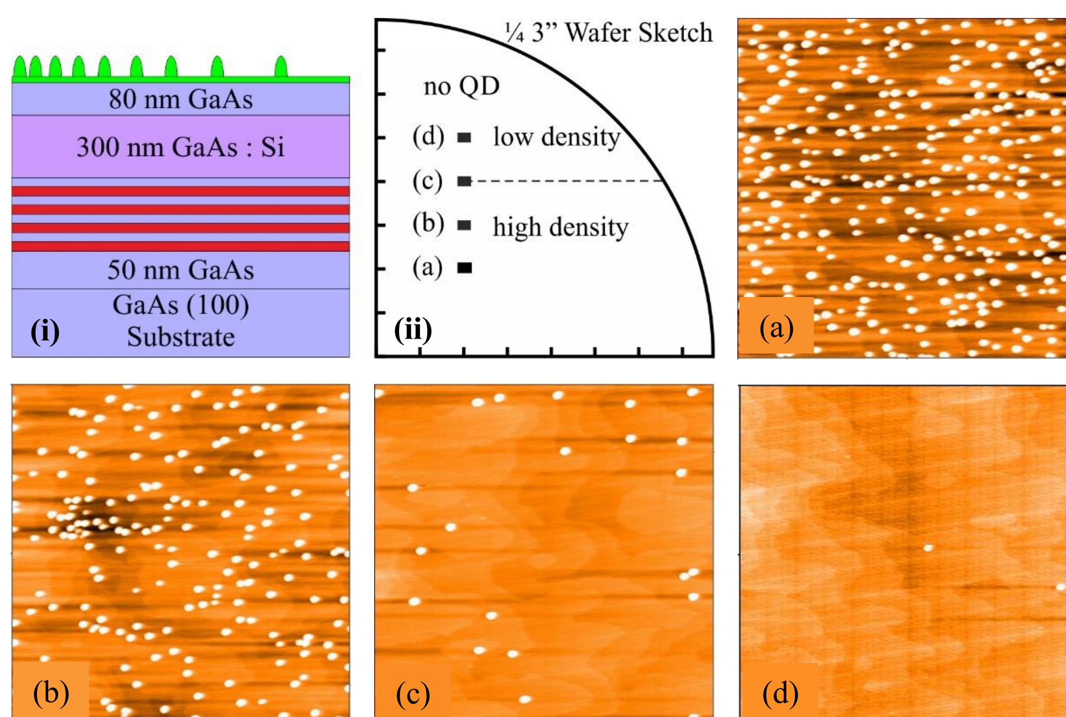

Figure 6.3: *(i) Schematic of the sample structure, (ii) Sketch of ¼ 3" wafer with marked positions where AFM measurements have been performed, and (a-d) AFM images at various positions along the gradient axis. Images (a) and (b) represents the high density region, (c) is from the transition region and (d) represents the low density region.*

For the first set of QDM samples, the *ex-situ* AFM is employed to measure the density of top QDs. Figure 6.4(i) & (ii) shows the sample layer structure and wafer sketch respectively. Wafer sketch is marked with different positions where AFM measurement is performed. The QD layers are separated by 6 nm thick GaAs barrier. For the top QD layer, InAs amount is varied from 1.84 ML to 1.30 ML employing cycled growth.

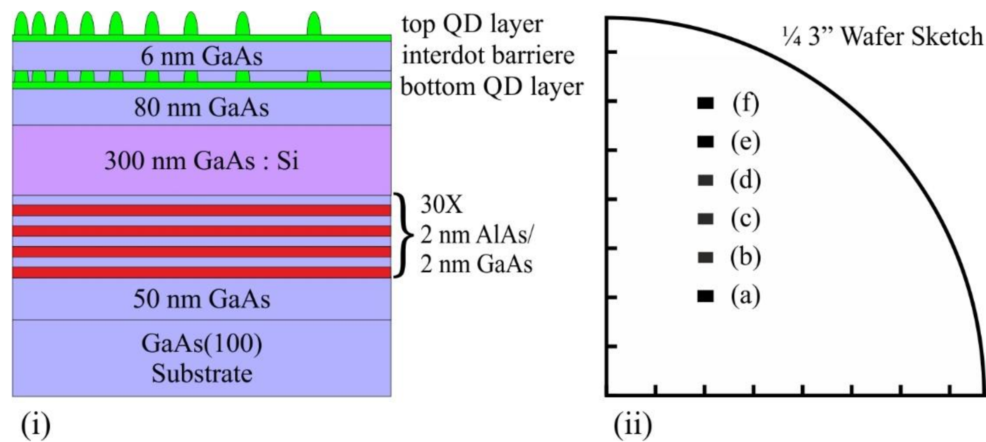

Figure 6.4: *(i) QDMs sample structure and (ii) ¼ 3" wafer sketch. The Bottom QDs are 2.2 nm flushed and grown with gradient approach. The top QDs are grown with homogeneous InAs deposition. In wafer sketch, rectangular squares show the positions where AFM is performed.*

The AFM images were taken at different positions along the In-gradient axis and for each set of samples, a set of identical positions was chosen with respect to the substrate edge within the accuracy of our setup (±0.5 mm). For each position, several images were taken at slightly different positions to ensure that images with representative QD densities were recorded. In the high density regions (QD densities above 1×10^9 cm^{-2}), deviations of less than ±10 % between the individual images are observed, whereas, for lower densities, the density value depends more strongly on the exact image position.

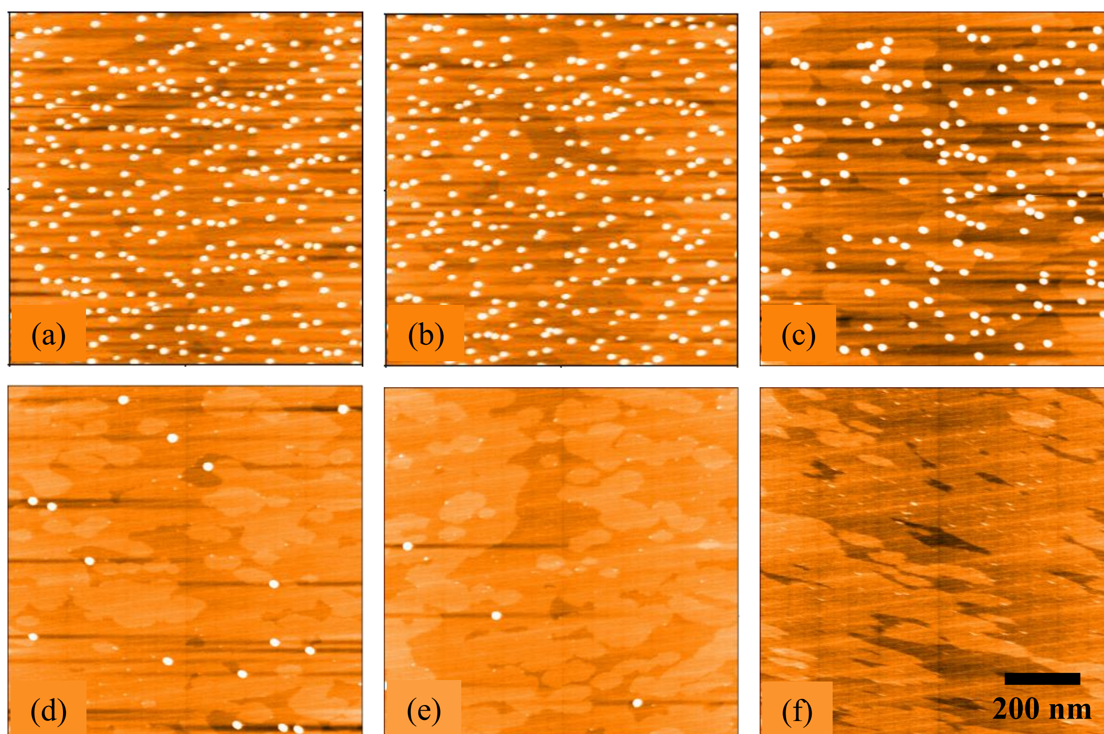

Figure 6.5: *AFM images (a-f) along the In-gradient axis for top layer quantum dots grown with 15 cycles with substrate rotation. The positions of the recorded images are indicated in Fig. 6.4(ii).*

Figure 6.5 shows AFM images of top QDs at various positions as marked in Figure 6.4 (ii). A clear gradient is present in top QD layer. As discussed above the top QDs are grown with 15 cycles (1.62 ML of InAs) with homogeneous deposition, i.e. with substrate rotation. In single QD layer growth, with 15 cycles no QDs growth take place with substrate rotation. This suggests that the top QD forms with less than a critical amount of InAs for single QD layer. The QD densities at different positions and the location of the low density region are comparable to the reference sample with a single QD layer within the range of sample to sample variations. This suggests that the gradient in top QD layer reproduce the gradient in the bottom QD layer. The bottom QD layer influences the growth kinetics, formation and characteristics of the top QDs. The strain field around the QDs in bottom layer alter the migration rate of In

adatoms during top QD layer formation and also provides preferential migration to In adatoms towards regions above the buried QDs. Also the low growth rate (0.027ML/sec.) and growth interruption method provides In adatoms longer migration length [103] and they have a higher chance of finding a lower energy position at which to be incorporated [104]. This indicates that the top QDs are vertically aligned with bottom QDs. So the vertical alignment is strain driven and therefore creates gradient in the top layer. The strain field from bottom QD layer also decreases the critical thickness for QD formation compared to single layer. It has been already shown that for 6 nm thick interdot barrier, the alignment probability is close to 100% [9].

The dots in the top layer are larger than the dots in the bottom layer, although the lower amount of InAs is deposited for top layer growth. The height of top QDs along the In-gradient axis grown with 15 cycles increases similar to the single layer QDs grown with 16 cycles. In single layer QDs the height is increased from 6 nm to 10 nm and top QDs height increased from 6.5 nm to 11 nm. This points to strain driven intermixing or a thinner wetting layer [104].

In summary, we have grown low density QDMs with an approach where bottom QD layer grown with an In-gradient provides a gradient to the top QD layer. The vertical alignment and gradient in the top layer are driven by the strain field from bottom QD layer. In the next section, we describe the effect of In amount for top layer QDs.

6.3.1 QDMs: Effect of In Amount for Top QD Layer

The top QD layer is grown with different number of the cycles to see the effect of strain field from bottom QD layer. Figure 6.6 shows AFM images of top QDs in the high density region, which are grown with different number of cycles. The QD density at the high density region looks quite similar for 17, 16 and 15 cycles. The densities variation are within sample to sample variation. This suggests that for each bottom QD, there is a top QD formed. For 14 cycles, the QD growth happens, but the density is slightly lower so may be not for every bottom QD, there is a top QD formed (see Figure 6.6d). For 13 cycles, very few QDs are formed in the top layer, most of the bottom QDs are without top QDs. Disk shaped bottom QDs can be seen in the AFM images without top QDs (see Figure 6.6e). For 12 cycles or less, no QD growth happens in the top layer. The height of top QDs also decreases with decreasing the In-amount. The presence of top QDs for 14 cycles indicates that the critical thickness for QD formation is

decreased by 10-12% due to strain field from bottom QD layer. The height of top QDs for 17 cycles is around 7 nm and for 13 cycles is around 4 nm. Figure 6.7 shows the height and density variations for different In-amount at high density regions.

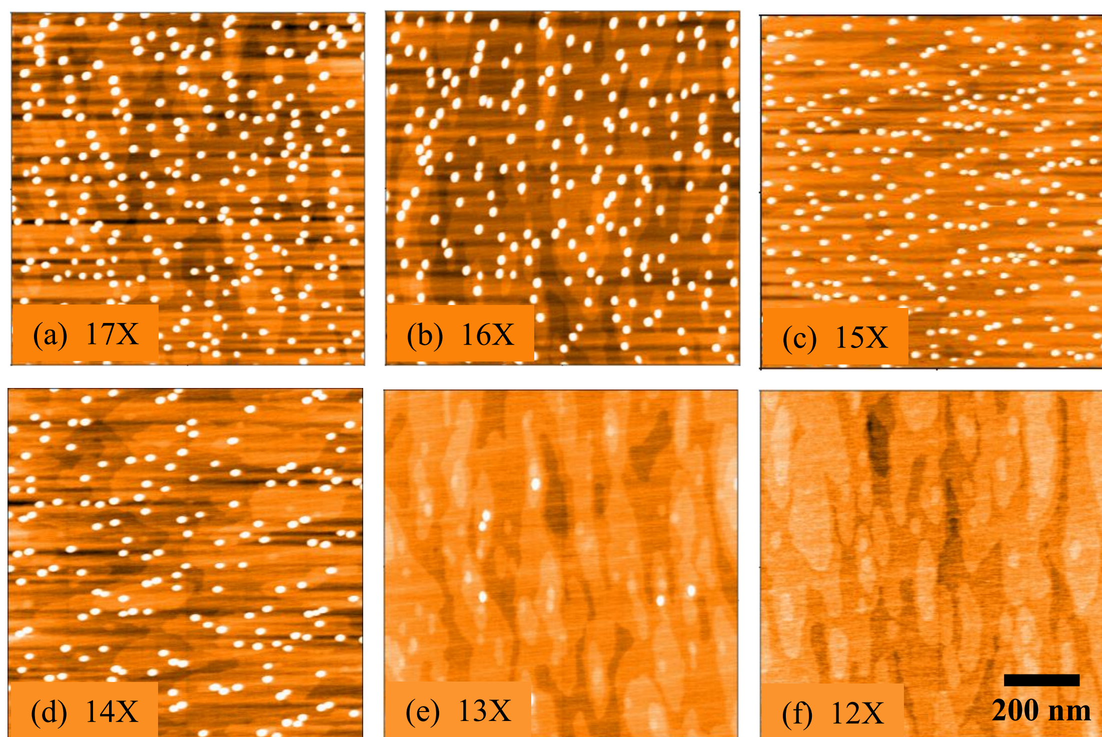

Figure 6.6: *AFM images of top QDs with different In amount. The images are taken from high density region in bottom QD layer.*

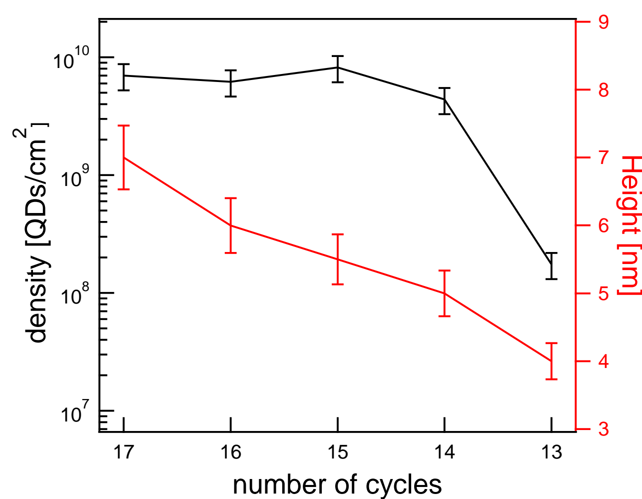

Figure 6.7: Density and height of top QDs as a function of growth cycles at high density region. The density stays almost constant for 17 to 14 cycles. The height decreases with decreasing cycles

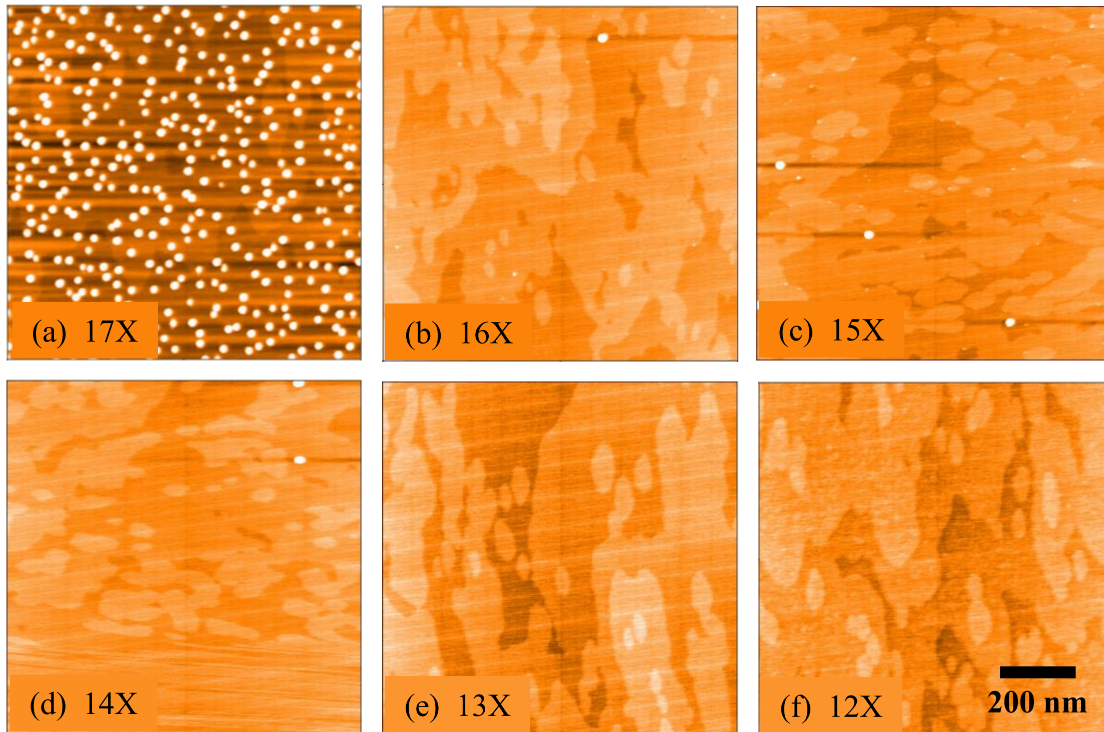

Figure 6.8: *AFM images of top QDs with for different In amount. The images are taken from the low density region in bottom QD layer.*

For a low QD density in the bottom layer, the results differ from those from the high density region discussed above, (see Fig. 6.8 for AFM images). With 17 cycles, the density is the same as on the high density side, hence at least one order of magnitude higher than in the bottom layer. This means that due to the large amount of In many top QDs are formed at positions without a bottom QD. In contrast to the high density region, not enough sites for preferential QD formation induced by the bottom QDs are present for the QD density corresponding to the deposited In amount. Thus, also QDs are formed between the sites corresponding to bottom QDs. For 16 and 15 cycles, a density similar to the expected bottom QD density is observed. From this, we can conclude that approximately all top QDs are formed vertically aligned to a bottom QD. The overall In amount is so low that due to diffusion towards the strain field maximum [Xie-PRL, Legrand-APL] only here the critical thickness is exceeded and QDs are formed. For 14 cycles only very few QDs are observed and it seems that only above a small fraction of the bottom QDs top QDs are formed. Probably the overall In amount is too small to form above all bottom QDs a top QD. For 13 and 12 cycles no top QDs at all are observed. We conclude that for a rather narrow In range (15 and 16 cycles), one obtains QDMs with probably almost 100 % pairing probability and a density gradient despite homoge-

-neous In deposition is realized for the top QD layer. The density gradient reproduces the QD density gradient in the bottom layer induced by inhomogeneous In deposition. For higher and lower In amount, deviations from this behaviour are found. In the next paragraph, the influence of the interdot barrier thickness will be discussed.

6.3.2 QDMs: Effect of Interdot Barrier Thickness

Figure 6.9 shows the results for the high density regions for interdot-barrier thicknesses of 6, 12 and 18 nm, respectively. As already discussed, in the case of a 6 nm barrier a high density is observed and we assume that almost all top QDs grow vertically aligned with the bottom QDs. This changes significantly for a 12 nm barrier, were the density is at least a factor 4 lower. We conclude that for a 12 nm barrier by far not on each bottom QD a top QD is formed. This is attributed to the reduced strain field at the top-layer position due to the thicker GaAs barrier and size of the bottom QDs [96]. For 18 nm barrier thickness, the influence of the strain field is even more reduced and only very few top QDs are observed at some positions. The experiments with different barrier thicknesses show the strong influence of this parameter and reveal that only for the 6 nm barrier we obtain stacked QDs with a density gradient and a high pairing probability.

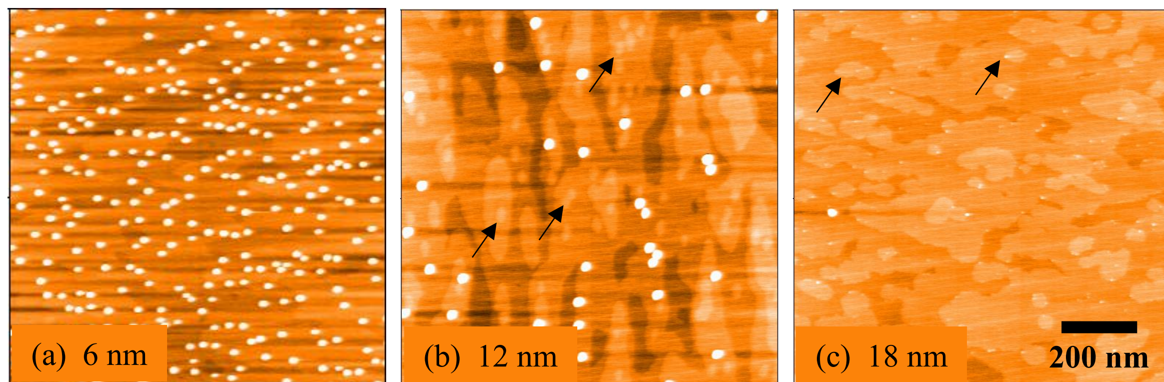

Figure 6.9: *AFM images from the high density region along the In-gradient for the top QD layer for different interdot barrier thickness d_B. The interdot barrier d_B is (a) 6 nm (b) 12 nm (c) 18 nm. For 6 nm the arrows in Figure (b) indicate humps on the surface due to bottom QDs. The arrows in Fig. (c) shows 2d islands (~ 3 Å) which are a consequence of the strained growth.*

6.4 QDMs: Optical Properties

The optical properties of the QDMs are investigated by PL spectroscopy. The measurements are performed in the confocal PL setup, described in Chapter 3. The QDMs excitation is done by semiconductor laser source of a wavelength of 635 nm (1.95 eV). The emission energies of dot layer are tuned using the In-flushing technique (see Sub-Chapter 5.5). As mentioned above the bottom QDs are 2.2 nm flushed, top QDs are 1.8 nm flushed and the interdot barrier is 6 nm thick GaAs. Such QDMs are embedded in a Schottky diode structure (see Appendix II) to allow for charge carrier tunnelling between two dots [102]. Here we have measured PL spectra of such samples to see their emission and presence of density gradient in the sample. Figure 6.10 shows room temperature PL spectra of QDMs at various positions along the gradient axis.

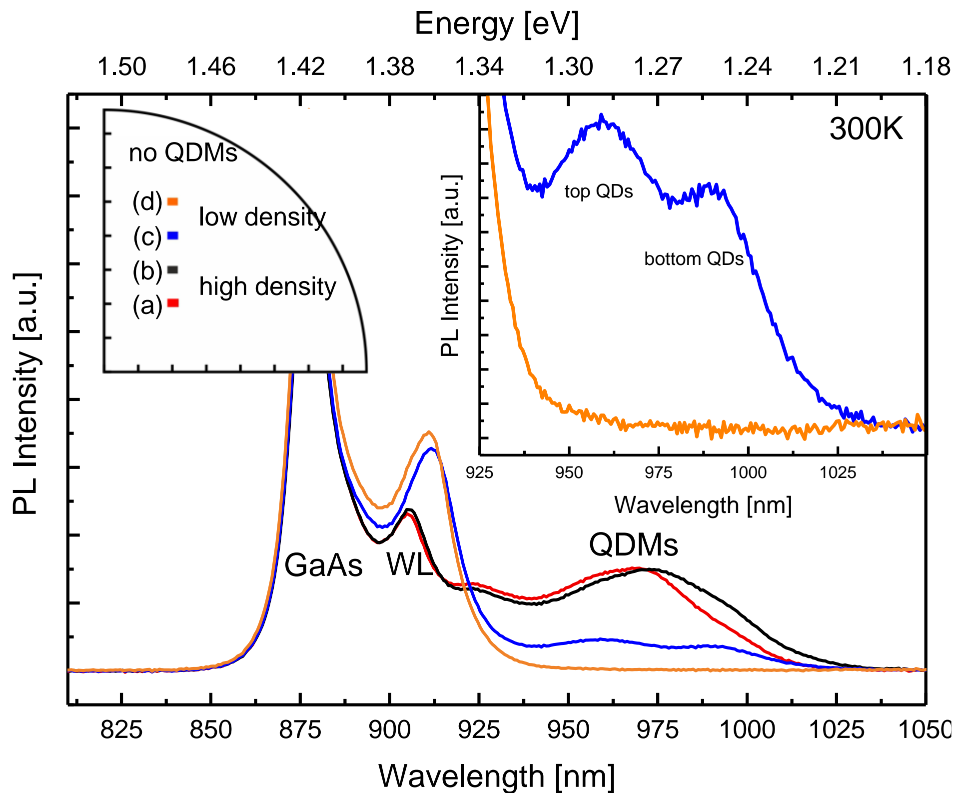

Figure: 6.10: *Room temperature PL spectra of QDMs at various positions along the gradient. (main graph) The inset (top left) shows the wafer sketch with marked positions where PL measurement are performed and the inset (top right) shows the PL spectra at position (c) and (d)with higher resolution.*

As we move from high density to low density area on the sample, emission intensity from QDMs is decreased and intensity from GaAs and WL is increased. At position (d) only emission from GaAs and WL is observed. The position between (c) and (d) is the low density region where single molecule spectroscopy can be performed.

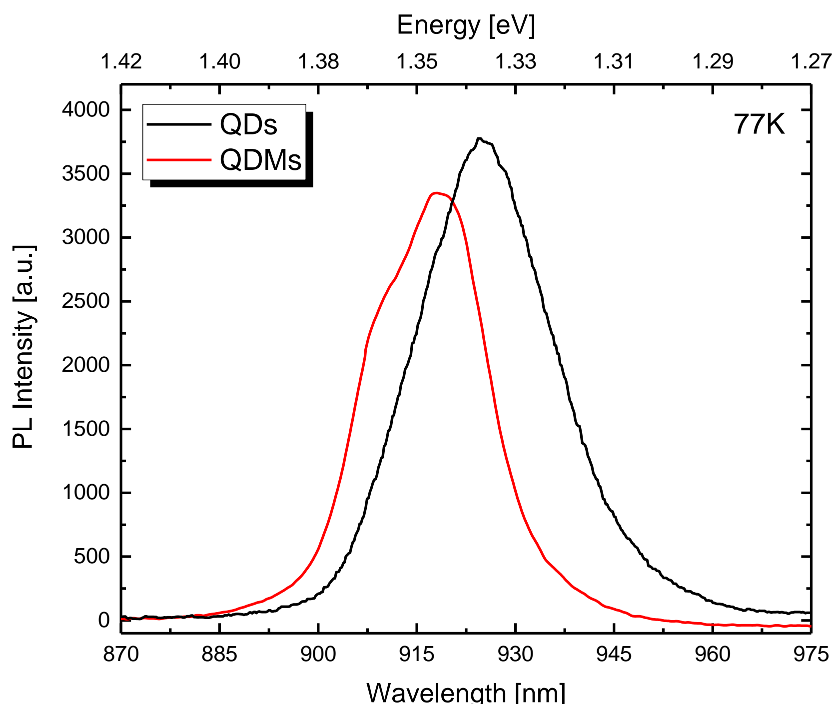

Figure 6.11: *PL spectra of 2.2 nm flushed QDs and QDMs (B-QDs_2.2 nm / T-QDs 1.8 nm) for high density region at 77K. For both spectra the same excitation and detection parameters have been used (0.045mW power and 1 sec integration time). The intensity of QDMs is comparable to the QDs. The slight change in the intensity is probably due to the density variations between the samples.*

It is also worth noting that the optical quality of QDMs is very similar to the single QD layers. Figure 6.11 shows the PL spectra of 2.2 nm flushed QDs and QDMs (B-QDs_2.2 nm / T-QDs 1.8 nm) at 77K where both samples are excited with same laser power. The slight change in the intensity of QDMs and QDs are may be due to statistical variations of the QD densities. At low excitation powers, only bottom QDs show emission. The QDMs PL emission shows a blue shift in the spectra which is also observed by other groups [105], which is due to the strain fields, that exist in and around these QDMs.

Figure 6.12 shows PL spectra of QDM ensemble as a function of laser excitation power at 77K. At low powers, emission from bottom QDs is observed due to the low carrier generation and electronic coupling between dots. For thin tunnel barriers, charge carriers tunnel non-resonantly from smaller QDs to bigger QDs through the barrier. As we increase the power, the emission intensity increases and additional emission peaks appear from top QDs (smaller QDs). At high excitation power, emission from WLs and GaAs are also observed. At very low power (0.05mW), the ground state emission from bottom QDs shows a narrow full width at half maximum (FWHM) of 14 meV. This indicates that the bottom QDs are very uniform due to In-flushing process.

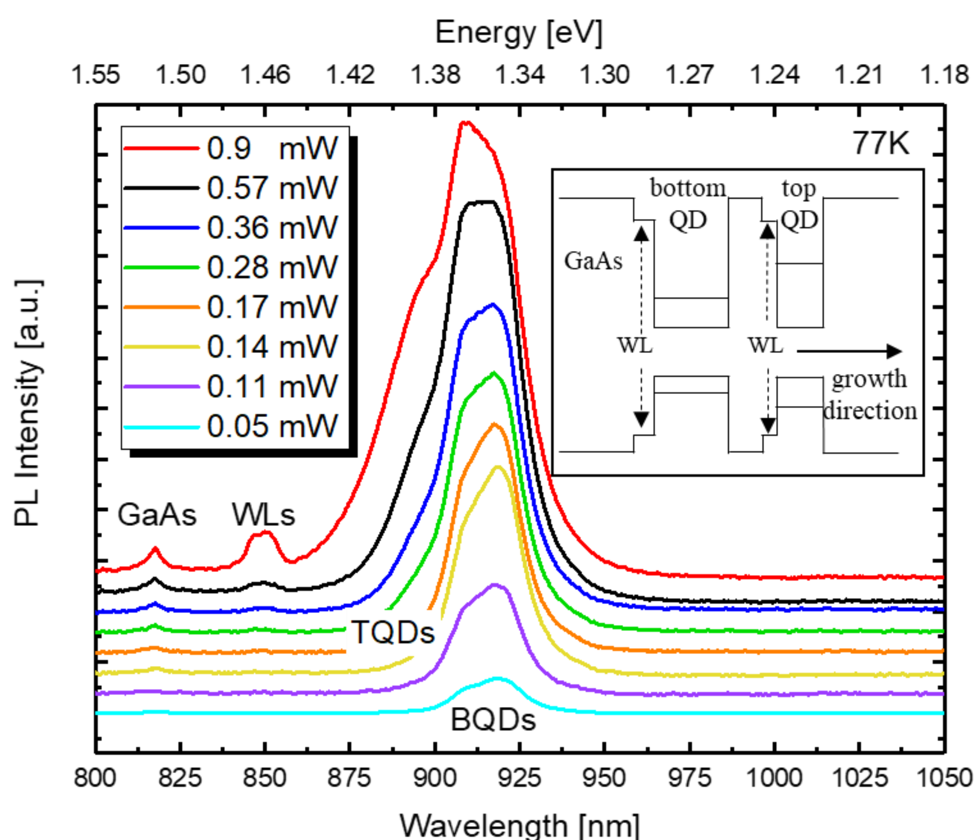

Figure: 6.12: *Power dependent PL spectra of QDMs at high density region at 77K. The spectra are vertically displaced for clarity. Inset shows the band structure of a QDM along the growth direction (neglecting the band tilting due to built-in field). At low powers emission from bottom QDs is observed. As power increased emission form top QDs, wetting layers and from GaAs is observed. Two peaks at WL position also indicate the presence of two WLs with different thickness.*

In conclusion, we have demonstrated the growth of low density self-assembled InAs QDMs on GaAs(100) via a simplified gradient approach where bottom QD layer is grown with density gradient using the In-gradient technique. For the top QD layer growth, the InAs is deposited with homogeneously and still realized in a density gradient in top layer similar to the bottom layer. The density gradient in the top layer is induced by the strain from the bottom QD layer and indicates the vertical alignment of QDs. It is also observed that the strain field from bottom QDs decreases the critical thickness for top QDs. For 6 nm interdot barrier, the vertical alignment probability is close to 1. For larger interdot barriers (12 nm and 18 nm), the influence of the bottom layer is strongly reduced and modified gradient approach is not reliable for the formation of low density QDMs. The PL measurement of QDMs show similar luminescence intensities as single QD layer, showing the good optical quality of the stacked QDs. This also indicates that there are no strain relaxation processes during growth of top QD layer. The presence of two WL peaks in PL spectra at high excitation powers indicates the presence of two WLs with different thickness.

This page has been intentionally left blank.

Chapter 7

7 Site-Controlled Quantum Dots

This chapter describes the fabrication process of site-controlled InAs quantum dot fabrication on GaAs(100) using pre-patterning and re-growth technology. After a brief introduction about site-controlled QDs, the fabrication process is described. The effect of buffer layer thickness and InAs amount on QDs occupancy is discussed in section 7.3. In last section of this chapter the optical properties of site-controlled QD ensemble is studied by PL spectroscopy.

7.1 Introduction

Spatial and spectral control of QDs are important technological goal for the scalable fabrication of novel devices on single photon emitters or entangled photon pair sources [69, 6]. InAs/GaAs based system is widely studied for such application in the recent years because of high quality QDs. The growth of self-assembled InAs QDs on GaAs(100) is strain driven process which provides random nucleation of QDs over the surface. The resulting density of the QDs is also very high [10^9-10^{10}/cm^2] for such process. To address a single QD with nm precision and with isolation for single dot based devices is very challenging. There are various approaches [18, 21, 83] used to grow low density QDs [~10^8/cm^2] for better isolation and conventional lithography processes are used to define mesa structures to integrate them into devices.

The most promising approach for growth of positioned QDs is pre-patterning of the substrate. Initially optical lithography is has been for patterning process but it provides clusters of QDs in the groves [106]. Later the size of the pattern structures is reduced to nanometre range and single QDs are grown on pre-patterned location. There are various techniques to define nanopattern on GaAs substrates such as focus ion beam lithography [107, 108], nanoimprint lithography (NIL) [109, 110], AFM nanooxidation lithography [111], and especially electron beam lithography (EBL) [112, 113, 114]. In all these processes the surface curvature is modified for preferential migration of In adatoms. There are some other approaches where the local strain filed is modified for preferential nucleation of QDs [115, 116].

There are several advantages of site-controlled QDs:

1. Positioned QDs allow better device scaling for single QD based devices and allow integrating them into the device using conventional patterning process.
2. Provides better control over size and shape fluctuations during stacking of the layers.

The nanoholes patterned on the flat GaAs(100) surface provides local minima for surface energy which is the driving force for the preferential nucleation of QDs. Figure 7.1 shows the schematic illustration of the growth process of site-controlled QDs. In Figure 7.1a, the preferential migration of In adatoms to the hole site is shown and Figure 7.1b shows that the strain drives accumulation of adatoms at the hole site. By this the critical thickness is reached earlier at hole sites compare to the flat region as shown in Figure 7.1c, which gives preferential nucleation of QDsin the holes. In other words, the preferential migration of In adatoms increases strain energy within the hole region and provides the preferential nucleation site. A good control over cleaning process after patterning, growth temperature, InAs amount and III/V flux is required for good site selectivity.

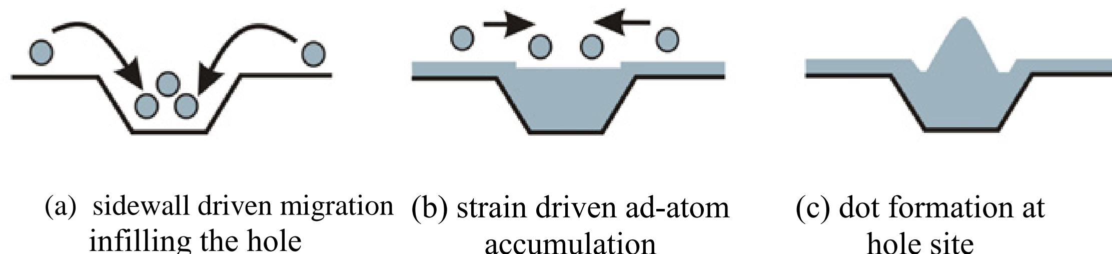

Figure 7.1: *Schematic diagram of the mechanism of site-controlled InAs QD formation on GaAs(100) substrate after* [117].

In this work, we have optimized the growth process to grow single QD per hole with high probability without nucleating QDs in between.large ordering. We have used conventional electron beam lithography technique with a standard wet etching process to pattern GaAs with nanoholes prior to growth. In this chapter fabrication process of positioned QDs via lithography technique and re-growth technology is discussed.

7.2 Growth of InAs QDs on Patterned Substrate

GaAs(100) substrate is patterned by optical lithography and EBL. Optical lithography and wet chemical etching (WCE) is employed to define the alignment marks and mesa structures (300 µm×300 µm) as described in Chapter 4. After pre-patterning of nanoholes in centre of each mesa by EBL, the wafer is subjected to two stage cleaning procedure. *Ex-situ* chemical cleaning is employed to remove resist residuals and other surface contaminants. The remaining residuals of the resist and native oxide are removed by hydrofluoric (HF) acid which gives hydrophilic surface. The substrate is then loaded to the loadlock degassed at 120°C for 8 hours. After degassing the wafer in preparation chamber at 200°C for 1 hour, *in-situ* atomic hydrogen (AH) cleaning is employed at 350°C substrate temperature as discussed in Chapter 4. This low temperature cleaning process leaves the surface clean and undamaged whereas thermal desorption of oxide cause pitting of the surface which prevents the patterned holes from acting as preferential nucleation sites [118]. The process also preserved the hole shapes due to low temperature during the cleaning process.

After removal of surface oxide by AH cleaning, the patterned substrate is transferred to the MBE growth chamber. The substrate temperature is increased to 520°C in presence of arsenic and substrate is degassed for 5 min. After that a thin GaAs buffer layer with a thickness of 15-25 nm depending on the initial depth of the hole is grown at 510°C substrate temperature to smooth the surface and isolate any interface defects or contaminants. Mostly these defects are Ga or As antisite defects which can act as non-radiative recombination centres and degrade the luminescence of QDs [117]. Buffer layer growth also helps to recover the surface stoichiometry at regrowth interface which might have changed due to HF cleaning and elevated temperature annealing (520°C for 5 minutes). The InAs is deposited in a cycled mode where for 4 seconds In cell is opened and for 4 seconds closed at 510°C substrate temperature as described in Chapter 5. After that, a 5 minute growth interruption is provided under As_4 overpressure as an annealing step. The growth rate of InAs is 0.027ML/sec. The amount of InAs is less than the critical thickness to ensure the dot formed at patterned site. To investigate the optical properties of SCQDs, QDs were overgrown with 10 nm thick GaAs at 510°C and then the substrate temperature is increased to 600°C and 200 nm GaAs is grown. PL spectroscopy is employed to study the optical properties. For samples for investigation of the morphology and the hole occupancy, the substrate temperature is lowered to 300°C after QD s growth and the sample is taken out.

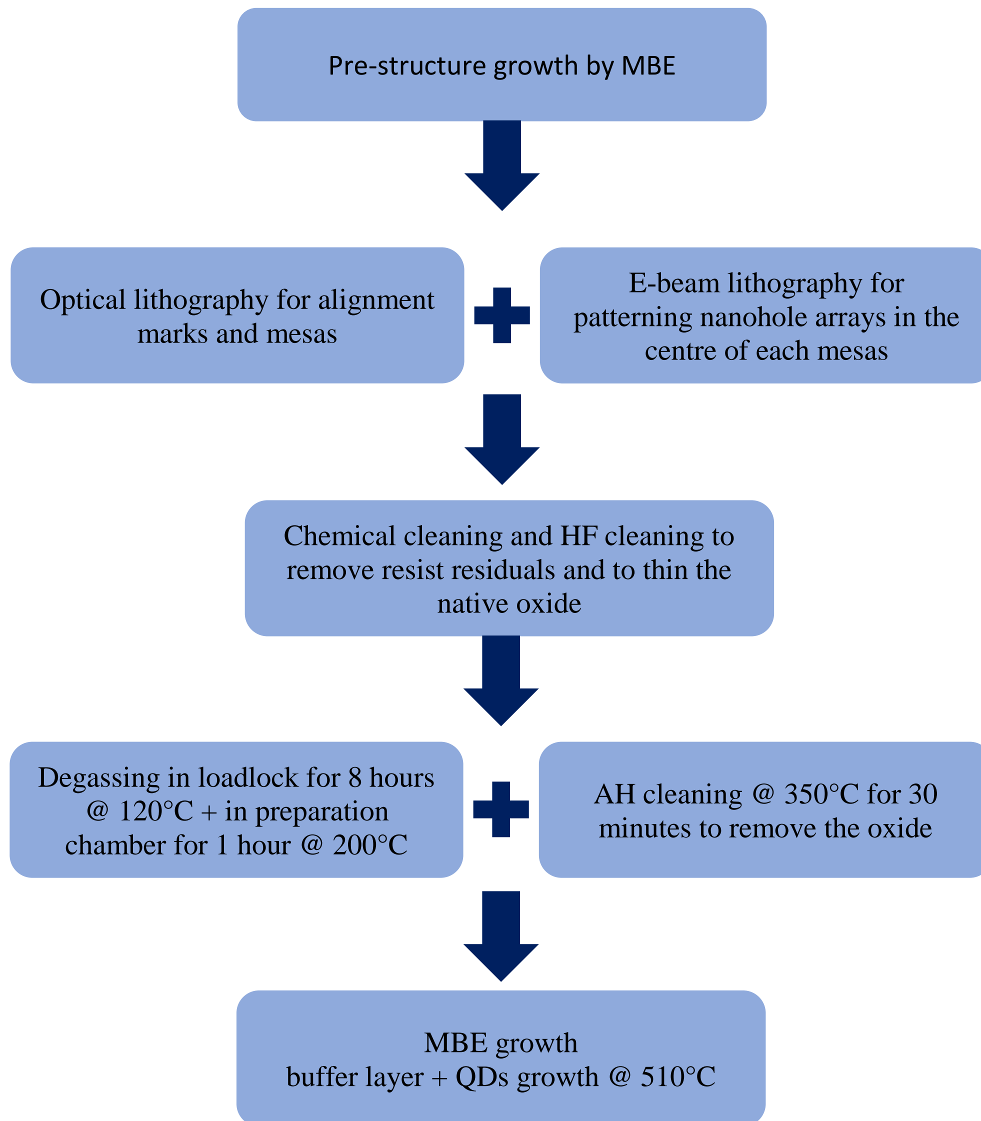

Figure 7.2: *Schematic of the fabrication process for site-controlled InAs quantum dots on GaAs(100) substrate.*

Figure 7.2 shows the schematic of the complete fabrication process of site-controlled InAs QDs on GaAs(100) substrates. Pre-growth, optical and electron beam patterning process, and cleaning process are described in Chapter 4. The results of the site-controlled QDs are described in the next part of the chapter.

7.3 SCQDs: Morphological Characterization

The growth of buffer layer before QDs growth changes the morphology of the patterned nanoholes due to growth anisotropy on GaAs. Figure 7.3(a) and (b) show the AFM images of nanoholes before and after growth of buffer layer, respectively. The nanoholes get elongated along the [011] direction during overgrowth process due to preferential migration of Ga adatoms [112, 119]. The elongation of the holes increases with increasing the buffer layer thickness. Initially, the holes are circular shaped and have a diameter of about 75 nm (Fig. 7.3a). The growth of 25 nm buffer layer changes hole shape, elongated along [011] and narrowed along [01-1] directions. The elongated holes provide two or more preferential nucleation sites for QDs growth.

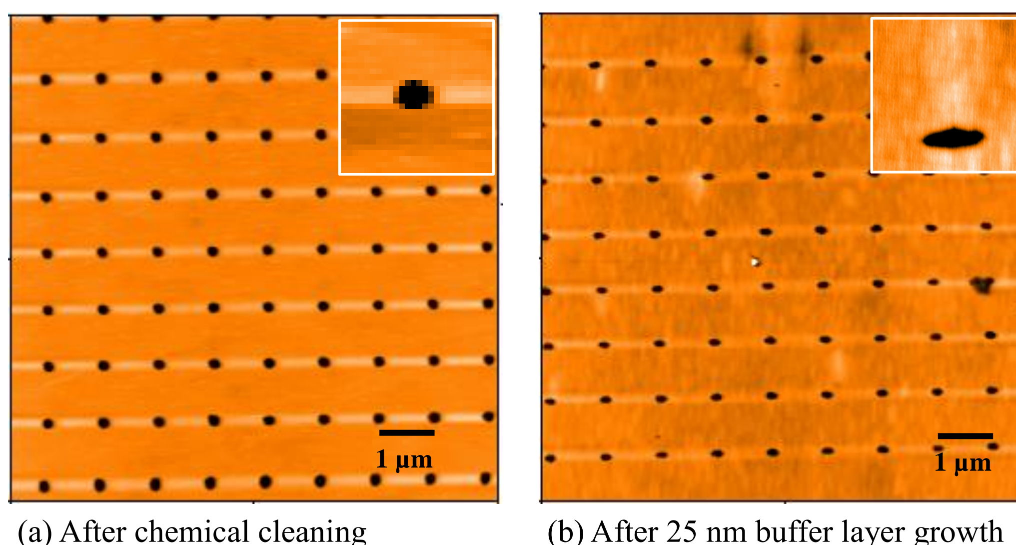

(a) After chemical cleaning (b) After 25 nm buffer layer growth

Figure 7.3: *AFM images (8.8 × 8.8 μm^2) of patterned nanoholes on GaAs (a) after chemical cleaning and (b) after growth of 25 nm GaAs buffer layer. Inset AFM images (500 × 500 nm^2) shows the shape evolution of the nanoholes after buffer layer growth, in more detail.*

The buffer layer growth is done at the low growth temperature (510°C) to avoid large thermal diffusion which elongates the hole along [011] direction. After buffer layer growth, a 2 minute annealing step is provided to smooth the GaAs surface. During annealing step, As_4 flux is reduced to grow InAs QDs.

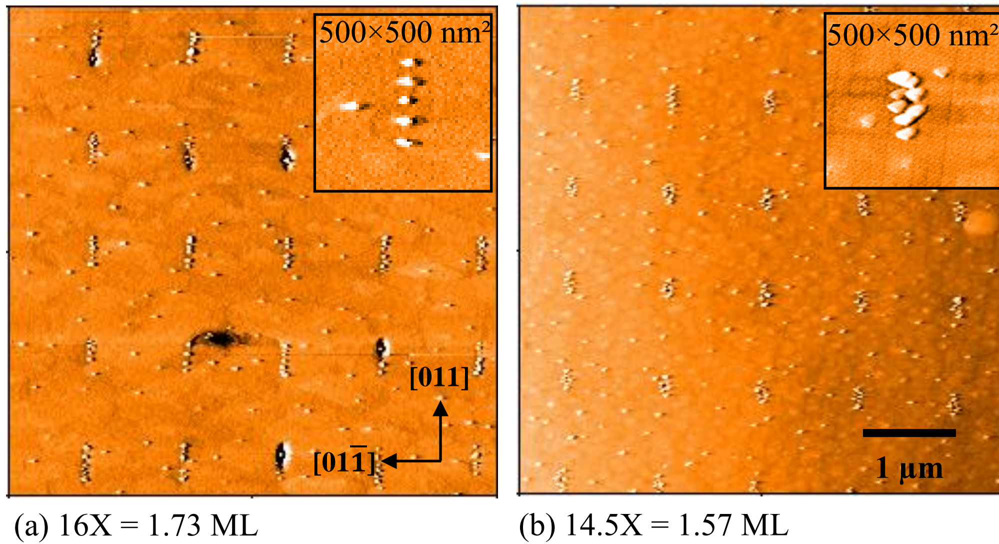

(a) 16X = 1.73 ML (b) 14.5X = 1.57 ML

Figure 7.4: *AFM images (5 ×5 μm^2) of positioned InAs QDs on GaAs (a) at 1.73 ML of InAs and (b) at 1.57 ML of InAs deposited at 510°C. In the inset of both images (500 × 500 nm^2) shows QDs in single nanohole.*

Initially, the site-controlled QDs are grown with 16 cycles as used for the planner surface. In figure 7.4, we see a cluster of the positioned QDs in patterned nanoholes and additionally QDs are present on the flat surface. In each hole around 4-8 QDs are present due to elongation of holes during buffer layer growth and higher amount of InAs. The height of QDs which are grown in the holes have in the range of 3-5 nm and QDs which are grown on the flat surface have in the range of 1-2 nm. In Figure 7.4a, InAs amount is 1.73 ML, deposited in 16 cycles whereas in Figure 7.3b, the deposited amount is 1.57 ML corresponding to 14.5 cycles. The inset shows 500 × 500 nm^2 area where single hole contains a few QDs. The hole size is about 75 nm after patterning and becomes about 150 nm along [011] after overgrowth of 25 nm buffer layer, which provides more than one nucleation site for QDs growth. The InAs QDs are aligned along [011] direction due to the preferential incorporation of In on B-type facets (As-terminated). In next step, the InAs amount is decreased to 1.46 ML for the growth of QDs in nanoholes.

Figure 7.5 shows SEM image of multiple QDs per nanoholes with 15% less InAs (1.46 ML) deposition than the critical thickness. This suggests that the larger size of the holes in the [011] direction compared to the lateral size of QDs (30-40 nm), each hole provides multiple nucleation sites for QD formation. The inset shows the histogram of the dot occupancy per hole where 70% of the holes are occupied by three or more dots while single dot occupancy is zero.

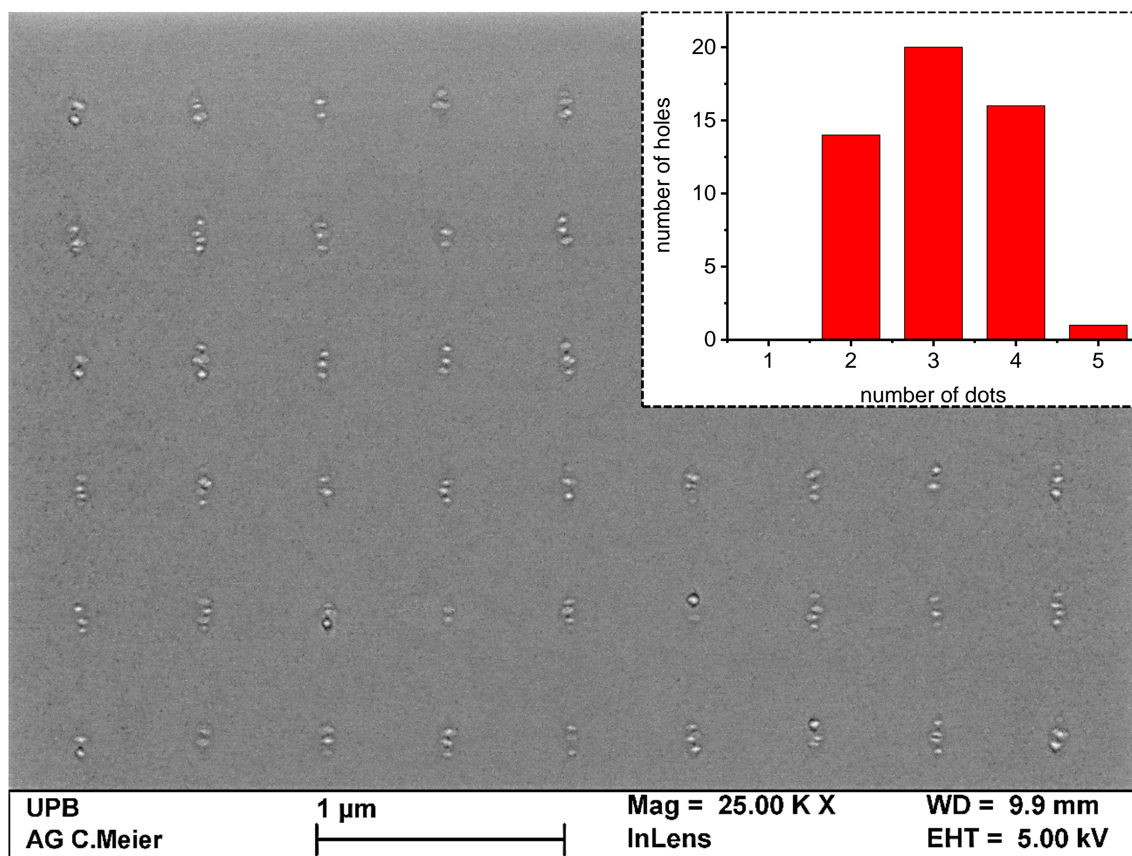

Figure 7.5: *SEM image of site-controlled InAs/GaAs QDs on patterned nanoholes. Appropriate position control is achieved with 1.46 ML InAs deposition. The inset shows a histogram of dot occupancy per hole.*

We further decrease the diameter of the patterned holes to 65 nm to achieve single dot per hole occupancy. The hole diameter is defined to 65 nm during EBL process on PMMA which becomes around 70 after WCE and chemical cleaning. To form QDs in at patterned holes, 1.46 ML of InAs deposited. Figure 7.6(a), (b) and (c) shows AFM images of positioned QDs grown with 13.5 cycles (1.46 ML). Figure 7.6(a) shows positioned QDs on a mesa which is patterned with 500 nm pitch and figure 7.6(b) and (c) shows positioned QDs on mesas which are patterned with 1 µm and 2 µm pitch respectively. In all cases, most of the hole contains quantum dot pair because of the hole shape changes from circular to the eight shape during buffer layer growth [112]. Further decreasing InAs amount (13 cycles ~1.4ML) results in no QD growth in the nanoholes, so at least 84% of the critical thickness of InAs is required for positioned QDs growth. Similar observations have been made by P. Atkinson et al [117]. Also increasing substrate temperature to 520°C, prevents the QD formation due to an increase of the critical thickness for QD formation.

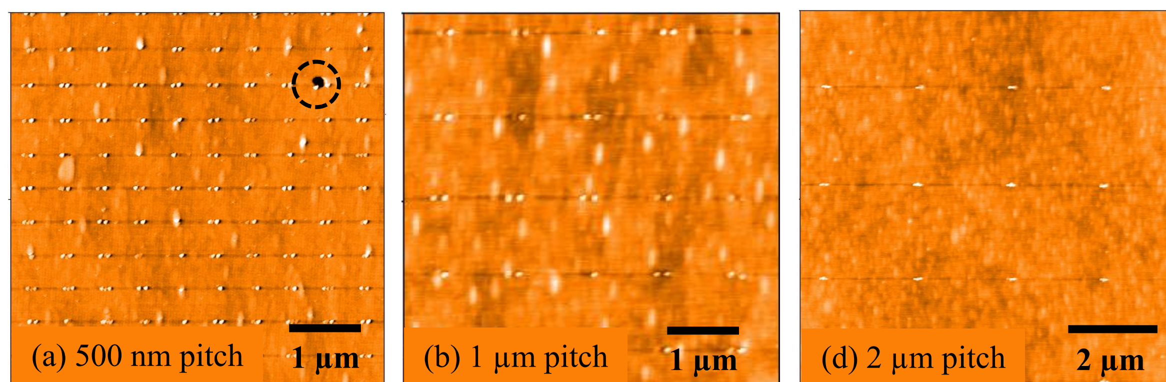

Figure 7.6: *AFM images of positioned InAs QDs grown on GaAs(100). The deposited InAs amount is 1.46 ML. (a) shows 500 nm pitch, (b) shows 1 µm pitch and (c) shows 2 µm pitch. Almost each of hole contains 2 QDs. The height of QDs is in the range of 3-4 nm and diameter is in the range of 25-30 nm. The dotted circle in (a) indicates the presence of defect during regrowth process.*

The other point is that, in the case of 13.5 cycles (1.46 ML of InAs), there is no S-K growth is observed in the flat surface region, which demonstrating highly selective QDs formation. Using this process, QD pairs with 2 µm pitch is successfully fabricated. In many approaches like NIL [110], AFM lithography single dot per hole occupancy is often very challenging due to much larger patterned holes than the dots. In addition, the growth of GaAs buffer layer before QDs growth also elongates the holes, provides several nucleation sites per hole. To get single QD per hole, we should decrease further the hole diameter or should decrease elongation of holes during buffer layer growth. The combination of EBL and WCE process is limited to pattern nanohole arrays with ca. 60 nm hole diameter on GaAs(100). In next step, we further reduced the diameter of patterned nanoholes and also decreased the buffer layer thickness. Figure 7.7a shows an array of nanoholes in PMMA which are defined 50 nm in diameter via EBL and Figure 7.7b shows an array of nanoholes on GaAs wafer after transferring by WCE process. The PMMA is removed by acetone and isopropanol. The hole diameter is increased from 50 nm to 60 nm during WCE. The hole depth is around 10 nm. Using reactive ion etching (RIE) instead of WCE, patterning of nanohole arrays with 40-50 nm diameter is possible but RIE introduces additional defects as charge traps and degrades the optical and electrical performance of materials [120, 121] and has not been tried in this thesis.

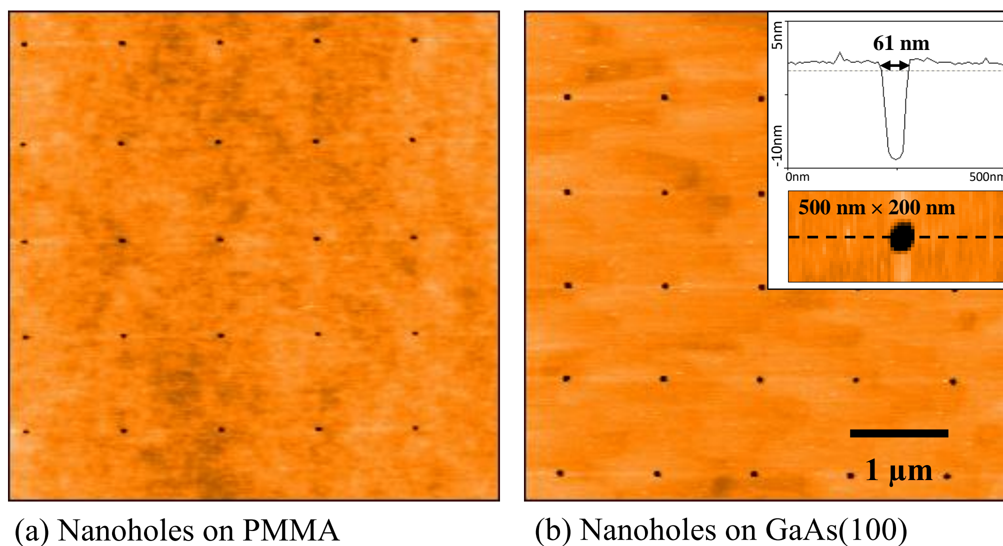

(a) Nanoholes on PMMA (b) Nanoholes on GaAs(100)

Figure 7.7: *(a) An AFM images of 50 nm diameter nanohole arrays on PMMA defined by e-beam lithography technique. (b) Shows an AFM image of nanoholes after transferring the pattern by WCE process. Inset of the (b) shows the line scan over the nanohole.*

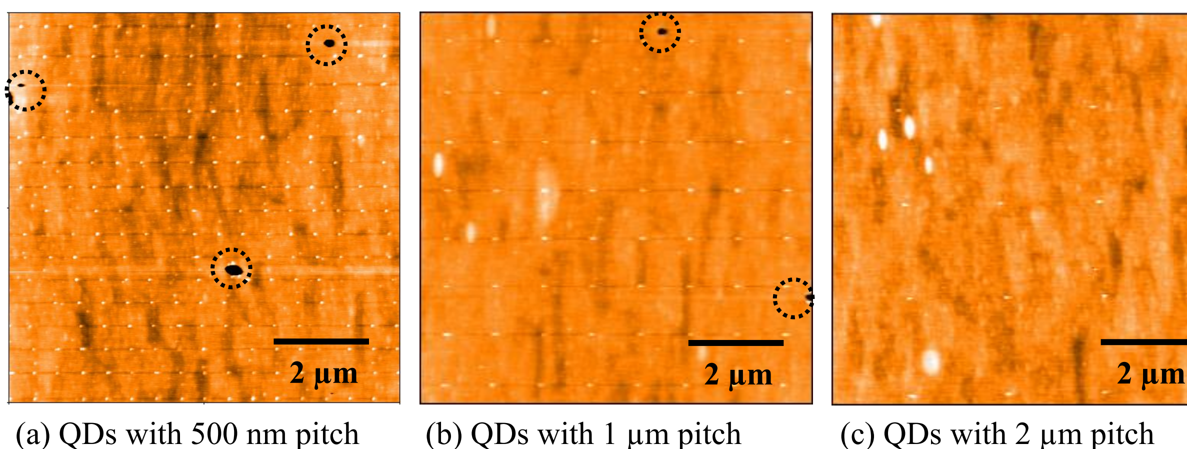

(a) QDs with 500 nm pitch (b) QDs with 1 µm pitch (c) QDs with 2 µm pitch

Figure 7.8: *AFM images of positioned InAs QDs with different pitch; (a) with 500 nm pitch, (b) with 1 µm pitch and (c) with 2 µm pitch. Most of the holes contain a single QD.*

To decrease the elongation of the nanoholes during overgrowth, the buffer layer thickness is decreased from 25 nm to 15 nm. For that nanohole were etched 10-12 nm deep in GaAs. Figure 7.8 shows AFM images of positioned QDs on different mesas with a different pitch. Most of the nanoholes contain single QD. On these mesas, the hole diameter was 50 nm during electron beam patterning process. The dotted circles in the AFM images show the hole defects which are present at regrowth interface. These holes are formed during regrowth process. The main reasons for the occurrence of hole defects can be due to incomplete removal of residual oxide or insufficient surface cleaning after lithography process. Figure 7.9 shows the SEM image of site-controlled QDs with 250 nm pitch where most of the holes are occupied with 1 or 2 QDs. The inset of Figure 7.9 shows the histogram of the QDs occupancy. Around 60% holes are occupied with single dots and 35% holes with 2 dots.

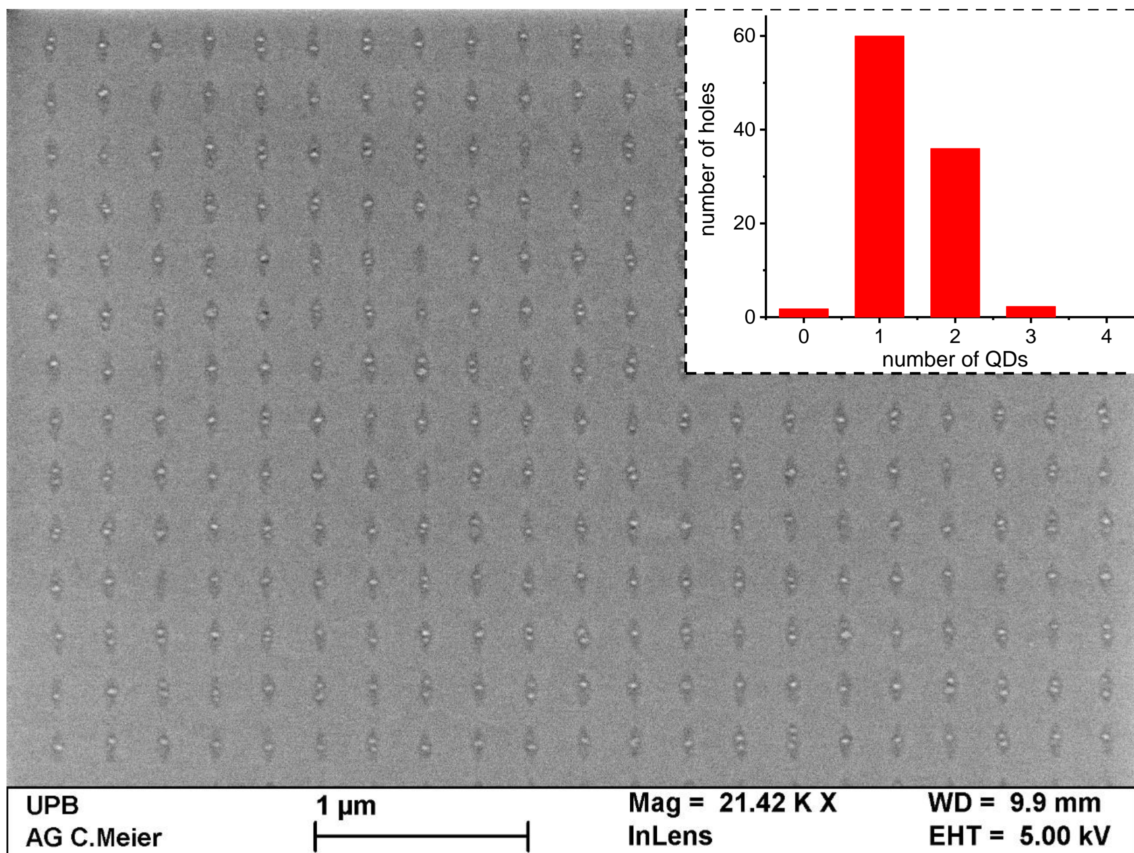

Figure 7.9: *SEM image of positioned InAs QDs grown at patterned nanoholes by MBE. The inset shows histogram of QDs occupancy per hole.*

These results show that control of patterning process and growth kinetics, occupation statistics of QDs in patterned holes can be controlled. Generally, the number of QDs per nanohole and morphology of SCQDs depends strongly on the initial size of nanoholes as well as buffer layer thickness. With smaller hole diameter and with thin GaAs buffer layer (15 nm), the occupancy of single dot per hole is achieved. The optical properties of SCQDs buried in GaAs matrix is described in the following section.

7.4 SCQDs: Optical Characterization

Samples with SCQDs buried in GaAs matrix were fabricated for optical characterization. The positioned QDs were overgrown with 200 nm GaAs and the PL measurements are performed in confocal PL setup, described in Chapter 3. The samples are cooled by continuous flow cryostat to 8K by liquid helium. Figure 7.10 shows PL spectra of positioned QDs with different pitch and a broad emission at 970 nm is observed. The broad PL peak (FWHM ≈ 65 meV) points to a large size distribution of QDs as observed in the AFM images. The large blue shift in the emission of SCQDs compared to planar QDs is mainly due to the smaller height of SCQDs (2-3 nm) and higher degree of In-Ga intermixing. The higher degree of In-Ga intermixing is due to lower arsenic pressure and longer interruption time before capping of the QDs. The lower arsenic pressure is used to increase single dot occupancy per hole [111]. Moreover, the PL intensities of SCQDs are three to four times lower than of QDs grown on planner GaAs surface (QD density~10 ^{8}/cm^{2}).

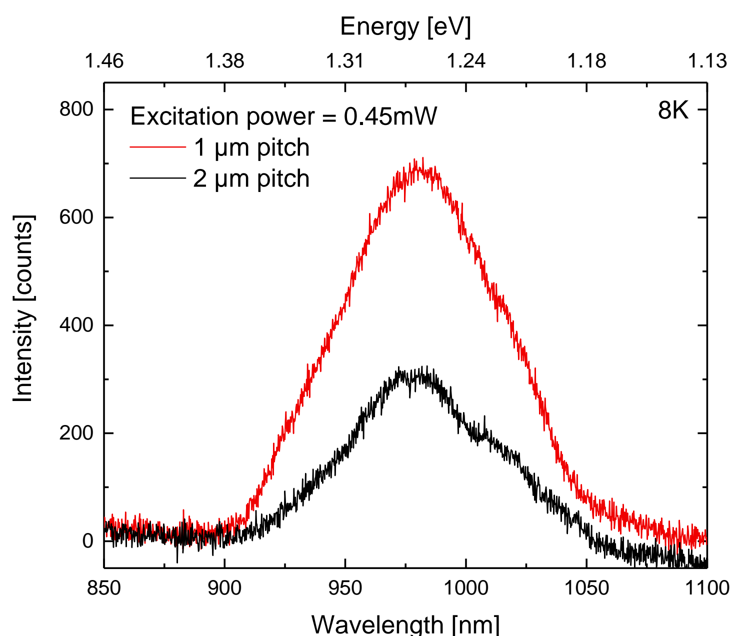

Figure 7.10: *PL spectra of positioned QDs with different pitch. For 1 µm pitch, around 10-15 QDs contributes to the emission.*

Figure 7.11 shows PL spectra of positioned QDs at different arsenic flux. At low arsenic flux ($P_{As} = 1.5 \times 10^{-5} mbar$) during QDs growth, the emission peak is around 970 nm and at higher arsenic flux ($P_{As} = 1.6 \times 10^{-5} mbar$), the emission peak is around 1070 at low temperature (8K). The shift in the PL emission peak is due to less In-Ga intermixing.

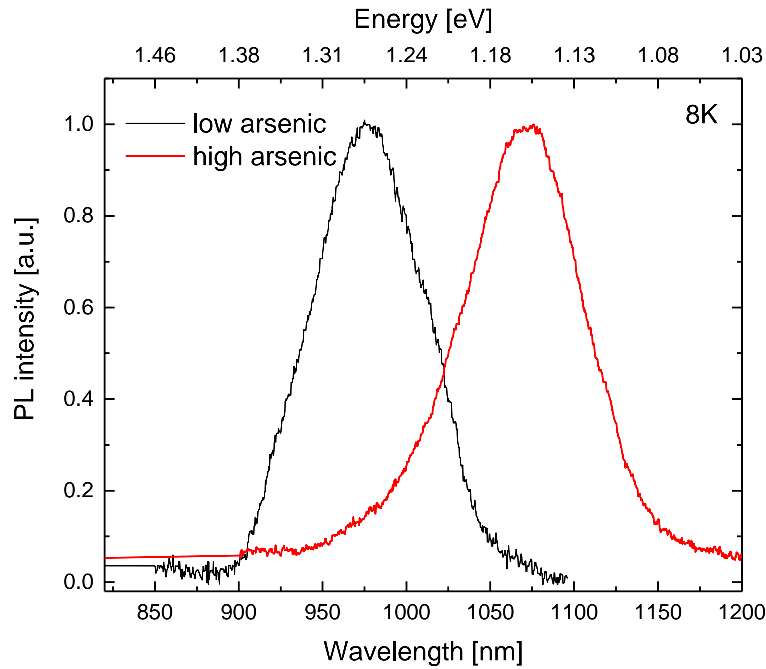

Figure 7.11: *Low temperature PL spectra of positioned InAs QDs. The higher arsenic pressure reduces the Ga-In intermixing and shifts the spectra to lower energy. Around 10-15 QDs contributes the PL emission.*

7.5 Summary

In summary, we have fabricated site-controlled InAs QDs on GaAs(100) substrate by per-patterning and re-growth technology. GaAs surface patterned with nanoholes is used to define the nucleation position of the InAs QDs. The occupancy of the nanoholes can be controlled by their size and InAs amount. The good lateral ordering of the QDs is achieved for pitches up to 2 µm. Limitations due anisotropic growth of GaAs buffer layer is a major challenge for the growth of single dot per hole for thick buffer layers. With 15 nm thick GaAs buffer layer, 60% holes are occupied with single QDs. The PL spectra of SCQDs shows that dots are optically active and show emission around 970 nm, which is also suitable for efficient Si based detection technology.

This page has been intentionally left blank.

Chapter 8

8 Conclusions

The most important achievements of the thesis are optimization of the growth process of InAs and InGaAs QDs on a newly installed MBE system. In this work, we have produced high quality InAs(InGaAs) QDs on GaAs(100) system. A simplified gradient approach for growth of low density QDMs is demonstrated. To achieve spatial control of QDs, pre-patterning and regrowth technology is used.

At starting of the thesis work, the growth of GaAs, AlAs, and InGaAs layers is optimized on GaAs(100) substrate by growing several samples such as smooth GaAs layers, background doping test samples, QWs, HEMTs etc. Different substrate growth temperatures and III/V ratio are used for optimal growth parameters. GaAs smooth layers (S_q=0.2 nm) with very low surface defects (20-25 defects/cm^2) are grown for the growth of high quality heterostructures. The key growth parameters are optimized by structural, optical and electrical characterizations.

The QDs growth is done by migration enhanced MBE for good optical and electrical properties. The effect of growth rate and III/V flux ratio is studied by employing PL spectroscopy and AFM. The low density QDs is achieved utilizing In-gradient technique, which is acquired by pausing the substrate rotation during InAs deposition. The emission energies of QDs is tuned employing In-flush technique and by Ga-incorporation during InAs deposition.

A simplified gradient approach is established for the growth of low density QDMs. In this approach a density gradient in the bottom QD layer is employed by In-gradient technique and top QD layer is grown homogeneously with 6 nm thick GaAs interdot barrier. The presence of a gradient in the top QD layer and formation of top QDs below the critical thickness (13% less) suggest that the top QD layer growth is strain driven. The effect of the interdot barrier thickness is studied for the vertical coupling. For 6 nm GaAs interdot barrier, the density gradient in the top layer is showing spatial density variations similar to the bottom QD layer suggest that the vertical coupling is present while for 12 nm thick GaAs interdot barrier the density gradient is present but not for every bottom QD top QD is formed. For 18 nm GaAs barrier, no QD growth took place in the top layer. With increasing interdot barrier thickness, the strain field is decreased. The emission energy tuning of both QDs layer is done by In-flush technique. The optical quality of QDM ensemble is similar to the single QD layer ensemble.

Finally, site-controlled QDs are grown by patterning and regrowth technology. The patterning of pre-grown GaAs wafers is done by optical lithography and EBL process. An intense cleaning process is used to remove all resist residuals and to thin the oxide layer before loading to the loadlock for regrowth. An *in-situ* atomic hydrogen cleaning is used to remove the remaining oxide layer without damaging the surface. The 60% occupancy of single dot per hole is achieved with 15 nm thick GaAs buffer layer. The optical properties of site-controlled QD ensemble are studied by PL spectroscopy.

Further work on the low-density QDs may include the fabrication of low density QDs over the whole wafer. In this approach the depositing InAs will be below the critical thickness (<1.7 ML) and annealing of the sample should be performed. Few samples already tested for surface QDs, where the density of QDs is around $5\times10^7/cm^2$ over the wafer. For further work on site-controlled QDs may include optimization of regrowth process to reduce anisotropy growth which will improve occupancy of single QD per hole. Additionally, to increase the distance between patterned interface and QDs, QD seed layers work as a stressor where the top dots are spectrally isolated from the lower ones. In this way, one will be able to increase the buffer layer thickness, which will improve the optical quality of the QDs.

Appendix

Appendix I

Patterning and Cleaning Procedure

1. Wafer preparation (pre-grown wafer)
   (a) Clean with Acetone and Isopropanol (IPA)
   (b) Dry with N2
2. Photoresist coating
   (a) ARP 3510 : AR 300-12 (1 : 1) spin coated (3000 rpm, 30 sec)
   ⇨ 1-1.2 µm thick
   (b) Baking at 100°C for 60 sec at hot plate
3. Optical lithography using UV lamp and mask aligner (SÜSS KSM MJB3)
4. Development
   (a) AR 300-35: dip for 30 sec
   (b) Stopped by DI water: dip for 30 sec
   (c) Dry with N2
5. Pattern transfer
   (a) Wet chemical etching (H_2SO_4 : H_2O_2 : H_2O ≈ 1 : 1 : 50)
   (b) 300 nm etching (etch rate ≈ 100 nm/min)
   (c) Stopped by DI water
6. Resist removal and cleaning
   (a) Resist removed by Acetone
   (b) Ultrasonic bath in Acetone for 5 min
   (c) Ultrasonic bath in IPA for 5 min
   (d) NMP (n-methyl pyrollidine) cleaning for 20 min at 150°C
   (e) TCE (trichloroethylene) cleaning for 20 min at 75°C
   (f) Clean with acetone and IPA

Substrate is ready for next lithography process

7. PMMA coating
   (a) 2% PMMA 950K (ARP 671.02) at 5500 rpm for 30 sec
      ⇨ 75-80 nm thick PMMA

   (b) Baking at 150°C for 90 sec. at hot plate
8. Patterning defined by electron beam lithography (Raith Pioneer 150)
9. Development
   (a) Developed in MIBK : IPA (1:3) solution: dip for 30 seconds at room temperature
   (b) Stopped by IPA: dip for 30 sec.
   (c) Dried by N2
10. Pattern transfer
   (a) By wet chemical etching ($H_2SO_4 : H_2O_2 : H_2O \approx 1 : 8 : 800$)
   (b) Etch rate 1 nm/sec.
   (c) Stopped by DI water (30 sec.)
11. Step 6 is repeated for resist removal and cleaning
12. HF cleaning
   (a) 50%HF +IPA for 5 minutes
   (b) Rinse with flowing DI water for 10 minutes.
   (c) Dried with N2

Substrate after this step is transferred to locklock chamber to avoid oxidation and contamination.

13. Good Luck

Appendix II

Schottky Diode Structure (Charge Tunable Structure)

One of the major advantages of QDs is the ability to exactly control their charge state. By doing this, one not only suppresses the random charge fluctuations which might occur in the sample but this also opens up ways to study and even control the interaction of single charge or spin with various reservoirs by having a specific number of carriers in the QD. In order to deterministically charge a QD on a single electron level, they are embedded in a Schottky structure, sandwiched between two metallic layers. One layer consists of a 200 nm thick highly n-doped GaAs layer below the QD layer and is referred to as the back contact or as a source of electron gas. The QDs are separated by a layer of intrinsic GaAs, which acts as a tunnel barrier from the back contact. The thickness of the tunnel barrier depends on the particular experiment and varies between 25 and 40 nm within this work. The other metallic layer is a thin, semi-transparent film of Ti/Au is processed on the sample surface.

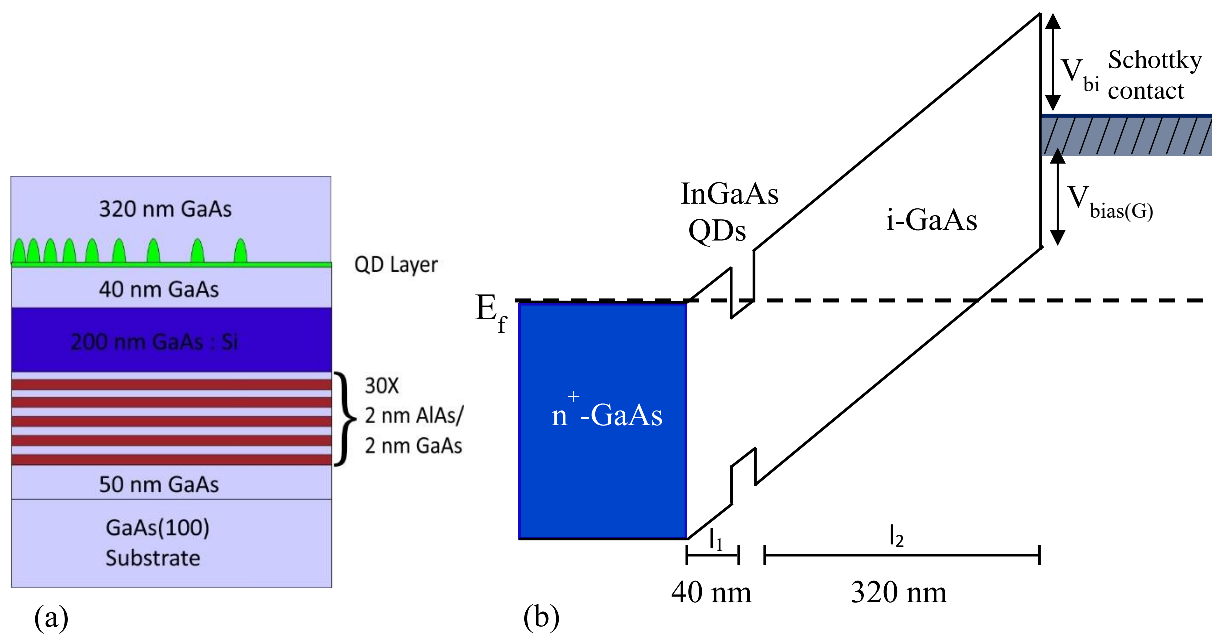

(a) Schematic of the charge tunable structure and (b) shows the band structure of Schottky diode structure

The thickness of the sample between the QD´s and the sample surface is of significant importance for controlling the different charge states of the QD [122]. The thickness of the top

layer (l_2) can be varied 5 to 11 times of the tunnel barrier thickness(l_1), for above sample it is 8 times of the tunnel barrier. A schematic of the sample structure is shown in Figure (a) where InGaAs QDs are grown with gradient approach. Figure (b) shows the band structure of a such Schottky diode structure.

Figure (c) shows the Voltage-dependent photoluminescence (VPL) spectra of single QD in a charge-tunable device where different excitonic states are observed. In this measurement, the voltage is applied to the Schottky diode structure and PL spectra are recorded. In PLV spectra, different gate voltages correspond to the different charge states in the QD. In this spectroscopy, electrostatically induced electrons or optically trapped holes through tunnelling in the QDs are optically observed [123].

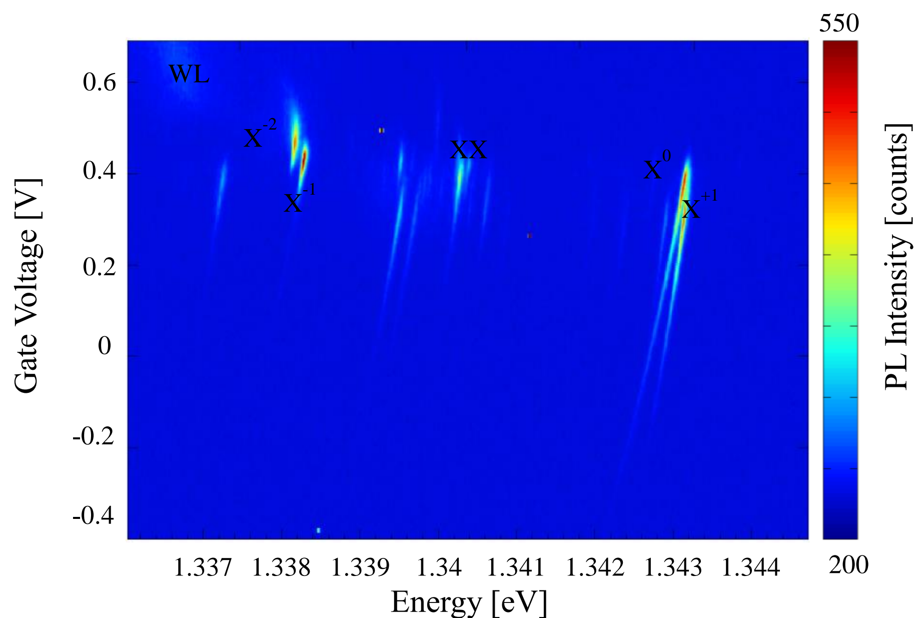

(c) PLV spectra of single quantum dot in colour map at the excitation power of 1 mW laser power (courtesy: Alex Widhalm)

Bibliography

[1] K. Hinzer, C. N. Allen, J. Lapointe, D. Picard, Z. R. Wasilewski, S. Fafard and A. J. SpringThorpe, “Widely tunable self-assembled quantum dot lasers,” *J. Vac. Sci. Technol. A,* vol. 18, pp. 578-581, 2000.

[2] O. E. Semonin, J. M. Luther and M. C. Beard, “Quantum dots for next-generation photovoltaics,” *Materials Today,* vol. 15, pp. 508-515, 2012.

[3] M. X. Zhao and B. J. Zhu, “The research and applications of quantum dots as nano-carriers for targeted drug delivery and cancer therapy,” *Nanoscale Res. Lett.,* pp. 1-9, 2016.

[4] M. Fang, C. Peng, D. W. Pang and Y. Li, “Quantum dots for cancer research: current status, remaining issues, and future perspectives,” *Cancer Biol Med,* vol. 9, pp. 151-163, 2012.

[5] P. Bhattacharya, S. Ghosh and A. Stiff-Roberts, “Quantum dot opto-electronic devices,” *Annu. Rev. Mater. Res.,* vol. 34, pp. 1-40, 2004.

[6] A. J. Shields, “Semiconductor quantum light sources,” *Nat. Photon.,* vol. 1, pp. 215-223, 2007.

[7] W. B. Gao, A. Imamoglu, H. Bernien and R. Hanson, “Coherent manipulation, measurement and entanglement of individual solid-state spins using optical fields,” *Nature Photonics,* vol. 9, pp. 363-373, 2015.

[8] D. Bimberg, Semiconductor Nanostructures, Berlin: Springer, 2008.

[9] Q. Xie, A. Madhukar, P. Chen and N. P. Kobayashi, “Vertically self-organized InAs quantum box islands on GaAs(100),” *Phys. Rev. Lett.,* vol. 75, pp. 2542-2545, 1995.

[10] Q. Xie, P. Chen and A. Madhukar, “InAs island-induced-strain driven adatom migration during GaAs overlayer growth,” *Appl. Phys. Lett.,* vol. 65, pp. 2051-2053, 1994.

[11] S. Kiravittaya, A. Rastelli and O. G. Schmidt, “Advanced quantum dot configurations,” *Rep. Prog. Phys.,* vol. 72, p. 046502, 2009.

[12] M. Ohring, The Material Science of Thin Films, New Jersey: Academic Press, 1992.

[13] K. K. N. S. M. Sze, Physics of Semiconductor Devices, New York: Wiley, 2006.

[14] I. Vurgaftman, J. R. Meyer and L. R. Ram-Mohan, “Band parameters for III–V compound semiconductors and their alloys,” *J. Appl. Phys.,* vol. 89, pp. 5815-5875, 2001.

[15] A. R. Woll, P. Rugheimer and M. G. Lally, “Self-Organized Quantum Dots,” in *Quantum Dots*, Singapore, World Scientific Publishing Co. Pte. Ltd., 2003, pp. 45-78.

[16] G. H. Carey, A. L. Abdelhady, Z. Ning, S. M. Thon, O. M. Bakr and E. H. Sargent, "Colloidal Quantum Dot Solar Cells," *Chem. Rev.,* 2015.

[17] K. H. S. G. Medeiros-Ribeiro, U. Kunze, G. Abstreiter, M. Hagn and P. M. Petroff, "Size distribution of coherently strained InAs quantum dots," *Appl. Phys. Lett.,* vol. 84, pp. 4268-4272, 1998.

[18] J. Sun, P. Jin and Z.-G. Wang, "Extremely low density InAs quantum dots realized in-situ on (100) GaAs," *Nanotechnology,* vol. 15, pp. 1763-1766, 2004.

[19] J. A. Floro, M. Sinclair, E. Chason, L. B. Freund, R. D. Twesten, R. Q. Hwang and G. A. Lucadamo, "Novel SiGe Island Coarsening Kinetics: Ostwald Ripening and Elastic Interactions," *Phy. Rew. Lett,* vol. 84, pp. 701-704, 2000.

[20] A. J. Bennett and R. Murray, "Nucleation and ripening of seeded InAs/GaAs quantum dots," *J. Crystal Growth,* vol. 240, pp. 439-444, 2002.

[21] F. Zhan, S. S. Huang, Z. C. Niu, H. Q. Ni, Y. H. Xiong, Z. D. Fang, H. Y. Zhou and Y. Luo, "Desorption and Ripening of Low Density InAs Quantum dots," *J. Nanosci. Nanotechnol.,* vol. 9, pp. 844-847, 2009.

[22] N. Perret, D. Morris, L. Franchomme-Fossé, R. Côté, S. Fafard, V. Aimez and J. Beauvais, "Origin of the inhomogeneous broadening and alloy intermixing in InAs/GaAs self-assembled quantum dots," *Phys. Rev. B,* vol. 62, pp. 5092-5099, 2000.

[23] M. Herman and H. Sitter, "Molecular Beam Epitaxy: Fundamentals and Current Status," *Springer-Verlag,* 1989.

[24] M. Henini, Molecular Beam Epitaxy: from research to mass production, Oxford, UK: Elsevier Science, 2012.

[25] W. Brawn, "Reflection High Energy Diffraction during MBE Growth".

[26] M. Ohring, "The material science of thin films," *Academic Press, New York,* 1992.

[27] J. H. Neave, B. A. Joyce, P. J. Dobson and N. Norton, "Dynamics of film growth of GaAs by MBE from RHEED observations," *Appl. Phys. A,* vol. 31, pp. 1-8, 1983.

[28] S. P. Bhattacharya, R. Fornari and H. Kamimura, "Comprehensive Semiconductor Science and Technology," *Elsevier,* vol. 3, p. 480, 2011.

[29] N. Hilal and W. Bowen, "Atomic Force Microscopy in Process Engineering: An Introduction to AFM for Improved Processes and Products," *Elsevier,* vol. 1, 2009.

[30] R. Kamper, "PhD thesis - Cubic GaN on Pre-Patterned 3C-SiC/Si (001) Substrates," 2004.

[31] W. Ma, R. Nötzel, H. P. Schönherr and K. H. Ploog, "Shape transition of coherent three-dimensional (In,Ga)As islands on GaAs(100)," *Applied Physics Letters,* vol. 79, pp. 4219-4221, 2001.

[32] S. K. Park, J. Tatebayashi and Y. Arakawa, "Structural and optical properties of high-density (>) InAs QDs with varying Al(Ga)As matrix layer thickness," *Physica E,* vol. 21, pp. 279-284, 2004.

[33] P. M. Mooney, "Electrical properties of DX centers in GaAs and AlGaAs," *Radiation Effects and Defects in Solids,* vol. 111, pp. 281-298, 1989.

[34] P. J. Dean, "Photoluminescence as a diagnostic of semiconductors," *Prog. Crystal Growth Charact.,* vol. 5, pp. 89-174, 1982.

[35] S. M. Sze, "VLSI Technology," *McGraw-Hill,* vol. 2, 2003.

[36] T. Chang, M. Mankos, K. Y. Lee and L. P. Muray, "Multiple electron-beam lithography," *Microelectronic Engineering,* vol. 57, pp. 117-135, 2001.

[37] S. Weng, C. Webb, Y. G. Chai and S. G. Bandy, "Particulates: An origin of GaAs oval defects grown by molecular beam epitaxy," *Applied Physics Letters,* vol. 47, pp. 391-393, 1985.

[38] G. Laurence, F. Simondet and P. Saget, "Combined RHEED-AES study of the thermal treatment of (001) GaAs surface prior to MBE growth," *Appl. Phys.,* vol. 19, pp. 63-70, 1979.

[39] G. W. Smith, A. J. Pidduck, C. R. Whitehouse, J. L. Glasper and J. Spowart, "Real-time laser-light scattering studies of surface topography," *Journal of Crystal Growth,* vol. 127, pp. 966-971, 1993.

[40] A. Guillen-Cervantes, Z. Rivera-Alvarez, M. Lopez-Lopez, E. Lopez-Luna and I. Hernandez-Calderon, "GaAs surface oxide desorption by annealing in ultra high vacuum," *Thin Solid Films,* vol. 373, pp. 159-163, 2000.

[41] E. H. C. Parker, The Technology and Physics of Molecular Beam Epitaxy, New York: Plenum Press, 1985.

[42] J. H. Neave and B. A. Joyce, "Dynamics of film growth of GaAs by MBE from RHEED observations," *Applied Physics A,* vol. 31, pp. 1-8, 1983.

[43] K. Ploog and K. Graf, Molecular Beam Epitaxy of III-V Compounds, Berlin: Springer-Verlag, 1984.

[44] C. T. Lee and Y. Chou, "Types of oval effects on GaAs grown by MBE," *Journal of Crystal Growth,* pp. 167-172, 1988.

[45] H. Kawada, S. Shirayone and K. Takahasi, "Reduction of surface defects in GaAs layers grown by MBE," *Journal of Crystal Growth,* vol. 128, pp. 550-556, 1993.

[46] P. Kopev, S. Ivanov, A. Y. Yegorov and D. Y. Uglov, “Influence of growth parameters and conditions on the oval defect density in GaAs layers grown by MBE,” *Journal of Crystal Growth,* vol. 96, pp. 533-540, 1989.

[47] C. E. C. Wood, L. Rathbun, H. Ohno and D. DeSimone, “On the origin and elimination of macroscopic defects in MBE films,” *Journal of Crystal Growth,* vol. 51, pp. 299-303, 1981.

[48] N. Chand and S. N. G. Chu, “A comprehensive study and methods of elimination of oval defects,” *Journal of Crystal Growth,* vol. 104, pp. 485-497, 1990.

[49] L. Däwertiz and R. Hey, “Reconstruction and defect structure of vicinal GaAs(001) and AlxGa1-xAs(001) surfaces during MBE growth,” *Surface Science,* vol. 236, pp. 15-22, 1990.

[50] J. R. Arthur, “Interaction of Ga and As2 molecular beams with GaAs surface,” *Journal of Applied Physics,* vol. 39, pp. 4032-4034, 1968.

[51] M. Shinohara, T. Ito and Y. Imamura, “Generation and propagation of defects into molecular beam epitaxially grown GaAs from an underlying GaAs substrate,” *Journal of Applied Physics,* vol. 58, pp. 3449-3455, 1985.

[52] T. Shitara and T. Nishinaga, “Surface diffusion length of gallium during MBE growth on the various misoriented GaAs(001) substrates,” *Japanese Journal of Applied Physics,* vol. 28, pp. 1212-1216, 1989.

[53] T. Nishinaga, “Elementry growth process of molecular beam epitaxy,” *Journal of Crystal Growth,* vol. 146, pp. 326-333, 1995.

[54] A. Ballestad, B. J. Ruck, J. H. Schmid, M. Adamcyk, E. Nodwell, C. Nicoll and T. Tiedje, “Surface morphology of GaAs during molecular beam epitaxy growth: Comparison of experimental data with simulations based on continuum growth equations,” *Physics Review B,* vol. 65, pp. 1-14, 2002.

[55] S. Yamauchi, K. Komori and T. Sugaya, “Optical characteristics of self-aligned InAs quantum dots in the presence of GaAs oval strain,” *Japanese Journal of Applied Physics,* vol. 45, pp. 1030-1032, 2006.

[56] M. Yamada and Y. Ide, “Direct observation of species liberated from GaAs native oxides during atomic hydrogen cleaning,” *Japanese Journal of Applied Physics,* vol. 2, pp. 671-674, 1994.

[57] P. Tomkiewicz, A. Winkler and J. Szuber, “Comparative study of the GaAs(1 0 0) surface cleaned by atomic hydrogen,” *Applied Surface Science,* vol. 33, pp. 7647-7658, 2006.

[58] L. S. Hirsch, K. S. Ziemer, M. R. Richards-Babb, C. D. Stinespring, T. H. Myers and T. Colin, “The use of atomic hydrogen for low temperature oxide removal from HgCdTe,” *Journal of Electronic Materials,* vol. 27, no. 6, pp. 651-656, 1998.

[59] K. G. Tschersich, J. P. Fleischhauer and H. Schuler, “Design and characterization of a thermal hydrogen atom source,” *Journal of Applied Physics,* vol. 104, pp. 34908_1-34908_7, 2008.

[60] K. G. Tschersich, “Intensity of a source of atomic hydrogen based on a hot capillary,” *Journal of Applied Physics,* vol. 87, pp. 2565-2573, 2000.

[61] T. Sugaya and M. Kawabe, “Low-temperature cleaning of GaAs substrate by atomic hydrogen irradiation,” *Japanese Journal of Applied Physics,* vol. 30, pp. 402-404, 1991.

[62] A. Khatiri, J. Ripalda, T. Krzyzewski, G. Bell, C. McConville and T. Jones, “Atomic hydrogen cleaning of GaAs(001): a scanning tunnelling microscopy study,” *Surface Science,* vol. 548, pp. 1-6, 2004.

[63] P. D. Wang, N. N. Ledentsov, C. M. S. Torres, P. S. Kop´ev and V. M. Ustinov, “Optical characterization of submonolayer and monolayer InAs structures in a GaAs matrix on (100) and high-index surfaces,” *Appl. Phys. Lett.,* vol. 64, pp. 1526-1528, 1994.

[64] V. Bressler-Hill, A. Lorke, S. Varma, P. M. Petroff, K. Pond and W. H. Weinberg, “Initial stage of InAs epitaxy on vicinal GaAs(001)-(2*4),” *Phys. Rev. B,* vol. 50, pp. 8479-8487, 1994.

[65] E. Placidi, F. Arciprete, R. Magri, M. Rosini, A. Vinattieri, L. Cavigli, M. Gurioli, E. Giovine, L. Persichetti, M. Fanfoni, F. Patella and A. Balzarotti, “InAs Epitaxy on GaAs(001): A Model Case of Strain-Driven,” in *Self-Assembly of Nanostructures: The INFN Lectures*, Heidelberg, Springer Science & Business Media, 2011, 2011, pp. 73-126.

[66] D. Leonard, K. Pond and P. M. Petroff, “Critical layer thickness for self-assembled InAs islands on GaAs,” *Physics Review B,* vol. 50, pp. 11687-11692, 1994.

[67] R. Nötzel, “Self-organised growth of quantum-dot structures,” *Semicond. Sci. Technol.,* vol. 11, pp. 1365-1397, 1996.

[68] F. Patella, F. Arciprete, M. Fanfoni, A. Balzarotti and E. Placidi, “Apparent critical thickness versus temperature for InAs quantum dot growth on GaAs(001),” *Appl. Phys. Lett.,* vol. 88, pp. 1619031-1619033, 2006.

[69] P. Michler, Single quantum dots: fundamentals, applications and new concepts, Heidelberg: Springer-Verlag, 2003.

[70] G. E. Cirlin, G. M. Guryanov, A. O. Golubok, S. Ya.Tipissev, N. N. Ledentsov, P. S. Kop’ev, M. Grundmann and D. Biberg, “Ordering phenomena in InAs strained layer morphological transformation on GaAs (100) surface,” *Appl. Phys. Lett.,* vol. 67, pp. 97-99, 1995.

[71] P. B. Joyce, T. J. Krzyzewski, G. R. Bell, T. S. Jones, S. Malik, D. Childs and R. Murray, “Effect of growth rate on the size, composition, and optical properties of InAs/GaAs quantum dots,” *Phys. Rev. B,* vol. 62, pp. 10891-10895, 2000.

[72] B. A. Joyce, P. C. Kelires, A. G. Naumovets and D. D. Vvedensky, Quantum Dots Fundamentals, Applications, and Frontiers, Dordrecht, Netherlands: Springer, 2003.

[73] D. M. Schaadt, D. Z. Hu and K. H. Ploog, “Stress evolution during ripening of self-assembled InAs/GaAs quantum dots,” *J. Vac. Sci. Technol. B,* vol. 24 (4), pp. 2069-2074, 2006.

[74] T. J. Krzyzewski and T. S. Jones, “Ripening and annealing effects in InAs/GaAs(001) quantum dot formation,” *J. Appl. Phys.,* vol. 96, pp. 668-674, 2004.

[75] E. Steimetz, T. Wehnert, K. Haberland, J.-T. Zettler and W. Richter, “GaAs cap layer growth and In-segregation effects on self-assembled InAs-quantum dots monitored by optical techniques,” *J. Crystal Growth,* vol. 195, pp. 530-539, 1998.

[76] J. G. Belk, C. F. McConville, J. L. Sudijono, T. S. Jones and B. A. Joyce, “Surface alloying at InAs-GaAs interfaces grown on (001) surfaces by molecular beam epitaxy,” *Surface Science,* vol. 387, pp. 213-226, 1997.

[77] A. Lemaitre, G. Glas and F. Patriarche, “Composition profiling of InAs⁄GaAs quantum dots,” *Appl. Phys. Lett.,* vol. 85, pp. 3717-3719, 2004.

[78] I. Kegel, T. H. Metzger, A. Lorke, J. Peisl, J. Stangl, G. Bauer, J. M. García and P. M. Petroff, “Nanometer-Scale Resolution of Strain and Interdiffusion in Self-Assembled InAs/GaAs Quantum Dots,” *Phys. Rev. Lett.,* vol. 85, p. 1694, 2000.

[79] P. B. Joyce, T. J. Krzyzewski, G. R. Bell, B. A. Joyce and T. S. Jones, “Composition of InAs quantum dots on GaAs(100): Direct evidence for (In, Ga)As alloying,” *Phys. Rev. B,* vol. 58, pp. R15981-84, 1998.

[80] S. Guha, A. Madhukar and K. C. Rajkumar, “Onset of incoherency and defect introduction in the initial stages of molecular beam epitaxial growth of highly strained InxGa1-xAs on GaAs(100),” *Appl. Phys. Lett.,* vol. 57, pp. 2110-2112, 1990.

[81] B. Ilahi, M. Souaf, M. B. J. Alrashdi, L. Sfaxi, A. Abdulaziz and H. Maaref, “Evolution of InAs QDs size with the growth rate: a numerical investigation,” *Journal of Nanomaterials,* pp. 1-6, 2015.

[82] D. Gammon, E. S. Snow, B. Shanabrook, D. S. Katzer and D. Park, “Homogeneous linewidths in the optical spectrum of a single gallium arsenide quantum dot,” *Science,* vol. 273, no. 5271, pp. 87-90, 1996.

[83] P. Jin, X. L. Ye and Z. G. Wang, “Growth of low-density InAs/GaAs quantum dots on a substrate with an intentional temperature gradient by molecular beam epitaxy,” *Nanotechnology,* vol. 16, pp. 2775-2778, 2005.

[84] J. S. Kim and N. Koguchi, “Near room temperature droplet epitaxy for fabrication of InAs quantum dots,” *Appl. Phys. Lett.,* vol. 85, pp. 5893-5895, 2004.

[85] S. Fafard and C. N. Allen, “Intermixing in quantum dot ensembles with sharp adjustable cells,” *Appl. Phys. Lett.,* vol. 75, pp. 2375-2376, 1999.

[86] Z. R. Wasilewski, S. Fafard and J. P. McCaffrey, “Size and shape engineering of vertically stacked self-assembled quantum dots,” *J. Cryst. Growth,* vol. 201/202, pp. 1131-1135, 1999.

[87] S. Fafard, Z. R. Wasilewski, C. N. Allen, D. Picard, M. Spanner and J. P. McCaffrey, “Manipulating the energy levels of semiconductor quantum dots,” *Phys. Rev. B,* vol. 59, pp. 15368-15373, 1999.

[88] F. Guffarth, R. Heitz, A. Schliwa, O. Stier, N. Ledentsov, A. R. Kovsh, V. Ustinov and D. Bimberg, “Strain engineering of self-organized InAs quantum dots,” *Phys. Rev. B,* vol. 64, no. 8, p. 085305, 2001.

[89] D. Litvinov, H. Blank, R. Schneider, D. Gerthsen, T. Vallaitis, J. Leuthold, T. Passow, A. Grau, H. Kalt and C. Klingshirn, “Influence of InGaAs cap layers with different In concentration on the properties of InGaAs quantum dots,” *J. Appl. Phys. ,* vol. 103, p. 083523, 2008.

[90] S. Malik, C. Roberts, R. Murray and M. Pate, “Tuning self-assembled InAs quantum dots by rapid thermal annealing,” *Appl. Phys. Lett.,* vol. 71, p. 1987, 1997.

[91] R. Leon, S. Fafard, P. G. Piva, S. Ruvimov and Z. Liliental-Weber, “Tunable intersublevel transitions in self-forming semiconductor quantum dots,” *Phys. Rev. B,* vol. 58, p. R4262, 1998.

[92] L. Wang, A. Rastelli and O. G. Schmidt, “Structural and optical properties of In(Ga)As/GaAs quantum dots treated by partial capping and annealing,” *J. Appl. Phys.,* vol. 100, p. 064313, 2006.

[93] R. M. Roescu, Wavefunction and carrier-carrier interactions in InAs quantum dots studied by capacitance-voltage spectroscopy, Bochum, Germany: Ruhr-Universität Bochum, 2009.

[94] E. Biolatti, R. C. Iotti, P. Zanardi and F. Rossi, “Quantum information processing with semiconductor macroatoms,” *Phys. Rev. Lett.,* vol. 85, pp. 5647-5650, 2000.

[95] X.-Q. Li and Y. Yan, “Quantum computation with coupled quantum dots embedded in optical microcavities,” *Phys. Rev. B,* vol. 65, p. 205301, 2002.

[96] B. Legrand, J. Nys, B. Grandidier, D. Stievenard, A. Lemaitre, J. M. Gerard and V. Thierry-Mieg, “Quantum box size effect on vertical self-alignment studied using cross-sectional scanning tunnelling microscopy,” *Appl. Phys. Lett.,* vol. 74, pp. 2608-2610, 1999.

[97] J. Tersoff, C. Teichert and M. G. Lagally, “Self-organization in growth of quantum dot superlattices,” *Phys. Rev. Lett.,* vol. 76, pp. 1675-1678, 1996.

[98] K. L. Janssens, B. Partoens and F. M. Peeters, “Magnetoexciton in vertically coupled InP/GaInP quantum disks: Effect of strain on the exciton ground state,” *Phys. Rev. B.,* vol. 69, p. 235320, 2004.

[99] S. Fafard, Z. R. Wasilewski, C. N. Allen, D. Picard, M. Spanner and J. P. McCaffrey, “Manipulating the energy levels of semiconductor quantum dots,” *Phys. Rev. B,* vol. 59, pp. 15368-15373, 1999.

[100] M. Scheibner, M. Yakes, A. S. Bracker, I. V. Ponomarev, M. F. Dotty, C. S. Hellberg, L. J. Whitman, T. L. Reinecke and D. Gammon, “Optically mapping the electronic structure of coupled quantum dots,” *Nat. Phys.,* vol. 4, pp. 291-295, 2008.

[101] M. F. Doty, M. Scheibner, A. S. Bracker, I. V. Ponomarev, T. L. Reinecke and D. Gammon, “Optical spectra of doubly charged quantum dot molecules in electric and magnetic fields,” *Phys. Rev. B.,* vol. 78, p. 115316, 2008.

[102] A. S. Bracker, M. Scheibner, M. F. Doty, E. A. Stinaff, I. V. Ponomarev, J. C. Kim, T. L. R. L. J. Whitman and D. Gammon, “Engineering electron and hole tunneling with asymmetric InAs quantum dot molecules,” *Appl. Phy. Lett.,* vol. 89, pp. 233110_1-3, 2006.

[103] G. E. Cirlin, G. M. Guryanov, A. O. Golubok, S. Ya.Tipissev, N. N. Ledentsov, P. S. Kop’ev, M. Grundmann and D. Biberg, “Ordering phenomena in InAs strained layer morphological transformation on GaAs (100) surface,” *Appl. Phys. Lett.,* vol. 67, pp. 97-99, 1995.

[104] Z. Mi and P. Bhattacharya, “Molecular-beam epitaxial growth and characteristics of highly uniform InAs/GaAs quantum dot layers,” *J. Appl. Phys.,* vol. 98, pp. 023510_1-023510_5, 2005.

[105] H. Heidemeyer, S. Kiravittaya, C. Müller, N. Y. Jin-Phillipp and O. G. Schmidt, “Closely stacked InAs/GaAs quantum dots grown at low growth rate,” *Appl. Phys. Lett.,* vol. 80, pp. 1544-1546, 2002.

[106] D. S. L. Mui, D. Leonard, L. A. Coldren and P. M. Petroff, “Surface migration induced self-aligned InAs islands grown by molecular beam epitaxy,” *Journal of Appl. Phys.,* vol. 66, pp. 1620-1622, 1995.

[107] M. Mehta, D. Reuter, A. Melnikov and A. D. Wieck, “Focused ion beam implantation induced site-selective growth of InAs quantum dots,” *Appl. Phys. Lett.,* vol. 91, p. 123108, 2007.

[108] J. Lee, M. J. Noordhoek, P. Smereka, H. McKay and J. M. Millunchick, “Filling of hole arrays with InAs quantum dots,” *Nanotechnology,* vol. 20, p. 28505, 2009.

[109] K. S. Han, S. H. Hong and H. Lee, “Fabrication of complex nanoscale structures on various substrates,” *Appl. Phys. Lett.,* vol. 91, p. 123118, 2007.

[110] J. Tommila, A. Tukiainen, J. Viheriala, A. Schramm, T. Hakkarainen and A. Aho, “Nanoimprint lithography patterned GaAs templates for site-controlled InAs quantum dots,” *J. Cryst. Growth,* vol. 323, pp. 183-186, 2011.

[111] J. Herranz, L. Gonzalez, L. Wewior, B. Alen, D. Fuster and Y. Gonzalez, "Study of growth parameters for single InAs QD formation on GaAs(001) patterned substrate by local oxidation lithography," *Cryst. Growth Des.,* vol. 15, pp. 666-672, 2015.

[112] P. Atkinson, M. B. Ward, S. P. Bremner, D. Anderson, T. Farrow, G. A. C. Jones, A. J. Shields and D. A. Ritchie, "Site-control of InAs quantum dots using ex-situ electron beam lithographic patterning of GaAs substrates," *J. J. of Appl. Phys.,* vol. 45, pp. 2519-2521, 2006.

[113] S. Kiravittaya, A. Rastelli and O. G. Schmidt, "Photoluminescence from seeded three-dimensional InAs/GaAs quantum-dot crystals," *Appl. Phys. Lett. ,* vol. 88, p. 143112, 2006.

[114] H. Heidemeyer, C. M. Mueller and O. Schmidt, "Highly ordered arrays of In(Ga)As quantum dots on patterned GaAs (0 0 1) substrates," *J. Cryst. Growth,* vol. 261, pp. 444-449, 2004.

[115] A. Strittmatter, A. Schliwa, J. H. Schulze, T. D. Germann, A. Dreismann, O. Hitzemann, E. Stock, I. A. Ostapenko, S. Rodt, W. Unrau, U. W. Pohl, A. Hoffmann, D. Bimberg and V. Haisler, "Lateral positioning of InGaAs quantum dots using a buried stressor," *Appl. Phys. Lett.,* vol. 93111, p. 100, 2012.

[116] K. D. Jöns, P. Atkinson, M. Müller, M. Heldmaier, S. M. Ulrich, O. G. Schmidt and P. Michler, "Triggered indistinguishable single photons with narrow line widths from site-controlled quantum dots," *Nano Letter,* vol. 13, pp. 126-130, 2012.

[117] P. Atkinson, O. G. Schmidt, S. P. Bremner and D. A. Ritchie, "Formation and ordering of epitaxial quantum dots," *C. R. Physique,* vol. 9, pp. 788-803, 2008.

[118] Z. R. Wasilewski, J. M. Baribeau, M. Beaulieu, X. Wu and G. I. Sproule, "Studies of oxide desorption from GaAs substrates via Ga2O3 to Ga2O conversion by exposure to Ga flux," *J. Vac. Sci. Technol B,* vol. 22, pp. 1534-1538, 2004.

[119] X.Q.Shen, D. Kishimoto and T. Nishinaga, "Arsenic pressure dependence of surface diffusion of Ga on nonplanar GaAs substrate," *Jpn J Appl. Phys.,* vol. 33, pp. 11-17, 1994.

[120] R. Cheung, S. Thoms, M. Watt, M. A. Foad, C. M. Sotomayor-Torres, C. D. W. Wilkinson, U. J. Cox, R. A. Cowley, C. Dunscombe and R. H. Williams, "Reactive ion etching induced damage in GaAs and Al0.3Ga0.7As and SiCl4," *Semicond. Sci. Technol,* vol. 7, pp. 1189-1198, 1992.

[121] C. Schneider, A. Huggenberger, T. Sünner, T. Heindel, M. Strauß, S.Göpfert, P. Weinmann, S. Reitzenstein, L. Worschech, M. Kamp and S. H. a. A. Forchel, "Single site-controlled In(Ga)As/GaAs quantum dots: growth, properties and device integration," *Nanotechnology,* vol. 20, pp. 1-9, 2009.

[122] D. Reuter, "Capacitance Voltage Spectroscopy of InAs Quantum Dots," in *Self-Assembled Quantum Dots*, New York, Springer, 2008, pp. 337-357.

[123] A. K. Rai, "Optically pumped and electrically triggered single photon emission from a single quantum dot," Bochum, 2013.

[124] T. Passow, S. Li, P. Feinäugle, T. Vallaitis, J. Leuthold, D. Litvinov, D. Gerthsen and M. Hetterich, "Systematic investigation into the influence of growth conditions on InAs/GaAs quantum dot properties," *J. Appl. Phys.,* vol. 102, pp. 735111-9, 2011.

Publications

(1) **N. Sharma**, D. Reuter, "A Modified Gradient Approach for the Growth of Low Density InAs Quantum Dot Molecules by Molecular Beam Epitaxy, J. Cryst. Growth, vol. 447, (2017).

(2) A. Mukherjee, A. Widhalm, **N. Sharma**, P. Kölling, A. Thiede, J. Förstner, D. Reuter, and A. Zrenner "Rapid Adiabatic Passage using Electrically Controlled Transitions in Quantum Dots" (in preparation 2017).

(3) A. Mukherjee, A. Widhalm, **N. Sharma**, P. Kölling, A. Thiede, J. Förstner, D. Reuter, and A. Zrenner "Ultrafast Coherent Control of a Single Exciton Qubit by Optoelectronic Manipulation" (in preparation 2017).

Conference Contributions

05/2015	Oral presentation, SFB.TRR 142 Workshop: "Molecular Beam Epitaxy of Tailored InAs Quantum Dot Heterostructures", Bad Sassendorf (Germany)
09/2015	Oral presentation, German MBE Workshop: Growth of Low Density Quantum Dot Molecules", Paderborn (Germany)
03/2016	Poster presentation, DPG Spring Meeting: "Growth of low density InAs Quantum Dot Molecules", Regensburg (Germany)
09/2016	Poster presentation, 19th International Conference on Molecular Beam Epitaxy: A Modified gradient Approach for the Growth of Low Density InAs Quantum Dot Molecules", Montpiller (France)